ACTA PHARMACEUTICA SCIENCIA

International Journal in Pharmaceutical Sciences, Published Quarterly

Contents

Aims and Scope of Acta Pharmaceutica Sciencia

Acta Pharmaceutica Sciencia is a continuation of the former "Eczacılık Bülteni" which was first published in 1953 by Prof. Dr. Kasım Cemal GÜVEN's editorship. At that time, "Eczacılık Bülteni" hosted scientific papers from the School of Medicine-Pharmacy at Istanbul University, Turkey.

In 1984, the name of the journal was changed to "Acta Pharmaceutica Turcica" and it became a journal for national and international manuscripts, in all fields of pharmaceutical sciences in both English and Turkish. (1984-1995, edited by Prof. Dr. Kasım Cemal GÜVEN, 1995-2001, edited by Prof. Dr. Erden GÜLER, 2002-2011, edited by Prof. Dr. Kasım Cemal GÜVEN)

Since 2006, the journal has been published only in English with the name, "Acta Pharmaceutica Sciencia" which represents internationally accepted high-level scientific standards. The journal has been published quarterly except for an interval from 2002 to 2009 in which its issues were released at intervals of four months. The publication was also temporarily discontinued at the end of 2011 but since 2016, Acta Pharmaceutica Sciencia has continued publication with the reestablished Editorial Board and also with the support of you as precious scientists.

Yours Faithfully

Prof. Dr. Şeref DEMİRAYAK

Editor

Everything about your eyes.

World-class applications and treatment methods of eye health are provided in each specific branch of Ophthalmology with the latest technology and specialized doctor team in our center.

| LAZER VE GÖZ İÇİ LENS | RETİNA HASTALIKLARI | KORNEA HASTALIKLARI | GLOKOM | KATARAKT | ŞAŞILIK VE GÖZ TEMBELLİĞİ | NÖRO OFTALMOLOJİ | OKÜLOPLASTİK CERRAHİ |

Development and Validation of UPLC Method for the Determination of Olopatadine Hydrochloride in Polymeric Nanoparticles

Umay Merve Güven[1*], Murat Sami Berkman[2], Yasemin Yazan[2]

1 Cukurova University, Faculty of Pharmacy, Pharmaceutical Technology, Adana, Turkey.
2 Anadolu University, Faculty of Pharmacy, Pharmaceutical Technology, Eskişehir, Turkey.

ABSTRACT

A new, simple, rapid, precise, accurate and specific stability indicating reverse phase UPLC method developed for the determination of encapsulated olopatadine hydrochloride (OLO) in the polymeric nanoparticle formulations. Studies were carried out on a 2.1x50 mm, 1.8 μm Zorbax Eclipse Plus C$_{18}$ column with an optimized mobile phase of methanol, water and sodium acetate buffer solution (40:50:10, v/v/v) at a flow rate of 0.5 mL/min. OLO was detected and quantitated using a photodiode array detector at a wavelength of 246 nm and the column temperature was adjusted to 40 °C. The proposed method validation was carried out for specificity, linearity, accuracy, precision, limit of detection, limit of quantitation and robustness according to the ICH harmonised tripartite guideline "validation of analytical procedures Q2(R1)". Analytical curve was linear over the concentration range of 5-50 μg/mL. All the validation parameters were within the acceptance range. LOD and LOQ for OLO were 0.7652 and 2.3188 μg/mL, respectively. The developed method fulfilled the requirements for reliability and feasibility for the quantitative analysis of OLO in polymeric nanoparticles.

Keywords: Olopatadine hydrocloride, Eudragit, UPLC, validation, nanoparticles.

INTRODUCTION

The conventional eye drops are the most convenient and patient compliant non-invasive route for topical ophthalmic drug delivery. Nasolachrymal drainage, epithelial membrane barriers and non-productive absorption of these ophthalmic preparations can result in poor ocular bioavailability and systemic absorption leading side effects. The limited duration time requires frequently dosing up to 4 times per day for many treatments [1]. The active ingredient can

be delivered to the posterior ocular tissue segments by different administrations routes such as intravitreal injections, periocular injections, and systemic administration, but all have limitations. To overcome the ocular drug delivery barriers and improve bioavailability, various conventional and novel drug delivery systems have been developed such as emulsion, ointments, suspensions, aqueous gels, nanomicelles, nanoparticles, liposomes, dendrimers, implants, contact lenses, nanosuspensions, microneedles and in situ thermosensitive gels [2,3].

Nanotechnology based ocular drug delivery systems such as polymeric nanoparticles have revealed promising results for dose optimization, bioavailability and sustained ocular drug delivery to the posterior ocular tissue segments.

Ultra-performance liquid chromatography (UPLC) is a new category of separation technique based upon well-established principles of liquid chromatograph[4,5]. UPLC provides the benefit of small injection volumes, shortened run times (<5 min), and reduced solvent usage, making it the more economical method for quantitation[6]. Because of its speed and sensitivity, this technique is gaining considerable attention in recent years for pharmaceutical and biomedical analysis[7,8]. In this study, UPLC was preferred for determination and quantification.

OLO (Figure 1) with histamine H1 receptor antagonistic action is used in ocular allergy and available on the market as eye drops for many years. OLO inhibits both mast cell degranulation and the release of arachidonic acid metabolites in various types of cells [9,10,11]. Therefore, OLO loaded polymeric nanoparticles were prepared as an alternative carrier to achieve the mentioned problems. The main purpose of this study was to describe a new assay for the determination of encapsulated OLO in the polymeric nanoparticle formulations.
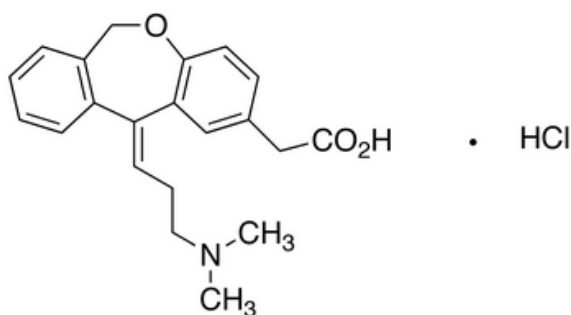
Figure 1. Olopatadine hydrochloride

METHODOLOGY

Materials

Olopatadine hydrocloride, methanol and sodium acetate were purchased from Sigma (Steinheim, Germany). Eudragit® RS 100 was obtained from Degussa Röhm Pharma Polymers (Germany). All other reagents and solvents were of analytical grade and purchased from Sigma (Steinheim, Germany). High purity water was used throughout the experiment and prepared using a Millipore Milli-Q water (France) purification system.

Preparation of Polymeric Nanoparticles

Eudragit® RS 100 polymeric nanoparticles were prepared using spray-drying method[1]. Briefly, Eudragit® RS 100 and OLO were dissolved in 100 mL methanol and stirred for 12 hours at room temperature with a magnetic stirrer. Final transparent solution was then spray-dried using a Mini Spray Dryer (B-190, BUCHI Labortechnik AG, Flawil, Switzerland) with an inlet and outlet temperature of 120 °C and 70 °C, respectively. A white dry powder was obtained and kept in coloured vials at room temperature until analysis[12, 13]. Olopatadin hydrochloride-free nanoparticles were also prepared as described above. Compositions of the nanoparticles prepared were given in Table 1.

Table 1. Compositions of the polymeric nanoparticles

Code	OLO (mg)	Eudragit® RS 100 (mg)	Methanol (mL)
NP plasebo	-	500	100
NP1	50	500	100
NP2	75	500	100

Chromatographic Conditions

As a model of combined pharmaceutical applications, the chromatography analyses of the polymeric nanoparticles were performed using an Agilent 1290 Infinity UPLC system (Germany) equipped with a solvent degasser, quaternary pump, autosampler, column oven and diode array detector. Agilent ChemStation software was used for operation control and data collection. The method was developed using a 2.1x50 mm, 1.8 μm Zorbax Eclipse Plus C_{18} column with an isocratic mobile phase consisting methanol, water and buffer solution in different ratios. The column temperature was maintained at 40 °C and UV detection was performed at 246 nm. All prepared solutions were filtered through

0.22 μm membrane filters before injection. Statistics were computed using Microsoft Excel 2010 (Redmond, WA, USA).

Analytical Method Validation

The UPLC method was validated according to the International Conference Harmonization (ICH) guideline[2] with respect to specificity, linearity, accuracy and precision, limit of detection (LOD), limit of quantification (LOQ) and statistically evaluated for OLO quantification [14].

Linearity

A linear relationship was evaluated across the range of the analytical procedure. The linearity of peak normalization (PN) ratios versus concentrations were evaluated using the calibration curve obtained from 5, 10, 15, 20, 25, 30, 35, 40, 45, 50 μg/mL OLO solutions. Six individual replicates at each concentration were analyzed and PN ratios were calculated using the Equation 1.

PN = peak area / retention time (R_t)   **Equation 1.**

Linear least squares methodology was used for the calculation of regression line. The correlation coefficient (r), coefficient of determination (r^2), y-intercept, slope of the regression line, residual sum of squares (RSS) was submitted with a plot of the data.

Accuracy

The accuracy of the method was determined by recovery studies evaluated in 3 concentration levels of 10, 30 and 50 μg/mL. Six individual replicates of each concentration were analyzed. Theoretical known amount and calculated assay amount were evaluated with the percent recovery.

Precision

The analyses were performed on the same day to determine repeatability or intra-day variability and on different days to establish the intermediate precision or inter-day variability. Samples were prepared in 3 concentration levels of 10, 25, 50 μg/mL. Six individual replicate of each concentration were analyzed. The precision of the chromatographic method was reported as mean values, standart deviations (SD) and relative standart deviations (RSD) with confidence intervals.

Specificity

The specificity of the method was verified by comparing the chromatograms obtained from the placebo and OLO samples to show the detection ability of

the desired components. Absence of any interference between the measured peaks was demonstrated in the representative chromatograms.

Limit of Detection (LOD) and Limit of Quantification (LOQ)

The calibration curve obtained in linearity was used for the detection limits. The LOD and LOQ were theoretically calculated by Equation 2 and 3.

LOD = 3.3 σ/S   **Equation 2.**

LOQ = 10 σ/S   **Equation 3.**

where σ is the standard deviation of y-axis interception values of the calibration curve and S is is the slope of the calibration curve [15].

Robustness

The capacity of the analytical method was investigated by deliberate variation of the mobile phase composition, flow rate, column temperature and stability of OLO. Sample solutions were evaluated for each variation of the method conditions.

Determination of OLO in Polymeric Nanoparticles

Two different extraction methods were used to assess the encapsulation efficiency of the nanoparticles. 5 mg nanoparticle was weighed and dispersed in 2 mL distilled water for the determination of superficial and free OLO. This suspension was centrifuged at 5000 rpm for 3 minutes and filtered. The same amount of nanoparticles were dissolved in 2 mL methanol for the determination of total OLO. The mixture was vortexed for 1 minute and filtered. The loaded amount of OLO was determined by UPLC analyses of these two samples in triplicate. The measurements were also repeated at 3rd and 6th months for stability study. Encapsulation efficiency were calculated using the following Equation 4 [16].

EE (%) = [(OLO$_T$ - OLO$_S$) × (OLO$_T$)$^{-1}$] × 100   **Equation 4.**

EE: Encapsulation Efficiency

OLO$_T$: Total OLO content

OLO$_S$: Superficial and free OLO content

RESULTS AND DISCUSSION

Chromatographic Conditions

Initial runs were carried out on methanol and water in various proportions to determime the appropriate mobile phase. Irregular shaping and tailing of OLO

peaks were observed in isocratic mode. Satisfactory regular and symmetrical peaks were obtained by using 0.1 M sodium acetate buffer solution. Studies were carried out on a 2.1x50 mm, 1.8 µm Zorbax Eclipse Plus C18 column with an optimized mobile phase of methanol, water and sodium acetate buffer solution (40:50:10, v/v/v) and the sample injection volume was 0.5 µL.

Independent variables such as oven temperature, flow rate and wavelength were also optimized which could greatly influence the separation procedure. The effect of oven temperature was studied between 20 and 40 °C. The highest OLO peak area and shape/base compliance was achieved at an oven temperature of 40 °C. The UV spectrum of OLO was scanned in the range of 200-400 nm and maximum absorption to accomplish the detection and the quantification of OLO was observed at 246 nm. The role of the flow rate on retention time, elution and peak morphology was tested and mobile phase was found to be most reliable at flow rate of 0.5 mL.min^{-1}. Under these conditions, OLO showed an acceptable retention time of 1.5 min with a run time of 5 min. Analysis time was 7 min including the re-equilibration time.

Before analysis, the chromatographic column was equilibrated with the mobile phase for 30 minutes prior to injection. A summary of the chromatographic setup conditions for validation and analysis are represented in Table 2.

Table 2. Chromatographic conditions

stationary phase	Zorbax Eclipse Plus C_{18} 2.1x50 mm, 1.8 µm
mobile phase	Methanol: water:sodium acetate buffer solution (40:50:10, v/v/v)
oven temperature	40 °C
flow rate	0.5 mL/min
injection volume	0.5 µL
detection wavelenght	246 nm

Analytical Method Validation

Calibration curves were obtained by plotting the PN ratios versus concentrations after the analysis of the injected samples (Figure 2).
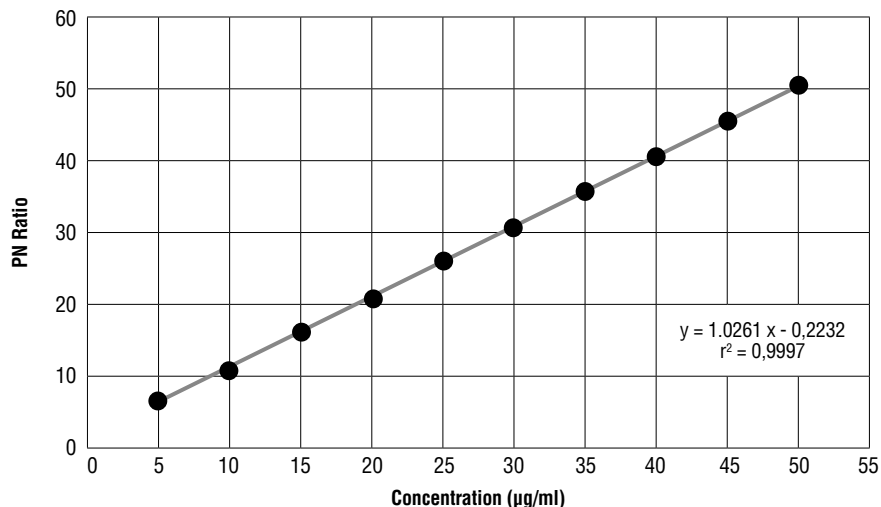
Figure 2. Linearity equation of OLO.

The linearity of the method was established in the 5-50 µg/mL OLO range and showed excellent correlation within the concentration range. Regression statistics data of the six individual replicates were summarized in Table 3.

Table 3. Regression statistics of linearity (n=6)

	pooled	*mean*
correlation coefficient (r)	0.9984	0.9999
coefficient of determination (r^2)	0.9968	0.9997
observations	60	10
y-intercept	-0.2232	
slope	1.0261	

The coefficient of determination close to unity was not the necessarily outcome of a linear relationship and the use of only this value could be potentially misleading according to the Analytical Methods Committee (AMC) technical brief [17]. Therefore, the lack-of-fit test was applied as an auxiliary indicator for linearity by evaluating the variance of the residual values (Table 4). Analysis of Vari-

ance (ANOVA) results were calculated by Minitab® 18 data analysis sofware and confirmed linearity significance of the curve, homogeneity of variances, and normality of the residues. The lack-of-fit was not statistically significant as P-value > 0.05 (0.754) which means the test did not detect any lack-of-fit at the α level in the simple linear regression model.

Table 4. ANOVA linearity pooled results (n=6) (DF: degrees of freedom; SS: sum of squares; MS: mean squares; F: F-value; P: P-value)

	DF	SS	MS	F	P
regression	1	13028.4	13028.4	17900.21	0.000
residual	58	42.2	0.7		
lack-of-fit	8	3.8	0.5	0.62	0.754
pure error	50	38.4	0.8		
total	59	13070.7			

The accuracy of the method was determined by recovery studies of the known contentrations. Analysis was carried out by the proposed method. The percentage recovery data were found to be accurate and in the acceptance limit of ±2%. The results indicated a low variability and a strong agreement between the theoretical known amount and calculated assay amount. The percentage recovery data, difference between mean and accepted true values and confidence intervals were presented in Table 5.

Table 5. Accuracy results (n=6)

concentration levels (µg/mL)	10	30	50
recovery %	100.8911	99.8584	100.4588
difference (µg/mL)	0.0891	0.0425	0.2294
confidence intervals (95%)	0.1354	0.2918	0.5817

The precision study was performed on three concentration levels (low, medium, and high) to evaluate the repeatability and intermediate precision of the analytical method. Analyses were carried out on three consecutive days to show the intra-day and inter-day variations. The precision of the method was verified and found to be within the targeted intervals since the RSD is below 2%. The precision data were presented in Table 6. The inter-day results of the three days were pooled and analyzed by GraphPad Prism 7 software.

Table 6. Intra-day and inter-day (pool-days) precision results (n=6)

concentration levels (µg/mL)		intra-day			inter-day
		day 1	day 2	day 3	
10 (low)	Mean	10.5235	10.0891	10.0709	10.2278
	SD	0.1965	0.1290	0.1906	0.2707
	RSD	1.8675	1.2786	1.8921	0.0277
	CI (95%)	0.2062	0.1354	0.2000	0.1346
25 (medium)	Mean	25.5769	25.6812	25.8976	25.7186
	SD	0.3612	0.4332	0.4008	0.3996
	RSD	1.4120	1.6867	1.5478	1.5538
	CI (95%)	0.3790	0.4546	0.4206	0.1987
50 (high)	Mean	49.7572	50.4572	50.2294	50.1479
	SD	0.7992	0.7875	0.5543	0.7420
	RSD	1.6063	1.5607	1.1036	1.4797
	CI (95%)	0.8387	0.8264	0.5817	0.3690

The specificity of the developed method was conducted with OLO loaded and placebo formulations. It was determined that overlapping effect of other formulation components did not affect the OLO peak (Figure 3). It was therefore concluded that the developed method was specific and the OLO peak was distinctly separated from other components in the formulations.
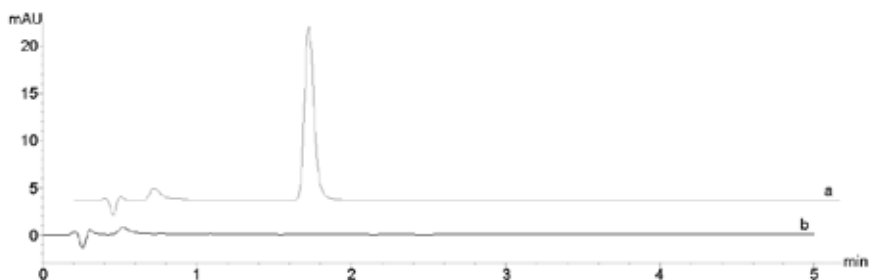
Figure 3. Chromotogram of OLO (a) and placebo formulations (b)

The parameters LOD and LOQ were calculated using the standard deviation of y-axis interception values of the calibration curve and the slope of the calibration curve. The lowest OLO concentration detected and quantified were 0.7652 and 2.3188 µg/mL respectively. Calculated LOD and LOQ concentrations could be considered as relatively high. The possible reasons of this situation were the use of PDA detector or high content of organic solvent and partial UV-cutoff effect. Nevertheless, these results proved that the chromatographic

method was suitable enough to detect and quantify OLO at a concentration range of 5 to 50.0 µg/mL.

The robustness of the developed method was investigated with slight changes in the column temperature, pH of the mobile phase and flow rate. However, these changes had an influence on the assay and stability, the method was considered robust as the RSD values were below 2% for the OLO content.

Determination of OLO in Polymeric Nanoparticles

The OLO content and encapsulation efficiency of the polymeric nanoparticles was carried out by the validated UPLC method. The results of characterizations and 6 months stability of the formulations (25°C and 60% RH) were presented in Table 7. The entrapment efficiency was evaluated according to Equation 4. Superficial and free OLO content was found higher than the encapsulated for both NP1 and NP2 formulations. Drug and polymer concentration ratios was found to be a significant factor for the entrapment efficiency [18]. Although the amount of OLO in the NP2 formulation was greater than NP1, NP2 was less loaded. As a result of the stability studies over 6 months, no statistically significant change was observed ($p > 0.05$) in OLO_T, OLOS and the entrapment efficiency.

Table 7. The entrapment efficiency of the polymeric nanoparticles

time	code	OLO_T (µg ± SE)	OLO_S (µg ± SE)	EE (%)
initial	NP1	140.007 ± 0.738	102.138 ± 0.874	27.048
	NP2	203.680 ± 0.532	184.990 ± 0.587	9.176
3 months	NP1	141.422 ± 0.560	103.436 ± 0.755	26.983
	NP2	208.602 ± 0.797	188.783 ± 0.847	9.530
6 months	NP1	144.755 ± 1.172	106.270 ± 0.847	26.706
	NP2	213.602 ± 1.161	192.783 ± 0.524	9.776

CONCLUSION

Analytical method validation was performed to confirm that the analytical procedure developed was adequate for its intended use, and that the results derived could be utilized to determine the reliability and consistency of the analytical data obtained. The method was completely validated for linearity, accuracy, precision, specificity, LOD, LOQ and robustness according to the ICH harmonised tripartite guideline "validation of analytical procedures Q2(R1)" and showed satisfactory data for all tested parameters. As a result, this method particularly exhibited an excellent sensitivity and speed performance for the

determination of OLO.

This newly developed UPLC method was also successfully applied for the determination of OLO in polymeric nanoparticle formulations, encapsulation efficiency and the stability studies. The results were found within higher confidence. In conclusion, this stability indicating method can be used and adaptable for the determination of OLO in similar pharmaceutical dosage forms.

ACKNOWLEDGEMENTS

CONFLICTS OF INTEREST

The authors report no conflict of interest. The authors alone are responsible for the content and writing of the paper.

REFERENCES

1. González-Chomón, C.; Silva, M.; Concheiro, A.; Alvarez-Lorenzo, C. Biomimetic contact lenses eluting olopatadine for allergic conjunctivitis. *Acta Biomaterialia.* **2016**, *41*, 302-311.

2. Patel, A.; Cholkar, K.; Agrahari, V.; Mitra, A. K. Ocular drug delivery systems: An overview. *World J Pharmacol.* **2013**, 2(*2*), 47-64.

3. Abelson, M. B.; Smith, L.; Chapin, M. Ocular allergic disease: mechanisms, disease subtypes, treatment. *Ocul Surf.* **2003**, 1(*3*), 127-149.

4. Nováková, L., Matysová, L., & Solich, P. (2006). Advantages of application of UPLC in pharmaceutical analysis. *Talanta*, **2006**, 68(*3*), 908-918.

5. Dewani, A. P.; Dabhade, S. M.; Bakal, R. L.; Gadewar, C. K.; Chandewar, A. V.; Patra, S. Development and validation of a novel RP-HPLC method for simultaneous determination of paracetamol, phenylephrine hydrochloride, caffeine, cetirizine and nimesulide in tablet formulation. *Arabian Journal of Chemistry*, **2015**, 8(*4*), 591-598.

6. Addo, R. T.; Davis, K.; Ubale, R.; Owen, J. S.; Watkins, E. B. Development and validation of a UPLC method for rapid and simultaneous analysis of proton pump inhibitors. *AAPS PharmSciTech*, **2015**, 16(*1*), 30-34.

7. Johnson, K. A; Plumb, R. Investigating the human metabolism of acetaminophen using UPLC and exact mass oa-TOF MS. *J Pharm Biomed Anal.* **2005**, 39(*3–4*), 805–810.

8. Kadav, A.A; Vora, D.N. Stability indicating UPLC method for simultaneous determination of atorvastatin, fenofibrate and their degradation products in tablets. *J Pharm Biomed Anal.* **2008**, 48(*1*), 120–126.

9. Reddy, Y.R; Kumar, K.K; Reddy. M.; Mukkanti, K. RP-UPLC method development and validation for the simultaneous estimation of ibuprofen and famotidine in pharmaceutical dosage form. *Pharm Methods.* **2012**, 3(*2*), 57–61.

10. Matsubara, M.; Masaki, S.; Ohmori, K.; Karasawa, A. Hasegawa, K. Differential regulation of IL-4 expression and degranulation by anti-allergic olopatadine in rat basophilic leukemia

(RBL-2H3) cells. *Biochemical Pharmacology*. **2004**, *67*, 1315-1326.

11. Tamura, T.; Komai, M. Effect of olopatadine hydrochloride, an anti-histamine drug, on rhinitis induced by intranasal instillation of toluene-2,4-diisocyanate in rats. *International Immunopharmacology*. **2008**, *8*, 916-921.

12. Shukla, M. H.; Patel, A. P.; Patel, M. G.; Patel, D. P.; Shah, R. R. Development and validation of first order derivative spectroscopic method for estimation of olopatadine hydrochloride and ambroxol hydrochloride in their synthetic mixture. *Pharma Science Monitor*, **2015**, 6(*1*).

13. Başaran, E. Ocular application of dirithromycin incorporated polymeric nanoparticles: An in vitro evaluation. *Turk J Pharm Sci*. **2017**, 14(*2*), 191-200.

14. ICH Harmonized Tripartite. Validation of analytical procedures: Text and methodology. *Guideline*. **2005**, *Q2(R1)*.

15. Berkman, M. S.; Yazan, Y. A validated HPLC method for the determination of octocrylene in solid lipid nanoparticle systems. *Pharmazie*. **2011**, *66*, 105-110.

16. Vardhan, H.; Mittal, P.; Adena, S. K. R.; Mishra, B. Long-circulating polyhydroxybutyrate-co-hydroxyvalerate nanoparticles for tumor targeted docetaxel delivery: Formulation, optimization and in vitro characterization. *Eur J Pharm Sci*. **2017**, *99*, 85-94.

17. Amc Technical Brief: Is my calibration linear? Analytical Methods Committee. **2005**.

18. Wang, H.; George, G.; Bartlett, S.; Gao, C.; Islam, N. Nicotine hydrogen tartrate loaded chitosan nanoparticles: Formulation, characterization and in vitro delivery from dry powder inhaler formulation. *Eur J Pharm Biopharm*. **2017**, *113*, 118-131.

Biosynthesis, Characterization and Cytotoxicity of Zinc Nanoparticles Using *Panax ginseng* Roots, Araliaceae

Mustafa Nadhim Owaid[1*], Tahseen Ali Zaidan[2], Rasim Farraj Muslim[2], Mohammed Abdulrahman Hammood[2]

1 Ministry of Education, Department of Heet Education, Hit, Iraq.
2 University Of Anbar, Department of Ecology, College of Applied Sciences-Hit, Hit, Anbar, Iraq.

ABSTRACT

This study aims to biosynthesize zinc nanoparticles from the aqueous extract of *Panax ginseng* (Red Ginseng) roots. The characteristics of ZnNPs were checked using change in color, UV-Vis, SEM, SPM, AFM, FT-IR, and EDS analyses, and assessed their cytotoxicity against L20B tumor cell line using MTT assay. The change in the solution color after 3 hr on 70 °C is from yellow to the brownish color with whitish sediments. The adsorption peak of UV-vis is 340 nm as evidence of formation the Zn nanoparticles. AFM, SEM and EDS observe shapes of zinc nanoparticles which are spherical to irregular particles with rate of size 59.76 nm. The concentration 100% Zinc nanoparticles significantly ($p<0.01$) recorded best inhibition percentage 41.70% against murine fibroblast cells (L20B) which have receptors of human polioviruses. Thus, this work is considered as an auspicious first test to reduce the growth of cancers using green ZnNPs of Ginseng (*Panax ginseng*) *in vitro*.

Keywords: Anticancer activity, EDS, Red Ginseng, SPM, ZnNPs.

INTRODUCTION

Ginseng is one of Korean herbs which was used in ancient world [1]. The scientific name of Ginseng is *Panax ginseng* and it is a perennial plant belongs to the Araliaceae family [2]. The Greek word of Panax is meaning drug for all diseases, and its origin from two words the first *pan* and the second *axos* meaning "all" and "medicine" respectively [3]. Korean Red Ginseng has been using as a health food and food additives [4] because of its potential role in the immune improvement [5], anti-fatigue, anti-stress, anti-aging effects [6], antifungal [7], anti-diabetic [8], anticancer activity [9], and improvement of blood circulation, and serum cholesterol [10].

The chemical composition of *Panax ginseng* mainly consists from saponin (ginsenoside) [4], water-soluble sugar, acidic polysaccharides, and phenolic compounds [11], thus *P. ginseng* had numerous pharmacological and physiological roles and opens the door toward using its extracts as a green agent to synthesize metallic nanoparticles. Few studies have enabled to Ginseng-mediated synthesize silver nanoparticles and gold nanoparticles [12–14].

Many studies were investigated the role of silver nanoparticles of Ginseng toward inhibiting human cancers which decreased the levels of mRNA and phosphorylation of receptors of epidermal growth factor in cancer cells [12] while [14] referred to antioxidant effects by gold nanoparticles biosynthesized from Ginseng. Silver and gold nanoparticles from leaves of this plant showed antimicrobial and potent anticoagulant agents [13]. In the last years, AuNPs were used as cosmetic products because of their role against inflammation, and to disinfect skin wounds [14].

The use of bacteria, fungi, parts of plant and their enzymes and extracts for synthesis of zinc nanoparticles have much benefits for pharmaceutical and biomedical applications [15]. Also, ZnNPs are used as preservative for different products like foods, pigments, plastics, ceramics, glass, etc. [16]. Most of the studies of Red Ginseng roots have referred to testing the bioactivity of its nanoparticles such as AgNPs and AuNPs. However, this recent study firstly indicates that Red Ginseng reduced zinc sulfate heptahydrate ($ZnSO_4.7H_2O$) and produce ZnNPs which inhibited mouse fibroblast cells (L20B cell line) *in vitro*. As you know that murine fibroblast cells have receptors of human polioviruses thus this study is important in the medical field.

METHODOLOGY

Red ginseng

Dried Red Ginseng roots, *Panax ginseng* (Figure 1), were purchased from the local market in Ramadi, Iraq which was obtained in October 2017. The pieces of roots of Red Ginseng were grinded using the Stand Blender (SAMiX, model LB6105D, China) to get its powder which will use in the extraction.

Extraction of *Panax ginseng* powder

About 20 g of the powder of *P. ginseng* was extracted in 200 mL Distilled Water (DW) in a 500mL-flask using magnetic stirrer hot plate for 20 minutes at 100 °C then cooled to 25 °C. The aqueous extract was filtered using filter paper Whatman No. 1 and then centrifuged for 10 minutes at 4000 cycle/min. The obtained aqueous extract was kept in the icebox as a stock solution until its use. The residue was emitted. FT-IR (Fourier Transform Infrared Spectroscopy) spectrum of this aqueous extract was performed for characterizing and com-

pared with FT-IR spectrum of the biosynthesized ZnNPs from it later.

Biosynthesis of zinc nanoparticles

About 0.86 g of zinc sulfate heptahydrate ($ZnSO_4.7H_2O$) was dissolved in 1 L of DW on the magnetic stirrer until the completion of dissolving was observed. The final concentration of $ZnSO_4.7H_2O$ solution is 3×10^{-3} M. Only, 100 mL of zinc sulfate solution 3×10^{-3} M was mixed with 30 mL of the crude aqueous Ginseng extract and heated on the magnetic stirrer hotplate at 70 °C for 3 hr to synthesize zinc nanoparticles. The same test was achieved at 25 °C for 24 hr. The change in the mixture color was individually recorded at 25 °C and 70 °C.

Characterization of ZnNPs

Ginseng-mediated biosynthesis of zinc nanoparticles (ZnNPs) was characterized using changing of the color of the mixture solution, UV-Visible spectrum (by EMC-LAB V-1100 digital spectroscopy, Germany), FT-IR spectroscopy, AFM, SPM, SEM, and EDS analyses.

In vitro Cytotoxicity

The cytotoxicity of ZnNPs toward L20B tumor cell line was investigated by MTT assay as mentioned by [17,18]. Firstly, 100 µl/well of 10^6 cell/mL L20B cells was cultured in 96-well tissue culture plate. Three concentrations of 50%, 75%, and 100% of colloid ZnNPs and extract of Ginseng roots were seperately applied in this test. About one hundred microliters of each concentration was added within each well then incubated at 37 °C for 48 hr. After that, 10 µl of 5 mg/mL MTT solution (3-(4,5-dimethylthiazol-2-yl)-2.5-diphenyltetrazolium bromide) was added to each well and re-incubated at 37 °C for 4 hr. Finally, 50 µl dimethyl sulfoxide (DMSO) was added to each well and incubated for 10 minutes. L20B cells were cultured in complete medium without ZnNPs or the extract of Ginseng solution as a control. ELISA reader was used to measure the absorbance of each well at 620 nm. The growth inhibition percentage was calculated using the equation below to give the cytotoxicity:

$$\text{Growth inhibition percentage} = \frac{(\text{Optical Density of control well} - \text{Optical Density of treatment wells})}{\text{Optical Density of control well}} \times 100$$

Statistical analysis

The data, in triplicates, has been subjected by its mean to one way analysis of variance (ANOVA) using SAS program, version 9. The significance of differences has been determined by using Duncan's Multiple Range Test and the probability least than 0.01 was considered to be statistically significant.

RESULTS AND DISCUSSION

UV-Visible spectrum of the biosynthesized ZnNPs from *P. ginseng* and their color were checked in this test to confirm the formation of nanoparticles. The color change of the mixture solution from yellow to the pale yellow close of the brownish color with whitish sediments was apparently recorded in tube B at peak 340 nm (Figure 1). The color arises due to excitement of surface Plasmon vibration in ZnNPs. These results agree with [19] who produced polydispersed brownish ZnNPs with absorbance peak at 310 nm using Actinomycestes. This case was achieved by the heating at 70 °C for 3 hr with absorption of 3.150 cm^{-1}. The absorption of tube A (performed at the room temperature) is 2.620 cm^{-1} that less than B tube. The heating to 70 °C is more suitable than 25 °C for forming ZnNPs from Red Ginseng roots extract due to increase of activation energy to reduce this organic molecules [20].
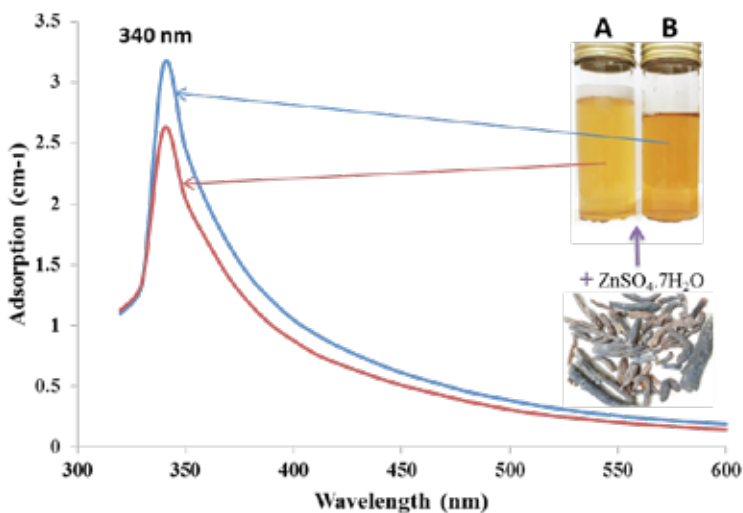
Figure 1. UV-Visible spectrum of the biosynthesized ZnNPs from *P ginseng* extract using at 25 °C (A) and 70 °C (B).

SEM image (Figure 2) observes shapes of zinc nanoparticles which are spherical to irregular particles with a clear accumulation. Figure 3 shows histogram of the particle size distribution of the biosynthesized zinc nanoparticles which reach to average 59.76 nm. Volumes of zinc nanoparticles of 45.00 nm, 60.00 nm, and 70.00 nm are ≤10%, ≤50%, and ≤90% respectively. The lower particles diameter is 45 nm while the higher diameter is 85 nm with volumes 8.16% and 1.53% respectively. The higher amount is 17.86% for the ZnNPs with the

diameter of 65 nm. Granularity Cumulation distribution of ZnNPs also has different accumulation according to their sizes as shown in Figure 3. The zinc nanoparticles of 45 nm have the lowest accumulation of 8.16%, followed 18.88% and 36.73% for ZnNPs with diameters 50.00 and 55.00 nm respectively. The higher accumulation percentage is 100% for ZnNPs of 85.00 nm followed 98.47% and 92.35% for the sizes 80.00 nm and 75.00 nm respectively.

Figure 2. Scanning Electron Microscopy (SEM) of the biosynthesized zinc nanoparticles.
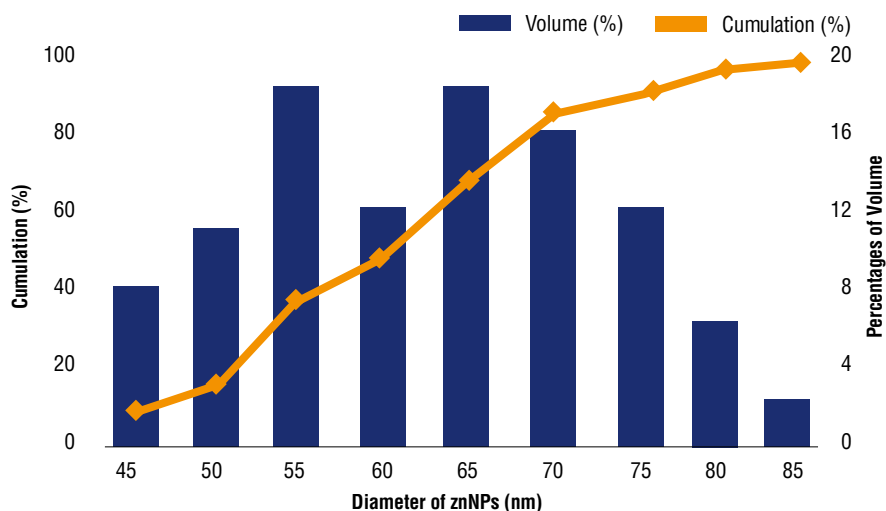
Figure 3. Histogram of particle size distribution of the biosynthesized zinc nanoparticles.

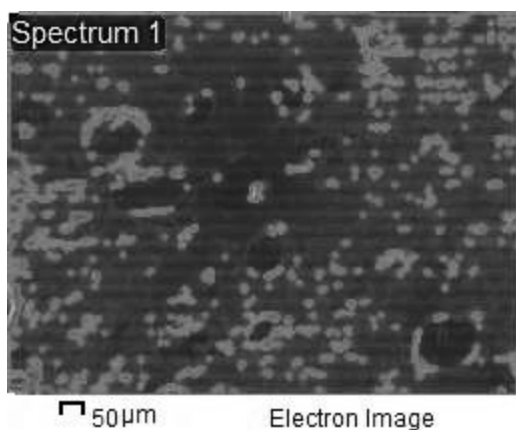AFM shows the lateral and three-dimensional images to screen surface roughness of the Ginseng-mediated zinc nanoparticles (ZnNPs) at size image 2042.09 nm×2052.20 nm as shown in Figure 4. Surface roughness analysis exhibits some functional parameters such as roughness average of 4.26 nm, reduced summit height of 0.65 nm, core roughness depth of 15.4 nm, and reduced valley depth of 4.81 nm. Hybrid parameters are measured like surface area ratio which reaches 7.75 and mean summit curvature reaches 0.43 nm^{-1}. This is an indicator for the formation Zn nanoparticles in small sizes less than 60 nm.

Figure 5 presented the Energy Dispersive X-ray (EDS) measurement which reconfirmed that the biosynthsized nanoparticles are actuality metal ZnNPs. The existence of carbon, phosphor, sulfur and oxygen peaks observed the presence of covering organic fractions of Ginseng on the Zn nanoparticles. Weight of Zinc 3.84% compared with 0.34% and 0.73% for S and P respectively. The presence of the elemental Zn can be seen in the EDS graph that indicates the reduction of Zn ions to elemental zinc. The appearance of other elements, like K after adsorption is from the organic moieties in the watery crude extract as mentioned by [21] who confirmed that potassium is adsorbed on the surface of ZnNPs.

A   **B**

Figure 4. AFM of the biosynthesized ZnNPs lateral (A), three-dimensional (B).
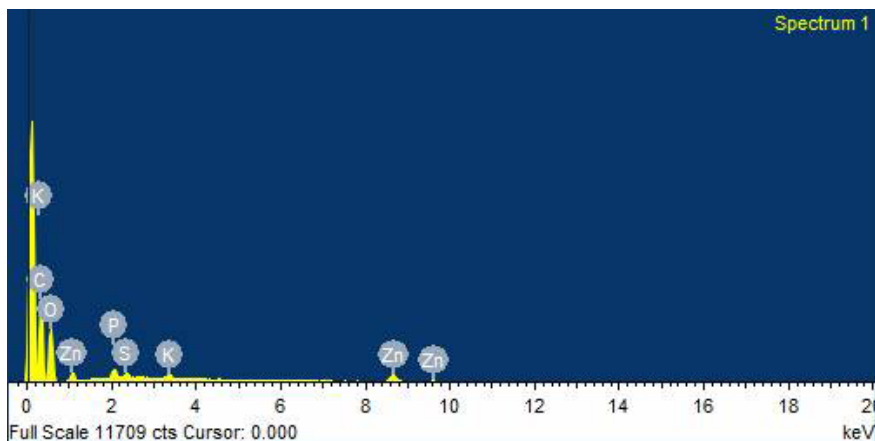
Figure 5. Energy Dispersive X-ray (EDS) spectrum of ZnNPs of *Panax ginseng.*

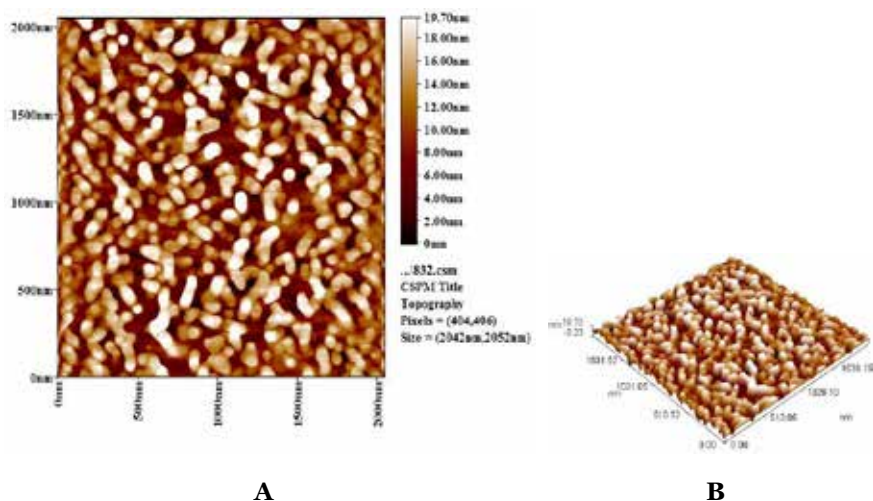The FT-IR spectroscopy was used to determine the chemical composition and active groups found in the studied samples (Ginseng extract and the biosynthesized ZnNPs from this extract) (Figure 6). The FT-IR spectrum of the Ginseng extract presented in Figure 6A showed finding two peaks the first 765 cm^{-1} due to the covalent bond between carbon and silicon (Si-C) and another peak 1107 cm^{-1}, which is evidence of the oxygen bond with silicon in (Si-O). As well as absorption peaks at 1359 cm^{-1} and 1419 cm^{-1} belong to the homogeneous and heterogeneous bending vibration of the methylene group (-CH$_2$) or the methyl (-CH$_3$) and the absorption bands at 2889 cm^{-1} and 2923 cm^{-1} belongs to the homogeneous and heterogeneous extension vibration of the methylene group (-CH$_2$) or the methyl (-CH$_3$). The mentioned four peaks belong to the methylene group (-CH$_2$) and the methyl group (-CH$_3$) in the synthesis of amino acids, peptides or proteins and the sign of that is finding the absorption band returns to the single bond (C-C).

The spectrum also showed an absorption peak at 1620 cm^{-1} due to the extension vibration of the group (C=C) in the alkene compounds and to the successive double bonds in the benzene ring in the aromatic structures. The presence of compensated aromatic rings is found in the composition of amino acids, peptides, and proteins [22]. The peak of 2290 cm^{-1} is a clear indication of the existence of stylenyl derivatives contains trinal bonds (C≡C). From the other hand, the existence of other peaks mentioned supporting the presence of double bond (C=C) on carbon atoms at 1419 cm^{-1} and 3178 cm^{-1} related to the extension vibration of groups C-O and =C-H respectively, which is due to alk-

ene compounds. Also, when reviewing the previous studies which studied the chemical composition of some Ginseng-derived compounds, it is certain that the extract in this study contains polyacetylenes may be in their three structures [1], (see Figure 7).

It is confirmed that the Ginseng extract contains polyacetylene compounds, amino acids, peptides, proteins, polyphenols, and polysaccharides. There is an extension vibration of the absorption bands at 3451cm⁻¹, and two bending vibration bands at 1261cm⁻¹ and 1359cm⁻¹ belong to the hydroxyl group (-OH) and the peak of 1419 cm⁻¹ due to an extension vibration for the group C-O.
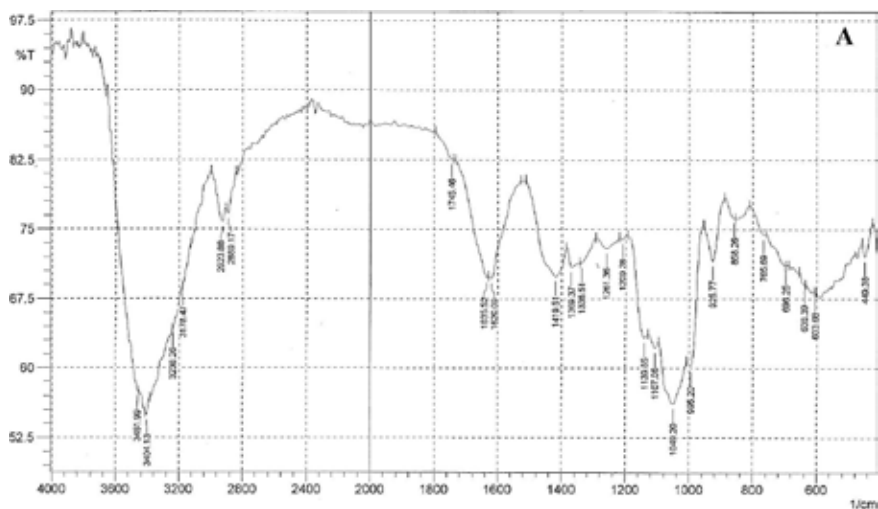
The absorption peak at 2705 cm⁻¹ indicates the presence of hydrogen bound to the carbonyl group in the aldehyde group (O=C-H). That is an evidence of the presence of non-cyclic monosugars. The two bands 603 cm⁻¹ and 638 cm⁻¹ showed the presence of the amide group (O=C-N-H) which binds successive two amino acids in the composition of proteins or peptides. Furthermore, the presence of the absorption peak at 3404 cm⁻¹ also belongs to the amine group (-NH) in the synthesis of the amino acid (Arginine), or belongs to the amide group in the peptide or protein synthesis [22,23]. The presence of the carboxylic group (-COOH) in amino acids is evidenced by the appearance of the broad absorption range from 2410 cm⁻¹ to 3620 cm⁻¹. Moreover, a bending vibration band at 925 cm⁻¹ is belonging to the hydroxyl group in the carboxyl group [24–27].

There is a band located at 1745 cm⁻¹ belongs to hexagonal-cyclic ketones, thus it belongs to the group of Carbonyl (C=O). This is evidence that the extract contains flavonoids, which belong to the category of phenols and its function to protect the plant from the harmful effects of ultraviolet radiation. The presence of flavonoids in the Ginseng extract was studied by others as shown in Figure 8. That also confirms that the Ginseng extract under study contains these compounds. It is believed that because of the presence of hydroxyl (-OH), carbon-oxygen (C-O), methylene (-CH$_2$) and methyl (-CH$_3$) groups, the presence of ginsenoside compounds in the Ginseng extract is similar in structure to the primary structure of cholesterol but is more complex in terms of the chemical composition [28].

The FT-IR spectrum of the biosynthesized zinc nanoparticles (Figure 6B) shows the sharp absorption peak located at 1141 cm⁻¹, the two clear peaks at 1371 cm⁻¹ and 1423 cm⁻¹ and the clear wideband at 1629 cm⁻¹. That is a clear indicator to presence of nano-zinc atoms in the composition of the biosynthesized ZnNPs from Ginseng extract, because in a study on mushrooms found that the FTIR spectrum of silver nanostructures when it binds with the hydrocarbons, it shows four bands located nearby and within the mentioned ranges

[29]. It was noted that this spectrum is very similar to the spectrum of FT-IR of the Ginseng extract (Figure 6A) in terms of the extension of the bands thus the chemical composition is similar, but the insulation, clarity, and the band width are better in the second spectrum (Figure 6B). The reason for this may be due to the presence of zinc atoms with good dispersion with a high surface area that enables the active groups in the electron-rich in the Ginseng extract to share their electron pairs with the empty orbitals in the outer shell of zinc.

It is known that zinc atoms have 30 electrons thus its fourth shell has one electronic pairs in the level (4s), thus the rest secondary levels 4p, 4d, and 4f which contain three, five, and seven orbitals respectively are empty and can assimilate coming electronic pairs from good atoms with negative charges are O, N, and S which find in monosaccharides, polysaccharides amino acids, peptides, proteins, polyphenols, flavonoids, polyacetylenes, and ginsenosides. Thus, the previous FT-IR spectrum (Figure 6B) exhibited that the structures of acidic polysaccharides, amino acids, ginsenosides, poly acetylenes, and polyphenols in the *Panax ginseng* extract are not affected because of interaction their active groups with zinc ions or zinc nanoparticles as reducing and capping agents to the synthesized ZnNPs.

Figure 6. FT-IR spectrum of extract of *P. ginseng* (A) extract and ZnNPs of *P. ginseng* (B)

Panaxynol

Panaxyldol

Panaxytriol

Figure 7. Structures of polyacetylene compounds expected in the extract of Ginseng [1]

Figure 8. Two structures of flavonoids compounds expected in the extract of Ginseng

Cytotoxicity of the biosynthesized ZnNPs and extracts of *Panax ginseng* Ginseng were applied against L20B tumor cell line using the colorimetric cell viability MTT assay. Three concentrations (50%, 75%, and 100%) of ZnNPs solution and aqueous extracts of Ginseng were individually achieved compared with the control. All concentrations of aqueous crude extracts did not exhibit any growth inhibition percentage as shown in Figure 9. Zinc nanoparticles of Ginseng showed growth inhibition percentages approx. 35.03%. The concentration of 100% significantly ($p<0.01$) recorded inhibition percentage of 41.70%, followed 33.30% and 30.10% by the concentration 75% and 50% respectively. The reason of that belongs to induce cytotoxicity and ROS generation in L20B tumor cell line [30] which cause apoptosis leading to cell death and preventing their replication. [31]. Extract of *P. ginseng* composes from some pharmacological compounds like polysaccharides, flavonoids, triterpenoids, and ginsenosides which caped ZnNPs, have been included anticancer activity [1,10,11]. The ability of the biosynthesized ZnNPs to inhibit L20B tumor cell line is considered as a potential indicator for biological activity of these green nanoparticles against the cancers *in vitro*. Saponin of Red Ginseng roots (Ginsenoside) is active compound against cancers [32] because of its role as antioxidant agent covering the ZnNPs. The zinc in many medical and nutritional products play a promising role in host defense to prevent the initiation, promotion and development of carcinoma.[33] A zinc nanoparicle model is useful as an approach to increase activity of zinc in treatment of cancers due to the high surface area of ZnNPs. Many studies were investigating the inhibitory role of AgNPs toward human cancers but not ZnNPs. These results agree with results of [12] who refereed to that silver nanoparticles of Ginseng decreased the levels of mRNA and phosphorylation of receptors of epidermal growth factor in cancer cells. While [14] prepared gold nanoparticles from this plant and have antioxidant effects.
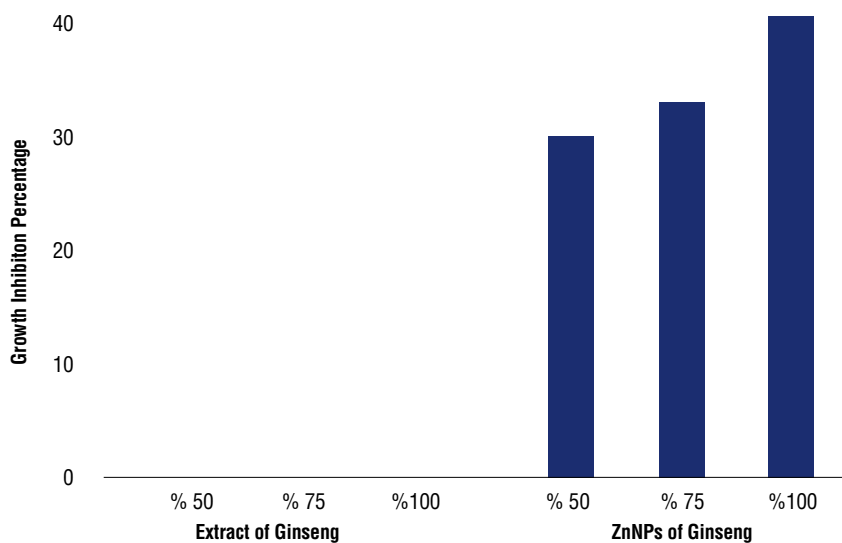
Figure 9. Cytotoxicity of extract of ginseng *(P. ginseng)* and its biosynthesized ZnNPs

CONCLUSION

This study aims to biosynthesize zinc nanoparticles from the aqueous extract of *Panax ginseng* (Red Ginseng) roots and characterize their properties. SEM image observes shapes of zinc nanoparticles which are spherical to irregular particles with rate of size 59.76 nm. The FT-IR spectrum of ZnNPs exhibited that the numerous structures of acidic polysaccharides, amino acids, ginseno-sides, polyacetylenes, and polyphenols in the Ginseng extract are not affected because of interaction their active groups to reduce and cap zinc ions to Zn^o and synthesizing zinc nanoparticles (ZnNPs). EDS reconfirmed that the nanoparticles formed are indeed metal ZnNPs. The concentration 100% Zinc nanoparticles significantly ($p<0.01$) recorded best inhibition percentage 41.70% against murine fibroblast cells (L20B) which have receptors of human polio-viruses, thus, this work is considered as an auspicious first test to reduce the growth of cancers using green ZnNPs of Ginseng (*Panax ginseng*) *in vitro*. A zinc nanoparticle model is useful as an approach to increase activity of zinc in treatment of cancers due to the high surface area of ZnNPs.

ACKNOWLEDGMENTS

REFERENCES

1. SM Lee, B Bae, H Park, N Ahn, B Cho, Y Cho and Y Kwak. Characterization of Korean Red Ginseng (Panax ginseng Meyer): History , preparation method , and chemical composition. *J Ginseng Res*. **2015**, *39*, 384–391. doi:10.1016/j.jgr.2015.04.009.

2. Y Kim, J Jeon, M-G Jang, J Oh, W-S Kwon, S-K Jung, D-C Yang. Ginsenoside profiles and related gene expression during foliation in Panax ginseng Meyer. *J Ginseng Res*. **2014**, *38*, 66–72.

3. H Jeong, H Hong, Y Kim, J Rho, K Kim and C Cho. The research trend of ginseng processing technology and the status of ginseng industry. *Food Sci Ind*. **2012**, *45*, 59–67.

4. W Yang, Y Hu, W Wu, M Ye and D Guo. Phytochemistry Saponins in the genus Panax L . (Araliaceae): A systematic review of their chemical diversity. *Phytochemistry*. **2014**, *106*, 7–24.

5. S Kang and H Min. Ginseng, the 'immunity boost': the effects of Panax ginseng on immune system. *J Ginseng Res*. **2012**, *36*, 354–368.

6. A Attele, J Wu and C Yuan. Ginseng pharmacology: multiple constituents and multiple actions. *Biochem Pharmacol*. **1999**, *58*, 1685–1693.

7. S Lam and T Ng. Isolation of a small chitinase-like antifungal protein from Panax notoginseng (sanchi ginseng) roots. *Int J Biochem Cell Biol*. **2001**, *33*, 287–292.

8. J Xie, S McHendale and S Yuan. Ginseng and diabetes. *Am J Chin Med*. **2005**, *33*, 397–404.

9. G Yang, D Park, J Lee, B Song, T Jeon, S Kang, J Jeon, S Shin, H Jeong, H Lee and Y Kim. Suppressive effects of red ginseng preparation on SW480 colon cancer xenografts in mice. *Food Sci Biotechnol*. **2011**, *20*, 1649–1653.

10. CH Lee and J Kim. Review article A review on the medicinal potentials of ginseng and ginsenosides on cardiovascular diseases. *J Ginseng Res*. **2014**, *38*, 161–166. doi:10.1016/j.jgr.2014.03.001.

11. C Cho, Y Kim, YK Rhee, Y Lee and K Kim. Chemical composition characteristics of Korean straight ginseng products. *J Ethn Foods*. **2014**, *1*, 24–28. doi:10.1016/j.jef.2014.11.007.

12. V Castro-Aceituno, S Ahn, SY Simu, P Singh, R Mathiyalagan, HA Lee and DC Yang. Anticancer activity of silver nanoparticles from Panax ginseng fresh leaves in human cancer cells. *Biomed Pharmacother*. **2016**, *84*, 158–165. doi:10.1016/j.biopha.2016.09.016.

13. P Singh, Y Kim and D Yang. A strategic approach for rapid synthesis of gold and silver nanoparticles by Panax ginseng leaves. *Artif Cell Nanomed B*. **2016**, *44*, 1949–1957.

14. ZE Jiménez-pérez, P Singh, Y Kim, R Mathiyalagan, D Kim, MH Lee and DC Yang. Applications of Panax ginseng leaves-mediated gold nanoparticles in cosmetics relation to antioxidant , moisture retention , and whitening effect on B16BL6 cells. *J Ginseng Res*. 42 (*3*) **2017**, 1–7. doi:10.1016/j.jgr.2017.04.003.

15. MA Willard, LK Kurihara, EE Carpenter, S Calvin and VG Harris. Chemically prepared magnetic nanoparticles. *Int Mater Rev*. **2004**, *49*, 125–170.

16. A Hernandezbattez, R Gonzalez, J Viesca, J Fernandez, J Diazfernandez, A MacHado, R Chou and J Riba. CuO, ZrO2 and ZnO nanoparticles as antiwear additive in oil lubricants. *Wear*. **2008**, *265*, 422–428.

17. PL Chih, JT Wei, LL Yuang and CK Yuh. The extracts from Nelumbonucifera suppress cell cycle progression, cytokine genes expression, and cell proliferation in human peripheral blood mononuclear cells. *Life Sci.* **2004**, *75*, 699–716.

18. RI Freshney. Culture of Animal Cell. 6th ed., Wily-Liss, New York, **2012**.

19. U Rajamanickam, S Viswanathan and P Muthusamy. Biosynthesis of Zinc Nanoparticles Using Actinomycetes for Antibacterial Food Packaging. in: Int Conf Nutr Food Sci IPCBEE, IACSIT Press, Singapore, **2012**, pp. 195–199.

20. C Burda, X Chen, R Narayanan and MA El-Sayed. Chemistry and properties of nanocrystals of different shapes. *Chem Rev.* **2005**, *105*, 1025–1102.

21. L Jia, Q Zhang, Q Li and H Song. The biosynthesis of palladium nanoparticles by antioxidants in Gardenia jasminoides Ellis : long lifetime nanocatalysts for p -nitrotoluene hydrogenation. *Nanotechnology.* **2009**, *20*, 0–9. doi:10.1088/0957-4484/20/38/385601.

22. BD Mistry. A Handbook of Spectroscopic Data CHEMISTRY (UV, JR, PMR, JJCNMR and Mass Spectroscopy). 2009th ed., Oxford Book Company, **2009**.

23. R Silverstein, F Webster and D Kiemle. Spectrometric identification of organic compounds. 7th ed., John Wiley and sons, Inc., London, UK, **2005**.

24. LD Field, S Sternhell and JR Kalman. Organic Structures from Spectra. 4th ed., John Wiley and Sons Ltd, **2008**.

25. K Nakamoto. Infrared and Raman Spectra of Inorganic and Coordination Compounds Part A: Theory and Applications in Inorganic Chemistry. 6th ed., A John Wiley and Sons, Inc., **2009**.

25. J Simek. Organic Chemistry. 8th ed., Pearson education, Inc., **2013**.

27. OH Abid, HM Tawfeeq and RF Muslim. Synthesis and Characterization of Novel 1,3-oxazepin-5(1H)-one Derivatives via Reaction of Imine Compounds with Isobenzofuran-1(3H)-one. *Acta Pharm Sci.* **2017**, *55*, 43–55.

28. D-H Kim. Chemical Diversity of Panax ginseng , Panax quinquifolium , and Panax notoginseng. *J Ginseng Res.* **2012**, *36*, 1–15.

29. S Sujatha, S Tamilselvi, K Subha and A Panneerselvam. Studies on biosynthesis of silver nanoparticles using mushroom and its antibacterial activities. *Int J Curr Microbiol App Sci.* **2013**, *2*, 605–614.

30. DR Nogueira, CMB Rolim and AA Farooqi. Nanoparticle induced oxidative stress in cancer cells: adding new pieces to an incomplete jigsaw puzzle. *Asian Pac J Cancer Prev.* **2014**, *15*, 4739–4743.

31. KS Siddiqi, A Husen and RAK Rao. A review on biosynthesis of silver nanoparticles and their biocidal properties. *J Nanobiotechnology.* **2018**, 16(*14*), 174-201. doi:10.1186/s12951-018-0334-5.

32. C-Z Wang, HH Aung, M Ni, J-A Wu, R Tong, S Wicks, T-C He and C-S Yuan. Red American Ginseng: Ginsenoside Constituents and Antiproliferative Activities of Heat-Processed Panax quinquefolius Roots. *Planta Med.* **2009**, *73*, 669–674. doi:10.1055/s-2007-981524. Red

33. D.K. Dhawan and V.D. Chadha. Zinc: A promising agent in dietary chemoprevention of cancer. *Indian J Med Res.* **2010**, *132*, 676–682. doi:10.2147/IJN.S16581.

Enhanced Solubility and Drug Release of Ketoprofen Using Lyophilized Bovine Serum Albumin Solid Dispersion

Meenakshi Bhatia[1*], Rupa Devi[1]

1 Guru Jambheshwar University of Science and Technology, Pharmaceutical Sciences, Hisar, India

ABSTRACT

Solid dispersions have been proved to be an effective method for the improvement of solubility and bioavailability of poorly water-soluble drugs. The study was designed to demonstrate the potential of ketoprofen loaded BSA solid dispersions on the solubility & *in-vitro* release of ketoprofen.

Ketoprofen-BSA solid dispersions were prepared by the freeze-drying method. A 2-factor, 3-level central composite experimental design was used to study the effect of varying concentration of BSA and ketoprofen on drug solubility & *in-vitro* drug release.

The combined effect of concentration of BSA & ketoprofen on % release and solubility exhibited a linear relationship between independent and dependent variables, suggesting that higher level of BSA & ketoprofen favours the expedited release and solubility.

Bovine serum albumin may be explored as a carrier for the preparation of solid dispersion for the enhancement of solubility and *in-vitro* drug release of BCS class II drug ketoprofen.

Keywords: Bovine serum albumin, Ketoprofen, Solid dispersion, Lyophilization.

INTRODUCTION

Biopharmaceutical classification system (BCS) divided the active pharmaceutical ingredient into four classes (I, II, III, IV) based on their solubility in water and membrane permeability. In recent years class II drugs (having low solubility & high permeability) have appeared oft times as candidate compound for development in drug discovery stage[1]. Various techniques including cyclodextrins complexes[2], nanoparticle technology[3], self emulsifying drug deliv-

ery systems (SEDDS)[4], liposomes[5], salt formation[6], use of surfactant "micellization"[7], amorphisation[8] and solid dispersion etc., have been attempted to overcome the poor solubility issues. Nowadays, solid dispersion has become the synonym for the solubility enhancement of poorly water-soluble drugs. Solid dispersion of poorly soluble drugs in water soluble carriers to improve the solubility and dissolution was reported decades ago[9]. Since then, the solid dispersion is explored colossally. Solid dispersion as group of solid products made up of both hydrophilic matrix and hydrophobic drug. The matrix can be either amorphous or crystalline[10]. For the improvement of bioavailability and dissolution rate of poorly water-soluble drugs use of various hydrophilic carriers like polyethylene glycol (PEG)[11], hydroxypropylmethyl cellulose (HPMC)[12], polyvinylpyrrolidone (PVP)[13], hydroxypropyl cellulose[14], hydroxypropylmethyl cellulose phthalate[15], gums[16], sugar[17], mannitol[18], urea[19], gelucires[20], eudragits[21], chitosan[22], sodium starch glycolate[23] and pregelatinized starch etc. has been investigated vastly[24].

Bovine serum albumin (BSA) also known as "Fraction V" is a serum albumin protein derived from cows is the most abundant protein in plasma that is also extensively used in pharmaceutical industry because of its low cost, ease of purification, biocompatibility and biodegradability and also due to its chemical similarity to human albumin[25]. BSA plays the role of an "*in-vivo* solubilizing agent" that enables the solubilisation of a wide range of biomolecules and drugs in plasma (a hydrophilic medium)[26,27]. Albumin has varied physiological functions like maintaining plasma osmotic pressure and neutralising free radicals[28,29]. The solubility enhancement properties of albumin are generally due to its incredible ability to form reversible binding complexes with ligands mainly by hydrophobic and electrostatic interaction[26,30]. This makes the bound molecule to flow in the blood at a higher concentration than its initial solubility. It possesses overall negative charge at physiological pH that endorses the binding of anionic molecules (weak acids) & hydrophobic molecules[27,30]. Moreover, it also contains a no. of free amino and carboxyl groups amenable to form highly soluble salts with acidic or basic drugs, respectively. This exceptional capacity of albumin to dissolve poorly soluble drugs is explored in this piece of research.

The aim of present study is to predominantly investigate the use of BSA as a carrier for solubility enhancement of ketoprofen. Ketoprofen is a non-steroidal anti-inflammatory drug belonging to class II that is having aqueous solubility of 0.5μg/ml. Ketoprofen binds with albumin molecule as its chemical structure is adaptable to form salt bridges with albumin amino groups. In this study, solid dispersion is prepared by freeze-drying or lyophilization technique. Ketoprofen-BSA solid dispersions are characterized by Fourier transform infrared

spectroscopy (FT-IR), X-ray diffraction (XRD), differential scanning calorimetry (DSC) and scanning electron microscopy (SEM) studies. In addition, the solubility and *in-vitro* release profile of ketoprofen are also evaluated.

METHODOLOGY

Materials

Ketoprofen was obtained as a gift sample from Infinity Laboratories, Behra (India). Bovine serum albumin (BSA), ethanol, sodium chloride, potassium chloride, di-sodium hydrogen orthophosphate, potassium di-hydrogen orthophosphate was procured from Hi-Media lab. Pvt. Ltd. All other chemicals & reagents used in the study were of analytical grade and used as received.

Preparation of freeze dried solid dispersion

Ketoprofen (0.1-0.5% w/v in aqueous ethanol) was added to BSA (0.1-2% w/v) that results in the formation of colloidal solution or colloidal suspension depending on the concentration of ketoprofen. The resulting solution/suspension was kept at -80°C for 4hrs and lyophilized for 48hrs in a lab scale lyophilizer.

Experimental design

A 2-factor, 3-level central composite experimental design was used to prepare solid dispersions. Based on preliminary trials, concentration of BSA (X_1) & concentration of ketoprofen (X_2) were selected as independent variables while solubility (Y_1) & in-vitro release (Y_2) were selected as the dependent variables (Table 1). The experimental design and statistical analysis of the data was carried out as per the design protocol by using Design Expert Software (Version 11).

Determination of drug content

The different solid dispersion (SD) batches and physical mixture (PM) equivalent to 10mg of ketoprofen were dissolved separately in 25 ml of phosphate buffer (pH 7.4). The solution was filtered and further diluted appropriately. Samples were filtered through 0.45μm milipore filters and analyzed by UV-visible spectrophotometer at 260nm.

Characterisation

Fourier Transform Infrared Spectroscopy (FT-IR)

Fourier Transform Infrared Spectroscopy was used to detect interaction between drug and carrier. FTIR spectral analysis of ketoprofen, BSA, PM and SD were done by FT-IR (FT-IR Spectrophotometer Perkin-Elmer BX II) in the range of 4000−400 cm $^{-1}$ using KBr pellets.

X-ray diffraction analysis (XRD)

The X-ray diffractometry was carried out for phase identification of the materials. The XRD spectra of ketoprofen, BSA, PM and SD were carried out using an X-ray diffractometer (Miniflex 2, Rigaku, Japan) at room temperature and at 30kV. The scanning diffraction angle (2θ) ranged from 0° to 80°.

Differential scanning calorimetry (DSC)

Differential scanning calorimetric thermogram of ketoprofen, BSA, PM and SD were recorded using differential scanning calorimeter (SDT Q600 V20.9 Build 20 TA instrument, USA) in the temperature range of (25°C–300°C) at a heating rate of 10°C/min in nitrogen atmosphere.

Scanning electron microscopy (SEM)

The shape and surface morphology of SD were examined using scanning electron micro-scope (JSM-6100 scanning microscopy, Japan) The sample were coated with gold and mounted on aluminium stub containing double adhesive carbon tape. The photographs were taken at acceleration voltages of 10 kV.

Solubility

The solubility of ketoprofen drug was determined by taking pure drug, PM and solid dispersion equivalent to 10 mg ketoprofen in 10 ml of distilled water and was kept for 48hrs on shaker at room temperature (25°C). The obtained solution was filtered by 0.45μm milipore filter paper and the drug content was determined by taking absorbance using UV-Visible Spectrophotometer at 260 nm. The amount of ketoprofen was calculated using the calibration curve in water. The Gibbs free energy of transfer (ΔG) of ketoprofen from pure water to the aqueous solution of carrier was also calculated as

$$\Delta G = -2.303RT \log S_o/S_s$$

Where S_o/S_s is the ratio of solubility of ketoprofen in aqueous solution of carrier to that of the same medium without carrier.

In vitro drug release

In vitro dissolution studies were performed using the USP type II dissolution apparatus. Dissolution studies of pure drug (ketoprofen), PM and solid dispersions containing ketoprofen equivalent to 10mg were conducted in 300ml phosphate buffer (pH 7.4) at 37±0.5°C with constant stirring rate of 50 rpm. The powders were dispersed over the dissolution medium. Aliquots of sample (5ml) was withdrawn at different time intervals and replaced with an equal amount of the dissolution medium to maintain a constant volume. Samples

were filtered through 0.45μm milipore filters and analyzed by UV-visible spectrophotometer at 260nm. The mechanism of drug release from the solid dispersion was determined by fitting the release data to several models like zero-order, first- order, Higuchi and Korsmeyer–Peppas plots.

RESULTS AND DISCUSSION

The BSA-Ketoprofen solid dispersions were prepared using 2-factor, 3-level central composite experimental design using concentration of BSA (X_1) and ketoprofen (X_2) as independent variable. Solubility (Y_1) and % release (Y_2) were chosen as dependent or response variables.

Drug content of formulations

Ketoprofen assay data for content uniformity of the drug in different batches of SD and PM are given in Table 1. From the data it is clearly indicated that the drug content in the formulated batches of SD and PM was within the range of the theoretical amount, indicating the method used for formulation was suitable and reproducible in nature.

Fourier Transform Infrared Spectroscopy (FT-IR)

Figure 1 exhibits the FTIR spectra of ketoprofen, BSA, SD and PM in the frequency region from 4000 to 450 cm^{-1}. The spectra of ketoprofen showed characteristic absorption band at 2979.54 cm^{-1} due to -CH stretching. The peak appearing at 1653.74 cm^{-1} can be ascribed to -C=O stretching, while peak appearing at 1598.70 cm^{-1} is due to -C=C stretching. The absorption band at 1445.03 cm^{-1} and 866.30cm^{-1} can be attributed to -C-C deformation and -CH deformation for substituted aromatic (out of plane), respectively. The spectra of Bovine serum albumin (BSA) present the characteristic absorption band of -NH bending vibration appearing at 3407.98 cm^{-1}, peak of -C=O stretching vibrations of the peptide bond (amide I band) appeared at1651.51cm^{-1} while peak appearing at 1546.85 cm^{-1} can be ascribed to -NH bending vibration / -CN stretching vibration (amide II band). The peak at 1239.16 cm^{-1} may be due to -CN stretching vibration / -NH bending vibration (amide III band). The spectra of SD revealed the characteristic peak appearing at 2962.52 cm^{-1} that can be ascribed to -CH stretching, the peak at 1654.55 cm^{-1} may be attributed to -C=O stretching while the peak at 1541.32 cm^{-1} is attributed to -C=C stretching and peaks appearing at 827.97cm^{-1},703.55cm^{-1} and 619.18cm^{-1} are of fingerprint region. The spectra of PM revealed that the characteristic peak appearing at 2930.49 cm^{-1} can be ascribed to --CH stretching, the peak at 1656.27 cm^{-1} may be attributed to -C=O stretching, while the peak at 1534.82 cm^{-1} is attributed to -C=C stretching and peaks at 968.27cm^{-1}, 827.92cm^{-1}, 717.55cm^{-1} and

618.92cm⁻¹ are of fingerprint region. The characteristic peaks of ketoprofen also seen in the SD and PM that indicate that ketoprofen is present in the solid dispersion and physical mixture.
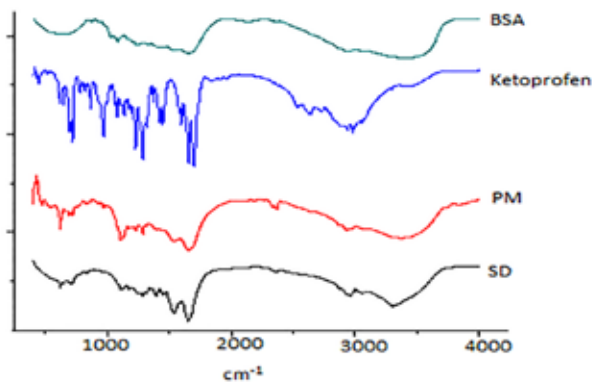
Figure 1. FT-IR spectra of ketoprofen, bovine serum albumin (BSA), physical mixture (PM) and solid dispersion (SD).

X-ray diffraction analysis (XRD)

The solid state of ketoprofen in the solid dispersion was examined using XRD (Figure 2). The XRD spectra of BSA is of typical amorphous material whereas the ketoprofen showed characteristics sharp peaks at 18.35ºC and 23.069ºC 2θ owing to its crystallinity. The X-Ray diffractogram of PM showed certain peaks corresponding to crystalline ketoprofen. However, XRD spectra of BSA-ketoprofen solid dispersion contain no sharp peaks thus unveiling amorphous characteristics of the final product.
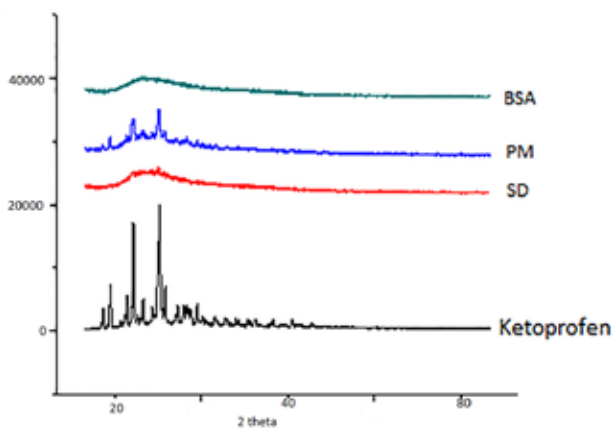
Figure 2. XRD spectra of bovine serum albumin (BSA), physical mixture (PM), solid dispersion (SD) and ketoprofen.

Differential scanning calorimetry (DSC)

Figure 3 displays the DSC thermogram of ketoprofen, solid dispersion (SD), physical mixture (PM) and bovine serum albumin (BSA). The thermogram of BSA appeared as broad peak at 94.26°C that is of typical amorphous material. The thermogram of ketoprofen showed a sharp peak at 93.08°C that corresponds to its melting point. A peak with decreased intensity at around 99.58°C is also seen in BSA-Ketoprofen physical mixture indicating the crystalline state of drug in the physical mixture. However, amorphous property of the solid dispersion can be inferred from the broad endotherm and disappearance of sharp peak in thermogram of SD.

Figure 3. DSC thermogram of ketoprofen, solid dispersion (SD), physical mixture (PM) and bovine serum albumin (BSA)

Scanning electron microscopy (SEM)

Figure 4 exhibits the scanning electron micrograph showing surface morphology of solid dispersion. The SEM micrograph of SD shows irregular structure with porous and rough surface.

Figure 4. SEM photomicrographs of solid dispersion

Solubility

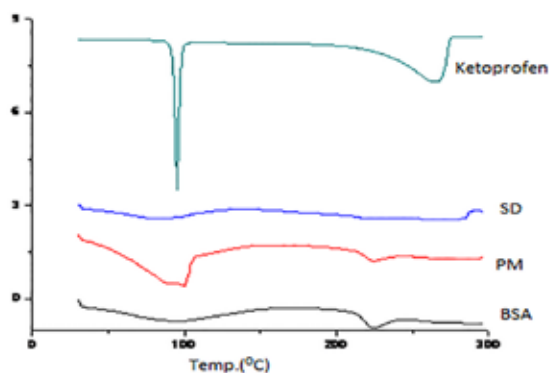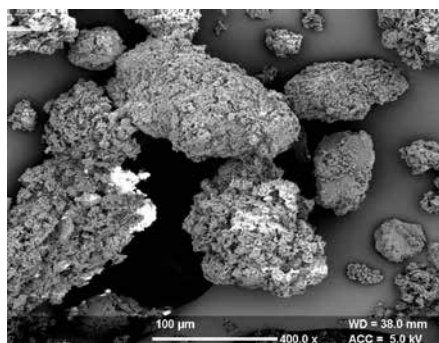The different batches of SD were prepared containing BSA (1-2%) and keto-profen (0.1-0.5%) as per the design protocol (Table 1). The pure ketoprofen dispensed a solubility of 18.79 µg/ml in water at room temperature whereas the physical mixture showed solubility of 34 µg/ml. The physical mixture presented solubility higher than the pure drug because of the BSA. However, the solid dispersion conferred solubility values ranging from 38-58 µg/ml. This increase may be due to formation of soluble complex between drug and BSA whereas the lower solubility in case of physical mixture as compared to SD may be explained on the basis of results obtained from DSC and XRD studies revealing that ketoprofen is still present in crystalline state.

Table 1. Solubility, in-vitro release, drug content and Gibb's free energy of different batches.

Batch	Conc. Of BSA (%) (X_1)	Conc. Of ketoprofen (%) (X_2)	Solubility (µg/ml) (Y_1)	% release in 60 min. (Y_2)	Drug content (%)	ΔG (KJ/Mol)
SD1	1	0.5	43±0.8	77.81±0.1	97.78±0.14	-1.8
SD2	1.5	0.3	51±0.25	89.67±0.1	98.17±0.08	-2.2
SD3	2	0.3	56±0.28	92.5±0.1	99±0.2	-2.4
SD4	1.5	0.3	51±0.25	85.44±0.21	97.89±0.61	-2.2
SD5	1.5	0.3	53±0.3	86.18±0.1	97.96±0.3	-2.3
SD6	1	0.3	40±0.1	76.33±0.23	97.39±0.2	-1.7
SD7	2	0.5	58±0.22	93.2±0.2	99.42±0.16	-2.5
SD8	1.5	0.3	5±0.6	88.37±0.17	98.05±0.1	-2.3
SD9	1.5	0.5	54±0.32	91.11±0.1	98.21±0.1	-2.3
SD10	1.5	0.1	47±0.71	80.11±0.3	97.56±0.25	-2.0
SD11	1	0.1	38±0.20	72.24±0.1	97±0.28	-1.5
SD12	2	0.1	48±0.16	85.21±0.28	97.88±0.22	-2.1
SD13	1.5	0.3	50±0.28	86.33±0.16	98.01±0.11	-2.2
PM	2	0.5	34±0.49	42±0.22	98.34±0.18	-1.3
Ketoprofen			18.79±0.29	26±0.17		

Table 1 shows the results of solubility of different batches of solid dispersions prepared as per the design protocol. The responses generated were fitted into various polynomial models using experimental design. The response solubility was fitted best into quadratic model with none transformation of the data. The adjusted polynomial equation obtained for the solubility (Y_1) shown in equation (i) with determination correlation (R^2) of 0.9740.

$$Y_1 = 51.62 + 6.83X_1 + 3.67X_2 + 1.25X_1X_2 - 3.6X_1{}^2 - 1.17X_2{}^2 \quad \text{(i)}$$

Table 2 summarizes the results of ANOVA on the response surface model. The polynomial model was found to be significant ($p < 0.05$) with non-significant lack of fit ($p > 0.05$). The good correlation between the experimental and predicted response is indicated by higher value of R^2 (> 0.9). Adequate precision that measures the signal to noise ratio was much above the required value of 4, indicating adequate signal and model fit to navigate the design space. Fig. 5 (a) display the combined effect of concentration of BSA & Ketoprofen on solubility. It can be inferred from the plots that there exists a curvilinear relationship between independent and dependent variables. It is inferred from the plot that higher level of BSA & ketoprofen results in increase in solubility.

To attain stability a natural tendency to acquire minimum Gibbs energy is always there. The plot of Gibbs free energy against varying concentration of BSA and ketoprofen (Fig. 5c) construed that the process is more favorable at higher level of BSA and ketoprofen possessing minimum value of ΔG. Further, all the values of ΔG are negative (Table 1) at all levels of carrier demonstrating spontaneity of drug solubilization process.
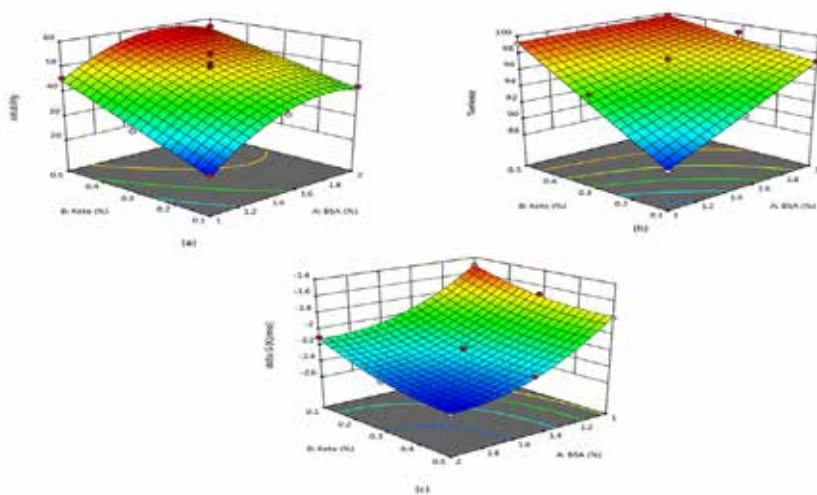

Figure 5. (a, b, c) Response surface plots showing effect of concentration of BSA & Ketoprofen on solubility (Y1), *in-vitro* release (Y2) and Gibb's free energy.

In vitro drug release

Table 1 shows the *in vitro* drug release data at 60 min. From these results, it is observed that only 26% of ketoprofen was released in 1 hr from drug solution and 42% from the PM whereas different batches of SD show 72.24 to 98.2% release of ketoprofen in 1hr study. The higher percentage release of drug in case of SD as compared to pure drug and PM may be related to the solubility data. As previously mentioned that the BSA form the soluble complex with the drug and thus increasing drug wettability and leads to a better solubility and thus better rate of drug release.

The polynomial equation obtained for the dependent variable Y_2 (*in vitro* release) is shown in equation (ii)

$$Y_2 = 87.30 + 7.42X_1 + 4.09X_2 + 0.605X_1X_2 - 3.13X_1{}^2 - 1.93X_2{}^2 \quad \text{(ii)}$$

Table 2 summarizing the results of ANOVA on response surface model (fitted best in quadratic model after none transformation of the data). The responses generated were fitted into various polynomials models using the experimental design. It was observed that response *in–vitro* release (Y_2) fitted best into quadratic response surface model.

Table 2. Model summary statistic

Response factor	Model					Lack of fit	
	F-value	Prob.>F	R^2	Adeq. prec.	C.V. (%)	F-value	Prob.>F
Y_1	52.36	< 0.0001	0.9740	24.2411	2.58	0.7745	0.5659
Y_2	34.42	< 0.0001	0.9609	20.0699	1.99	0.8202	0.5467

The polynomial model was found to be significant ($p < 0.05$) with non-significant lack of fit ($p > 0.05$). The higher value of R^2 (> 0.9) pertinent good correlation between the experimental and predicted response. Adequate precision that estimates the signal to noise ratio was much above the required value of 4, indicating adequate signal and model fit to navigate the design space. Figure 5 (b) display the combined effect of concentration of BSA & ketoprofen on % release that exhibited a linear relationship between independent and dependent variables, suggested that higher level of BSA & ketoprofen favours the expedited release. The numerical optimization tool using desirability approach was employed to prepare solid dispersion. The optimization of independent variables was done with constraints of maximum solubility and maximum % release. The

parameters suggested by the design were concentration of BSA (1.950%) & concentration of ketoprofen (0.480%) that provide SD with solubility of 58 µg/ml (predicted value 58.159 µg/ml) and % release 93.2% (predicted value 94.05%). The closer agreement between predicted and observed values indicated the high prognostic ability of the model. Figure 6 displays the in vitro release profile of ketoprofen as pure drug and from the optimised batch of formulation.
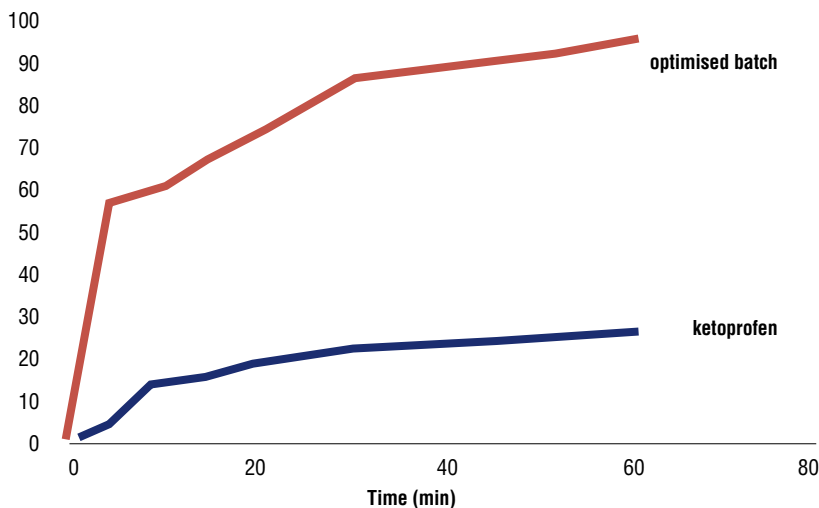
Figure 6. *In –vitro* release profile of pure ketoprofen and solid dispersion (optimized batch).

CONCLUSION

The solid dispersion has been the synonym for the enhancement of solubility of poorly water-soluble drugs. In this study, Bovine serum albumin (BSA) is used as solubility enhancer of ketoprofen (a model drug). The solid dispersion containing BSA and ketoprofen was prepared using 2-factor-3-level central composite experimental design. The preparation of SD was characterized by FT-IR, XRD, DSC and SEM studies. The DSC and XRD studies demonstrated the amorphous nature of the solid dispersion. Thereby, solid dispersion exhibited a fast release and enhanced solubility as compared to pure drug and physical mixture. Thus, overall study rendered the suitability of lyophilized BSA solid dispersion in improving the solubility of poorly water-soluble drug.

ACKNOWLEDGEMENTS

REFERENCES

1. Kaur, S., Jena, S. K., Samal, S. K., Saini, V., & Sangamwar, A. T. Freeze dried solid dispersion of exemestane: A way to negate an aqueous solubility and oral bioavailability problems. *European Journal of Pharmaceutical Sciences*, **2017**, *107*, 54-61.

2. Sherje, A. P., Murahari, M., Suvarna, V., & Patel, K. Study on effect of L-arginine on solubility and dissolution of Zaltoprofen: Preparation and characterization of binary and ternary cyclodextrin inclusion complexes. *Chemical Physics Letters*, **2018**, *694*, 120-128.

3. Lim, L. M., Cheow, W. S., & Hadinoto, K. Re-evaluating the presumed superiority of amorphous nanoparticles over amorphous microscale solid dispersion in solubility enhancement of poorly soluble drugs. *European Journal of Pharmaceutical Sciences*, **2017**, *109*, 455-463.

4. Vithani, K., Hawley, A., Jannin, V., Pouton, C., & Boyd, B. J. Solubilisation behaviour of poorly water-soluble drugs during digestion of solid SMEDDS. *European Journal of Pharmaceutics and Biopharmaceutics*, **2018**, *130*, 236-246.

5. Aloisio, C., Antimisiaris, S. G., & Longhi, M. R. Liposomes containing cyclodextrins or meglumine to solubilize and improve the bioavailability of poorly soluble drugs. *Journal of Molecular Liquids*, **2017**, *229*, 106-113.

6. Dwichandra Putra, O., Umeda, D., Fujita, E., Haraguchi, T., Uchida, T., Yonemochi, E., & Uekusa, H. Solubility Improvement of Benexate through Salt Formation Using Artificial Sweetener. *Pharmaceutics*, **2018**, 10(*2*), 64.

7. Strickley, R. G. Solubilizing excipients in oral and injectable formulations. *Pharmaceutical research*, **2004**, 21(*2*), 201-230.

8. Priemel, P. A., Laitinen, R., Grohganz, H., Rades, T., & Strachan, C. J. In situ amorphisation of indomethacin with Eudragit® E during dissolution. *European Journal of Pharmaceutics and Biopharmaceutics*, **2013**, 85(*3*), 1259-1265.

9. Sekiguchi, K., & Obi, N. Studies on Absorption of Eutectic Mixture. I. A Comparison of the Behavior of Eutectic Mixture of Sulfathiazole and that of Ordinary Sulfathiazole in Man. *Chemical and Pharmaceutical Bulletin*, **1961**, 9(*11*), 866-872.

10. Chiou, W. L., & Riegelman, S. Preparation and dissolution characteristics of several fast-release solid dispersions of griseofulvin. *Journal of Pharmaceutical Sciences*, **1969**, 58(*12*), 1505-1510.

11. Özkan, Y., Doğanay, N., Dikmen, N., & Işımer, A. (2000). Enhanced release of solid dispersions of etodolac in polyethylene glycol. *Il Farmaco*, **2000**, 55(*6-7*), 433-438.

12. Ghosh, I., Snyder, J., Vippagunta, R., Alvine, M., Vakil, R., Tong, W. Q. T., & Vippagunta, S. Comparison of HPMC based polymers performance as carriers for manufacture of solid dispersions using the melt extruder. *International Journal of Pharmaceutics*, **2011**, 419(*1-2*), 12-19.

13. Motallae, S., Taheri, A., & Homayouni, A. Preparation and characterization of solid dispersions of celecoxib obtained by spray-drying ethanolic suspensions containing PVP-K30 or isomalt. *Journal of Drug Delivery Science and Technology*, **2018**, *46*, 188-196.

14. Zecevic, D. E., Meier, R., Daniels, R., & Wagner, K. G. Site specific solubility improvement using solid dispersions of HPMC-AS/HPC SSL–Mixtures. *European Journal of Pharmaceutics and Biopharmaceutics*, **2014**, 87(*2*), 264-270.

15. Miyazaki, T., Aso, Y., Yoshioka, S., & Kawanishi, T. Differences in crystallization rate of nitrendipine enantiomers in amorphous solid dispersions with HPMC and HPMCP. *Interna-

tional Journal of Pharmaceutics, **2011**, 407(*1-2*), 111-118.

16. Babu, G. M. M., Prasad, C. D., & Murthy, K. R. Evaluation of modified gum karaya as carrier for the dissolution enhancement of poorly water-soluble drug nimodipine. *International journal of Pharmaceutics*, **2002**, 234(*1-2*), 1-17.

17. Van Drooge, D. J., Hinrichs, W. L. J., & Frijlink, H. W. Anomalous dissolution behaviour of tablets prepared from sugar glass-based solid dispersions. *Journal of Controlled Release*, **2004**, 97(*3*), 441-452.

18. Yadav, P. S., Kumar, V., Singh, U. P., Bhat, H. R., & Mazumder, B. Physicochemical characterization and in vitro dissolution studies of solid dispersions of ketoprofen with PVP K30 and d-mannitol. *Saudi Pharmaceutical Journal*, **2013**, 21(*1*), 77-84.

19. Mohammadi, G., Hemati, V., Nikbakht, M. R., Mirzaee, S., Fattahi, A., Ghanbari, K., & Adibkia, K. In vitro and in vivo evaluation of clarithromycin−urea solid dispersions prepared by solvent evaporation, electrospraying and freeze-drying methods. *Powder Technology*, **2014**, *257*, 168-174.

20. de los Santos, C. J. J., Pérez-Martínez, J. I., Gómez-Pantoja, M. E., & Moyano, J. R. Enhancement of albendazole dissolution properties using solid dispersions with Gelucire 50/13 and PEG 15000. *Journal of Drug Delivery Science and Technology*, **2017**, *42*, 261-272.

21. Singh, G., Pai, R. S., & Devi, V. K. Effects of the Eudragit and Drug coat on the release behaviour of poorly soluble drug by solid dispersion technique. *International Journal of Pharmaceutical Sciences and Research*, **2011**, 2(*4*), 816.

22. Prajapati, S. T., Gohel, M. C., & Patel, L. D. Studies to enhance dissolution properties of carbamazepine. *Indian Journal of Pharmaceutical Sciences*, **2007**, 69(*3*), 427.

23. Wren, S. A. C., Alhusban, F., Barry, A. R., & Hughes, L. P. Mechanistic understanding of the link between Sodium Starch Glycolate properties and the performance of tablets made by wet granulation. *International Journal of Pharmaceutics*, **2017**, 529(*1-2*), 319-328.

24. Modi, A. & Tayade, P. Enhancement of dissolution profile by solid dispersion (kneading) technique. *AAPS pharmscitech*, **2006**, 7(*3*), E87.

25. Yu, Z., Yu, M., Zhang, Z., Hong, G., & Xiong, Q. Bovine serum albumin nanoparticles as controlled release carrier for local drug delivery to the inner ear. *Nanoscale research letters*, **2014**, 9(*1*), 343.

26. Ghuman, J., Zunszain, P. A., Petitpas, I., Bhattacharya, A. A., Otagiri, M., & Curry, S. Structural basis of the drug-binding specificity of human serum albumin. *Journal of molecular biology*, **2005**, 353(*1*), 38-52.

27. Peters Jr, T. *All about albumin: biochemistry, genetics, and medical applications*. Academic press. **1995**.

28. Evans, T. W. albumin as a drug—biological effects of albumin unrelated to oncotic pressure. *Alimentary Pharmacology & Therapeutics*, **2002**, *16*, 6-11.

29. Liu, Z., & Chen, X. Simple bioconjugate chemistry serves great clinical advances: albumin as a versatile platform for diagnosis and precision therapy. *Chemical Society Reviews*, **2016**, 45(*5*), 1432-1456.

30. Urien, S., Tillement, J. P., & Barré, J. *The significance of plasma-protein binding in drug research* (pp. 189-197). **2001**, Wiley VCH: Zürich, Switzerland.

Microbial Efficacy and Two Step Synthesis of Uridine Derivatives with Spectral Characterization

Sumi R. Devi[1], Sanjida Jesmin[1], Mahfuz Rahman[1], Mohammad A. Manchur[2], Yuki Fujii[3], Yasuhiro Ozeki[4], Sarkar M. A. Kawsar[1*]

1 Laboratory of Carbohydrate and Nucleoside Chemistry, Department of Chemistry, Faculty of Science, University of Chittagong, Chittagong 4331, Bangladesh.

2 Department of Microbiology, Faculty of Biological Science, University of Chittagong, Chittagong-4331, Bangladesh

3 Department of Pharmacy, Faculty of Pharmaceutical Science, Nagasaki International University, 2825-7 Huis Ten Bosch, Sasebo, Nagasaki 859-3298, Japan

4 Department of Life and Environmental System Science, Graduate School of NanoBio Sciences, Yokohama City University, 22-2 Seto, Kanazawa-ku, Yokohama 236-0027, Japan

ABSTRACT

Uridine is a natural nucleoside precursor of uridine monophosphate in organisms and thus is considered to be safe and is used in a wide range of clinical settings. The far-reaching effects of pharmacological uridine have long been neglected. Here, we report a novel series of uridine esters were designed and synthesized by direct method with microbial efficacy. The structures of the prepared compounds have been characterized using various physico-chemical methods including C, H elemental analysis, melting point determination, IR and ^{1}H-NMR spectroscopy. The synthesized uridine derivatives were subjected to *in-vitro* antibacterial screening using agar disc diffusion method on some clinically isolated Gram-positive and Gram-negative bacterial strains. Also, antifungal functionality test was performed against a number of plant pathogenic fungi. The compounds showed varied antibacterial and antifungal activities. In addition, cytotoxic activity showed different rate mortality with different concentrations. In conclusion, it may useful for antibacterial and antifungal active agents after investigating their further analysis to develop safer and more potent drugs in the future.

Keywords: Synthesis, uridine, structure, efficacy, pathogens

INTRODUCTION

Uridine (**1**) is one of the four basic components of robonucleic acid (RNA). Upon digestion of foods containing RNA, uridine is released from RNA and is absorbed intact in the gut. Uridine is found in sugarcane, tomatos, broccoli, liver,

pancreas etc. Uridine has anti depression activity, asthmatic airway inflammation, hepatocyte proliferation[1,2]. In addition, uridine has been reported to have other physiological actions in animal studies, such as a vasoconstrictive effect in rats, which was reversed by adenosine[3] and hyperpolarized amphibian ganglia and superior cervical ganglia in rats, possibly related to an inhibitory activity[4]. In humans, uridine is administered to reduce the adverse effects of cancer chemotherapy including 5-fluorouracil, such as bone marrow and gastrointestinal toxicity[5]. Furthermore, a combination of uridine and benzylacyclouridine (uridine phosphorylase inhibitor) was shown to reduce neurotoxicity and bone marrow toxicity related to zidovudine used for treatment of HIV infection[6]. However, the physiological activities of uridine in humans remain undetermined.

Nucleotides and nucleosides are key compounds involved in major biological processes, such as nucleic acids and proteins synthesis, cell signaling, enzyme regulation, and metabolism. Indeed, many nucleoside analogues are already clinically used as antiviral[7,8] and antitumoral agents[9,10]. However, their efficiency is sometimes reduced by the appearance of resistance mechanisms[11]. The availability of new nucleoside derivatives[12], therefore, is still of prime importance.

A number of fruitful and efficient methods for selective acylation were reported by many carbohydrate chemists using many acylating agents and varying reaction conditions[13,14]. However, most of these methods are based on the blocking and deblocking of the hydroxyl groups which are not directly involved in the reaction[15,16]. Various methods for acylation of carbohydrates and nucleosides have so far been developed and employed successfully[17-19]. Of these, direct method has been found to be the most encouraging method for acylation of carbohydrates and nucleosides[20].

From literature survey revealed that a large number of biologically active compounds possess aromatic and heteroaromatic nucleus and acyl substituents[21,22]. It is also known that, if an active nucleus is linked to another nucleus, the resulting molecule may possess greater potential for biological activity[23]. The benzene and substituted benzene nuclei play important role as common denominator of various biological activities[24]. Results of an ongoing research work on selective acylation of nucleosides[25] and also evaluation of antimicrobial activities reveal that in many cases the combination of two or more aromatic or heteroaromatic nuclei[23]. It is also found that N, S and X containing substitution products showed marked antimicrobial activities i.e., enhance the biological activity of the parent compound[26,27]. Encouraged by literature reports and our own findings[28,29], we synthesized some selectively acylated derivatives of

uridine (**1**) (Scheme 1- 2 & Table 1) containing various substituents in a single molecular framework and evaluated their antibacterial and antifungal activities using a variety of bacterial and fungal pathogens.
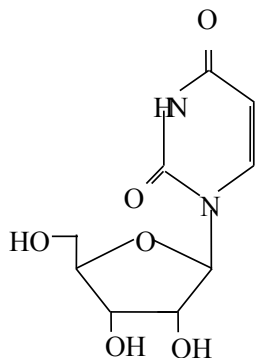
Figure 1. Uridine (Compound 1)

METHODOLOGY

Chemicals

Melting points were determined on an electro-thermal melting point apparatus (England) and are uncorrected. Evaporations were carried out under reduced pressure using VV-1 type vacuum rotary evaporator (Germany) with a bath temperature below 40°C. Thin layer chromatography (t.l.c) was performed on Kieselgel GF$_{254}$ and spots were detected by spraying the plates with 1% H$_2$SO$_4$ and heating at 150-200°C until coloration took place. Column chromatography was performed with silica gel G$_{60}$. All reagents used were commercially available (Aldrich) and were used as received, unless otherwise specified.

Structure and physical properties of uridine derivatives

The structures of newly synthesized compounds were determined through NMR spectroscopy and mass spectrometry. ¹H-NMR spectra (400 MHz) were recorded for solutions in deuteriochloroform (CDCl$_3$) (internal Me$_4$Si) with a Bruker DPX-40C spectrometer. Synthesized compounds were also conducted by liquid chromatography electrospray ionization-tandem mass spectrometry in positive ionization mode (LC/ESI(+)-MS/MS) by using a system that consisted of a JASSO LC (JASCO, Tokyo, Japan) at the Yokohama City University, Japan. IR spectra were recorded by KBr disc at the Chemistry Department, University of Chittagong, Bangladesh, with an IR Affinity Fourier Transform Infrared Spectrophotometer (SHIMADZU). The physical properties were de-

termined and characterized by melting point and elemental analysis (C and H).

Synthesis of uridine derivatives

5´-O-octanoyluridine (Compound 2)

A solution of the uridine (**1**) (200 mg, 0.83 mmol) in anhydrous pyridine (3 ml) was cooled to 0ºC when octanoyl chloride (0.3 ml, 1.1 molar eq.) was added. The reaction mixture was continuously stirred for 6 hours at 0ºC temperature and then the reaction mixture was standing for overnight at room temperature with continuous stirring. The progress of the reaction was monitored by t.l.c (methanol-chloroform, 1:24) which indicated full conversion of the starting material into a single product (R_f = 0.50). The solution was poured into ice water with constant stirring. It was then extracted with chloroform (3×10 ml). The combined chloroform layer was washed successively with dilute hydrochloric acid, saturated aqueous sodium hydrogen carbonate solution and distilled water. The organic layer was dried (Na_2SO_4), filtered and concentrated. The organic layer was dried ($MgSO_4$), filtered and concentrated. Purification by chromatography with methanol-chloroform (1:24) as eluant and furnished the octanoyl chloride derivative (**2**) (164 mg, 82%) as solid mass, which was used in the next stage. Physical properties are shown in the Table 2.

Colour: white, solubility: $CHCl_3$, DMF. FTIR (KBr) v_{max} (cm^{-1}) 1728 (C=O), 3358-3520 (br, -OH). ^{1}H-NMR (400 MHz, CDCl$_3$): δ_H 9.08 (1H, s, -NH), 7.53 (1H, d, J = 7.8 Hz, H-6), 5.98 (1H, d, J=5.6 Hz, H-1´), 5.88 (1H, s, 2´-OH), 5.81 (1H, dd, J = 2.1 and 12.1 Hz, H-5´a), 5.77 (1H, dd, J=2.2 and 12.3 Hz, H-5´b), 5.67 (1H, d, J = 8.1 Hz, H-5), 5.62 (1H, s, 3´-OH), 4.40 (1H, dd, J = 2.2 and 5.5 Hz, H-4´), 4.22 (1H, d, J = 5.6 Hz, H-2´), 4.17 (1H, dd, J = 7.4 and 5.4 Hz, H-3´), 2.34 {2H, m, CH$_3$(CH$_2$)$_5$CH$_2$CO-}, 1.61 {2H, m, CH$_3$(CH$_2$)$_4$CH$_2$CH$_2$CO-}, 1.26 {8H, m, CH$_3$(CH$_2$)$_4$(CH$_2$)$_2$CO-}, 0..87 {3H, m, CH$_3$(CH$_2$)$_6$CO-}. Mass spectra (MS) (positive ion LC-ESI, 8eV): m/z [M+H]$^+$ 371.18 (100). Anal calcd for C$_{17}$H$_{26}$O$_7$N$_2$ (370.18): C, 55.15; H, 7.02. Found: C, 55.18; H, 7.04.

General procedure for synthesis of 5´-O-octanoyl derivatives

A cooled (0ºC) and stirred solution of compound (**2**) (120.8 mg, 0.33 mmol) in dry pyridine (3 ml) was treated with 5 molar equivalents of pentanoyl chloride (0.14 ml, 5.1 mmol) and the solution was left standing overnight in the room temperature. The progress of the reaction was monitored by t.l.c (methanol-chloroform, 1:18) which indicated the complete conversion of the starting material into faster moving product (R_f = 0.54). Aqueous work-up procedure as described earlier and silica gel column chromatographic purification (methanol-chloroform, 1:18 as eluant), gave the pentanoylate (**3**) (110 mg, 91%) as a

pasty mass.

Using the similar reaction procedure, compound 3 was converted to compound **4**, **5**, **6**, 7, **8**, **9**, **10**, **11**, **12** and compound **13**.

5´-*O*-Octanoyl-2´,3´-di-*O*-pentanoyluridine (Compound 3)

Colour: off white, solubility: $CHCl_3$, DMF. FTIR (KBr) v_{max} (cm⁻¹) 1757 (C=O). ¹H-NMR (400 MHz, $CDCl_3$): δ_H 9.01 (1H, s, -NH), 7.41 (1H, d, J = 7.8 Hz, H-6), 6.08 (1H, d, J = 5.6 Hz, H-1´), 5.75 (1H, dd, J = 2.2 and 12.2 Hz, H-5´a), 5.61 (1H, dd, J = 2.1 and 12.2 Hz, H-5´b), 5.08 (1H, d, J = 7.8 Hz, H-5), 4.52 (1H, d, J = 5.2 Hz, H-2´), 4.33 (1H, dd, J = 7.7 and 5.6 Hz H-3´), 4.27 (1H, m, H-4´), 2.35 {4H, m, 2×$CH_3(CH_2)_2CH_2CO$-}, 2.31 {2H, m, $CH_3(CH_2)_5CH_2CO$-}, 1.61 (4H, m, 2×$CH_3CH_2CH_2CH_2CO$-), 1.57 {2H, m, $CH_3(CH_2)_4CH_2CH_2CO$-}, 1.38 {4H, m, 2×$CH_3CH_2(CH_2)_2CO$-}, 1.26 {8H, m, $CH_3(CH_2)_4(CH_2)_2CO$-}, 0.88 {6H, m, 2×$CH_3(CH_2)_3CO$-}, 0..87 {3H, m, $CH_3(CH_2)_6CO$-}. Mass spectra (MS) (positive ion LC-ESI, 8eV): *m/z* [M+H]⁺ 539.60 (100). Anal calcd for $C_{27}H_{42}O_9N_2$ (538.60): C, 60.17; H, 7.80. Found: C, 60.22; H, 7.84.

2´,3´-Di-*O*-hexanoyl-5´-*O*-octanoyluridine (Compound 4)

Colour: white, solubility: $CHCl_3$, DMF, DMSO. FTIR (KBr) v_{max} (cm⁻¹) 1742 (C=O). ¹H-NMR (400 MHz, $CDCl_3$): δ_H 9.98 (1H, s, -NH), 7.53 (1H, d, J = 7.6 Hz, H-6), 6.02 (1H, d, J = 5.7 Hz, H-1´), 5.89 (1H, dd, J = 2.2 and 12.2 Hz, H-5´a), 5.74 (1H, dd, J = 2.1 and 12.0 Hz, H-5´b), 5.45 (1H, d, J = 7.8 Hz, H-5), 4.95 (1H, d, J = 5.2 Hz, H-2´), 4.39 (1H, dd, J = 7.8 and 5.6 Hz H-3´), 4.18 (1H, m, H-4´), 2.40 {2H, m, $CH_3(CH_2)_5CH_2CO$-}, 2.35 {4H, m, 2×$CH_3(CH_2)_3CH_2CO$-}, 1.62 {4H, m, 2×$CH_3(CH_2)_2CH_2CH_2CO$-}, 1.60 {2H, m, $CH_3(CH_2)_4CH_2CH_2CO$-}, 1.27 {8H, m, 2×$CH_3(CH_2)_2CH_2CH_2CO$-}, 1.25 {8H, m, $CH_3(CH_2)_4(CH_2)_2CO$-}, 0.85 {6H, m, 2×$CH_3(CH_2)_4CO$-}, 0..84 {3H, m, $CH_3(CH_2)_6CO$-}.

Mass spectra (MS) (positive ion LC-ESI, 8eV): *m/z* [M+H]⁺ 567.5 (100). Anal calcd for $C_{29}H_{46}O_9N_2$ (566.50): C, 61.43; H, 8.12. Found: C, 61.46; H, 8.15.

2´,3´-Di-*O*-decanoyl-5´-*O*-octanoyluridine (Compound 5)

Colour: dark white, solubility: $CHCl_3$, DMF, DMSO. FTIR (KBr) v_{max} (cm⁻¹) 1738 (C=O). ¹H-NMR (400 MHz, $CDCl_3$): δ_H 9.05 (1H, s, -NH), 7.54 (1H, d, J = 7.8 Hz, H-6), 5.87 (1H, d, J = 5.6 Hz, H-1´), 5.79 (1H, dd, J = 2.0 and 12.0 Hz, H-5´a), 5.41 (1H, dd, J = 2.0 and 12.0 Hz, H-5´b), 5.41 (1H, d, J = 8.2 Hz, H-5), 5.02 (1H, m, H-2´), 4.38 (1H, m, H-3´), 4.28 (1H, m, H-4´), 2.36 {4H, m, 2× $CH_3(CH_2)_7CH_2CO$-}, 2.33 {2H, m, $CH_3(CH_2)_5CH_2CO$-}, 1.60 {4H, m, 2×$CH_3(CH_2)_6CH_2CH_2CO$-}, 1.57 {2H, m, $CH_3(CH_2)_4CH_2CH_2CO$-}, 1.26 {24H, m, 2×$CH_3(CH_2)_6CH_2CH_2CO$-}, 1.24 {8H, m, $CH_3(CH_2)_4(CH_2)_2CO$-}, 0.85 {6H,

m, 2×CH_3(CH$_2$)$_8$CO-}, 0.83 {3H, m, CH_3(CH$_2$)$_6$CO-}. Mass spectra (MS) (positive ion LC-ESI, 8eV): m/z [M+H]$^+$ 680.29 (100). Anal calcd for C$_{37}$H$_{62}$O$_9$N$_2$ (679.29): C, 65.36; H, 9.13. Found: C, 65.40; H, 9.14.

2´,3´-Di-*O*-lauroyl-5´-*O*-octanoyluridine (Compound 6)

Colour: deep white, solubility: CHCl$_3$, DMF, DMSO. FTIR (KBr) v$_{max}$ (cm^{-1}) 1758 (-CO). ^{1}H-NMR (400 MHz, CDCl$_3$): δ$_H$ 8.96 (1H, s, -NH), 7.42 (1H, d, J = 7.7 Hz, H-6), 6.00 (1H, m, H-1´), 5.76 (1H, m, H-5´a), 5.57 (1H, m, H-5´b), 5.48 (1H, d, J = 8.1 Hz, H-5), 5.29 (1H, d, J = 5.6 Hz, H-2´), 5.22 (1H, m, H-3´), 4.32 (1H, m, H-4´), 2.37 {4H, m, 2×CH$_3$(CH$_2$)$_9$CH_2CO-}, 2.31 {2H, m, CH$_3$(CH$_2$)$_5$CH_2CO-}, 1.59 {4H, m, 2×CH$_3$(CH$_2$)$_8$CH_2CH$_2$CO-}, 1.56 {2H, m, CH$_3$(CH$_2$)$_4$CH_2CH$_2$CO-}, 1.24 {8H, m, CH$_3$(CH_2)$_4$(CH$_2$)$_2$CO-}, 1.21 {32H, m, 2×CH$_3$(CH_2)$_8$CH$_2$CH$_2$CO-}, 0.88 {6H, m, 2×CH_3(CH$_2$)$_{10}$CO-}, 0..86 {3H, m, CH_3(CH$_2$)$_6$CO-}. Mass spectra (MS) (positive ion LC-ESI, 8eV): m/z [M+H]$^+$ 735.42 (100). Anal calcd for C$_{41}$H$_{70}$O$_9$N$_2$ (734.42): C, 67.04; H, 9.53. Found: C, 67.07; H, 9.56.

2´,3´-Di-*O*-myristoyl-5´-*O*-octanoyluridine (Compound 7)

Colour: deep white, solubility: CHCl$_3$, DMF, DMSO. FTIR (KBr) v$_{max}$ (cm^{-1}) 1736 (-CO). ^{1}H-NMR (400 MHz, CDCl$_3$): δ$_H$ 9.01 (1H, s, -NH), 7.50 (1H, d, J = 7.6 Hz, H-6), 6.08 (1H, d, J = 5.7 Hz, H-1´), 5.75 (1H, m, H-5´a), 5.73 (1H, m, H-5´b), 5.61 (1H, d, J = 7.7 Hz , H-5), 5.08 (1H, d, J = 5.3 Hz, H-2´), 4.78 (1H, m, H-3´), 4.37 (1H, dd, J = 2.1 and 5.5 Hz, H-4´), 2.35 {4H, m, 2×CH$_3$(CH$_2$)$_{11}$CH_2CO-}, 2.33 {2H, m, CH$_3$(CH$_2$)$_5$CH_2CO-}, 1.62 {2H, m, CH$_3$(CH$_2$)$_4$CH_2CH$_2$CO-}, 1.26 {44H, m, 2×CH$_3$(CH$_2$)$_{11}$CH$_2$CO-}, 1.25 {8H, m, CH$_3$(CH_2)$_4$(CH$_2$)$_2$CO-}, 0.88 {6H, m, 2×CH_3(CH$_2$)$_{12}$CO-}, 0.86 {3H, m, CH_3(CH$_2$)$_6$CO-}. Mass spectra (MS) (positive ion LC-ESI, 8eV): m/z [M+H]$^+$ 791.46 (100). Anal calcd for C$_{45}$H$_{78}$O$_9$N$_2$ (790.46): C, 68.37; H, 9.87. Found: C, 68.41; H, 9.89.

5´-*O*-Octanoyl-2´,3´-di-*O*-palmitoyluridine (Compound 8)

Colour: light white, solubility: CHCl$_3$, DMF, DMSO. FTIR (KBr) v$_{max}$ (cm^{-1}) 1722 (-CO) cm^{-1}. ^{1}H-NMR (400 MHz, CDCl$_3$): δ$_H$ 8.98 (1H, s, -NH), 7.58 (1H, m, H-6), 5.70 (1H, m, H-1´), 5.61 (2H, m, H-5´a and H-5´b), 5.46 (1H, d, J = 8.1 Hz , H-5), 5.02 (1H, d, J = 5.5 Hz, H-2´), 4.87 (1H, m, H-3´), 4.36 (1H, m, H-4´), 2.36 {4H, m, 2×CH$_3$(CH$_2$)$_{13}$CH_2CO-}, 2.33 {2H, m, CH$_3$(CH$_2$)$_5$CH_2CO-}, 1.60 {2H, m, CH$_3$(CH$_2$)$_4$CH_2CH$_2$CO-}, 1.25 {8H, m, CH$_3$(CH_2)$_4$(CH$_2$)$_2$CO-}, 1.24 {52H, m, 2×CH$_3$(CH_2)$_{13}$CH$_2$CO-}, 0.88 {6H, m, 2×CH_3(CH$_2$)$_{14}$CO-}, 0.86 {3H, m, CH_3(CH$_2$)$_6$CO-}. Mass spectra (MS) (positive ion LC-ESI, 8eV): m/z [M+H]$^+$ 847.5 (100). Anal calcd for C$_{49}$H$_{86}$O$_9$N$_2$ (846.50): C, 69.52; H, 10.16. Found: C, 69.55; H, 10.19.

5´-O-Octanoyl-2´,3´-di-O-pivaloyluridine (Compound 9)

Colour: white, solubility: CHCl$_3$, DMF, DMSO. FTIR (KBr) ν$_{max}$ (cm^{-1}) 1740 (-CO). ^{1}H-NMR (400 MHz, CDCl$_3$): δ$_H$ 9.06 (1H, s, -NH), 7.65 (1H, d, J = 7.6 Hz, H-6), 6.08 (1H, d, J = 5.6 Hz, H-1´), 5.78 (1H, m, H-5´a), 5.61 (1H, m, H-5´b), 5.29 (1H, d, J = 8.4 Hz, H-5), 5.01 (1H, m, H-2´), 4.60 (1H, m, H-3´), 4.38 (1H,, m, H-4´), 2.35 {2H, m, CH$_3$(CH$_2$)$_5$CH$_2$CO-}, 1.64 {2H, m, CH$_3$(CH$_2$)$_4$CH$_2$CH$_2$CO-}, 1.21 {18H, s, 2×(CH$_3$)$_3$CCO-}, 1.21 {8H, m, CH$_3$(CH$_2$)$_4$(CH$_2$)$_2$CO-}, 0..88 {3H, m, CH$_3$(CH$_2$)$_6$CO-}. Mass spectra (MS) (positive ion LC-ESI, 8eV): m/z [M+H]$^+$ 539.5 (100). Anal calcd for C$_{27}$H$_{42}$O$_9$N$_2$ (538.50): C, 60.17; H, 7.80. Found: C, 60.19; H, 7.84.

2´, 3´-Di-O-methanesulfonyl-5´-O-octanoyluridine (Compound 10)

Colour: white, solubility: CHCl$_3$, DMF, DMSO. FTIR (KBr) ν$_{max}$ (cm^{-1}) 1765 (-CO) and 1365 (-SO$_2$). ^{1}H-NMR (400 MHz, CDCl$_3$): δ$_H$ 8.91 (1H, s, -NH), 7.71 (1H, d, J = 7.8 Hz, H-6), 6.01 (1H, d, J = 5.6 Hz, H-1´), 5.88 (1H, m, H-5´a), 5.69 (1H, m, H-5´b), 5.22 (1H, d, J = 8.2 Hz, H-5), 5.15 (1H, m, H-2´), 4.96 (1H, m, H-3´), 4.41 (1H,, m, H-4´), 3.10, 3.05 {2×3H, 2×s, 2×CH$_3$SO$_2$-}, 2.36 {2H, m, CH$_3$(CH$_2$)$_5$CH$_2$CO-}, 1.61 {2H, m, CH$_3$(CH$_2$)$_4$CH$_2$CH$_2$CO-}, 1.26 {8H, m, CH$_3$(CH$_2$)$_4$(CH$_2$)$_2$CO-}, 0..86 {3H, m, CH$_3$(CH$_2$)$_6$CO-}. Mass spectra (MS) (positive ion LC-ESI, 8eV): m/z [M+H]$^+$ 527.32 (100). Anal calcd for C$_{19}$H$_{30}$O$_{11}$N$_2$S$_2$ (526.32): C, 43.36; H, 5.70. Found: C, 43.39; H, 5.73.

2´,3´-Di-O-benzenesulfonyl-5´-O-octanoyluridine (Compound 11)

Colour: light white, solubility: CHCl$_3$, DMF, DMSO. FTIR (KBr) ν$_{max}$ (cm^{-1}) 1741 (-CO) and 1362 (-SO$_2$). ^{1}H-NMR (400 MHz, CDCl$_3$): δ$_H$ 9.09 (1H, s, -NH), 7.90 (4H, m, Ar-H), 7.56 (2H, m, Ar-H), 7.41 (4H, m, Ar-H), 6.03 (1H, d, J = 7.7 Hz, H-6), 5.76 (1H, d, J = 5.5 Hz, H-1´), 5.30 (1H, m, H-5´a), 5.09 (1H, m, H-5´b), 4.94 (1H, d, J = 8.2 Hz, H-5), 4.76 (1H, m, H-2´), 4.56 (1H, m, H-3´), 4.35 (1H, m, H-4´), 2.33 {2H, m, CH$_3$(CH$_2$)$_5$CH$_2$CO-}, 1.62 {2H, m, CH$_3$(CH$_2$)$_4$CH$_2$CH$_2$CO-}, 1.26 {8H, m, CH$_3$(CH$_2$)$_4$(CH$_2$)$_2$CO-}, 0..87 {3H, m, CH$_3$(CH$_2$)$_6$CO-}. Mass spectra (MS) (positive ion LC-ESI, 8eV): m/z [M+H]$^+$ 651.42 (100). Anal calcd for C$_{29}$H$_{34}$O$_{11}$N$_2$S$_2$ (650.42): C, 53.55; H, 5.23. Found: C, 53.56; H, 5.27.

2´,3´-Di-O-(2-bromobenzoyl)-5´-O-octanoyluridine (Compound 12)

Colour: white, solubility: CHCl$_3$, DMF, DMSO. FTIR (KBr) ν$_{max}$ (cm^{-1}) 1780 (-CO). ^{1}H-NMR (400 MHz, CDCl$_3$): δ$_H$ 9.01 (1H, s, -NH), 7.81 (2H, m, Ar-H), 7.64 (4H, m, Ar-H), 7.36 (2H, m, Ar-H), 7.28 (1H, d, J = 7.6 Hz, H-6), 6.19 (1H, d, J = 5.6 Hz, H-1´), 6.03 (1H, m, H-5´a), 5.77 (1H, dd, J = 2.0 and 12.0

Hz, H-5´b), 5.55 (1H, d, J = 8.2 Hz, H-5), 5.49 (1H, m, H-2´), 4.62 (1H, m, H-3´), 4.36 (1H, m, H-4´), 2.34 {2H, m, CH$_3$(CH$_2$)$_5$CH$_2$CO-}, 1.62 {2H, m, CH$_3$(CH$_2$)$_4$CH$_2$CH$_2$CO-}, 1.24 {8H, m, CH$_3$(CH$_2$)$_4$(CH$_2$)$_2$CO-}, 0..84 {3H, m, CH$_3$(CH$_2$)$_6$CO-}. Mass spectra (MS) (positive ion LC-ESI, 8eV): m/z [M+H]$^+$ 737.41 (100). Anal calcd for C$_{31}$H$_{32}$O$_9$N$_2$Br$_2$ (736.41): C, 50.56; H, 4.35. Found: C, 50.59; H, 4.39.

2´, 3´-Di-*O*-(4-chlorobenzoyl)-5´-*O*-octanoyluridine (Compound 13)

Colour: off white, solubility: CHCl$_3$, DMF, DMSO. FTIR (KBr) v$_{max}$ (cm^{-1}) 1760 (C=O). ^{1}H-NMR (400 MHz, CDCl$_3$) δ$_H$: 9.0 (1H, s, -NH), 7.95 (4H, m, Ar-H), 7.75 (1H, d, J = 7.7 Hz, H-6), 7.50 (4H, m, Ar-H), 6.03 (1H, d, J = 5.5 Hz, H-1´), 5.79 (1H, m, H-5´a), 5.77 (1H, dd, J = 2.1 and 12.2 Hz, H-5´b), 5.59 (1H, m, H-5), 5.23 (1H, m, H-2´), 4.55 (1H, m, H-3´), 4.35 (1H, m, H-4´), 2.33 {2H, m, CH$_3$(CH$_2$)$_5$CH$_2$CO-}, 1.62 {2H, m, CH$_3$(CH$_2$)$_4$CH$_2$CH$_2$CO-}, 1.27 {8H, m, CH$_3$(CH$_2$)$_4$(CH$_2$)$_2$CO-}, 0..84 {3H, m, CH$_3$(CH$_2$)$_6$CO-}. Mass spectra (MS) (positive ion LC-ESI, 8eV): m/z [M+H]$^+$ 648.6 (100). Anal calcd for C$_{31}$H$_{32}$O$_9$N$_2$Cl$_2$ (647.60): C, 57.52; H, 4.94. Found: C, 57.55; H, 4.98.

Microbial screening studies

Test tube cultures of bacterial pathogens were obtained from the Microbiology Laboratory, Department of Microbiology, University of Chittagong. The synthesized test compounds (Table 2 & 3) were subjected to antibacterial screening against three Gram-positive and three Gram-negative bacterial strains (Table 1).

Preparation of bacterial suspension

About 10 ml of distilled water was taken in a clean screw cap test tube. A number of test tubes with water were sterilized in an autoclave. From 48 hours; old bacterial culture, one loop of bacterial culture was transferred to the sterilized distilled water and mixed it properly. These bacterial suspensions of the test tube were used to the pour plate during sensitivity test.

Table 1. List of used bacteria and fungus.

Types of organisms	Tested organisms & strain no.	
	Bacteria	
Gram +Ve	*Bacillus subtilis*	BTCC 17
	Bacillus cereus	BTCC 19
Gram -Ve	*Escherichia coli*	ATCC 25922
	Pseudomonas aeruginosa	ICDDR,B
	Salmonella typhi	AE 14612
	Fungus	
	Aspergillus niger	ATCC 16404
	Rhizopous nigricans	ATCC 6227b

Antibacterial efficacy test

The *in vitro* antibacterial activities of the synthesized chemicals were detected by disc diffusion method[30,31]. Paper discs of 4 mm in diameter and glass petri plate of 90 mm in diameter were used throughout the experiment. Paper discs were sterilized in an autoclave and dried at 100°C in an oven. Then the discs were soaked with test chemicals at the rate of 50μg (dry weight) per disc for antibacterial analysis. For pour plate technique, one drop of bacterial suspension was taken in a sterile petri dish and approximately 20 ml of melted sterile nutrient agar (NA) (~45°C) was poured into the plate, and then mixed thoroughly with the direction of clockwise and anticlockwise. After solidification of the seeded NA medium, paper disc after soaking with test chemicals (2% in CHCl$_3$) were placed at the centre of the inoculated petri dish. A control plate was also maintained in each case with chloroform. Firstly, the plates were kept for 4 hrs. at low temperature (4°C) and the test chemicals diffused from disc to the surrounding medium by this time. The plates were then incubated at (35± 2)°C for growth of test organisms and were observed at 24 hrs. intervals for two days. The activity was expressed in terms of inhibition zone diameter in mm. Each experiment was repeated thrice. The standard antibiotic Ampicillin from FISONS Ltd. (Bangladesh) was used as a positive control and compared with tested chemicals under identical conditions.

Antifungal efficacy test

The *in vitro* antifungal functionality tests of the synthesized chemicals were tested by mycelial growth test[32]. Required amount of medium was taken in a conical flask separately and was sterilized in autoclave. After autoclaving, weighted amount of test chemicals (2%) was added to the sterilized medium in

conical flask at the point of pouring to obtain the desired concentration. The flask was shaken thoroughly to mix the chemical with the medium homogeneously before pouring. The medium with definite concentration (2%) of chemical was poured at the rate of 10 µl in sterilized glass Petri dishes individually. Proper control was maintained separately with sterilized PDA (potato dextrose agar) medium without chemicals and three replications were prepared for each treatment. After solidification of medium, the fungal inoculums (5 mm approximately) were placed at the centre of each Petri dish in an inverted position. All the plates were inoculated at room temperature on the laboratory desk for five days. The linear growth of fungal colony was measured in two directions at right angle to each other after five days of incubation and average of three replicates was taken as the diameter of a colony in mm. The percentage inhibition of mycelial growth of test fungi was calculated as follow:

$$I = \left\{ \frac{C - T}{C} \right\} \times 100$$

Where, I = percentage of inhibition, C = diameter of the fungal colony in control, T = diameter of the fungal colony in treatment. The antifungal results were compared with that of the standard antibiotic, Nystatin (100 µg dw./disc, BEXIMCO Pharm. Bangladesh Ltd.).

Table 2. Molecular formula of the test compounds.

Compounds	Name of the tested compounds	Molecular formula
2	5´-*O*-Octanoyluridine	$C_{17}H_{26}O_7N_2$
3	5´-*O*-Octanoyl-2´,3´-di-*O*-pentanoyluridine	$C_{27}H_{42}O_9N_2$
4	2´,3´-Di-*O*-hexanoyl-5´-*O*-octanoyluridine	$C_{29}H_{46}O_9N_2$
5	2´,3´-Di-*O*-decanoyl-5´-*O*-octanoyluridine	$C_{37}H_{62}O_9N_2$
6	2´,3´-Di-*O*-lauroyl-5´-*O*-octanoyluridine	$C_{41}H_{70}O_9N_2$
7	2´,3´-Di-*O*-myristoyl-5´-*O*-octanoyluridine	$C_{45}H_{78}O_9N_2$
8	5´-*O*-Octanoyl-2´,3´-di-*O*-palmitoyluridine	$C_{49}H_{86}O_9N_2$
9	5´-*O*-Octanoyl-2´,3´-di-*O*-pivaloyluridine	$C_{27}H_{42}O_9N_2$

10	2´,3´-Di-*O*-methanesulphonyl-5´-*O*-octanoyluridine	$C_{19}H_{30}O_{11}N_2S_2$
11	2´,3´-Di-*O*-benzenesulphonyl-5´-*O*-octanoyluridine	$C_{29}H_{34}O_{11}N_2S_2$
12	2',3´-Di-*O*-(2-bromobenzoyl)-5´-*O*-octanoyluridine	$C_{31}H_{32}O_9N_2Br_2$
13	2´,3´-Di-*O*-(4-chlorobenzoyl)-5´-*O*-octanoyluridine	$C_{31}H_{32}O_9N_2Cl_2$

RESULTS AND DISCUSSION

Synthesis and characterization

In the present investigation, we carried out selective octanoylation of of uridine (**1**) with octanoyl chloride using the direct acylation method (Scheme 1-2 & Table 3 & 4). A series of derivatives of the resulting acylation products were prepared in order to gather supportive evidences for structure elucidation and also to obtain newer derivatives of synthetic and biological importance.

Our initial effort was to carry out selective acylation of uridine (**1**) with unimolecular amount of non-traditional acylating agent octanoyl chloride in dry pyridine at -5°C. Conventional work-up procedure, followed by removal of solvent and silica gel column chromatographic purification, we obtained the octanoyl derivative (**2**). This compound (**2**) was sufficiently pure for use in the next reactions. The IR spectrum of this compound showed the following characteristic peaks: 1728 (-CO) and 3358-3520 cm-[1] (br −OH stretching). In its ^{1}H-NMR spectrum, two two-proton multiplets at δ 2.34 {$CH_3(CH_2)_5CH_2CO$-} and 1.61 {$CH_3(CH_2)_4CH_2CH_2CO$-}, an eight-proton multiplet at δ 1.26 {$CH_3(CH_2)_4(CH_2)_2CO$-} and a three-proton multiplet at δ 0.87 {$CH_3(CH_2)_6CO$-} were due to the one octanoyl group, thereby suggesting the introduction of one octanoyl group in the molecule. The downfield shift of C-5[/] proton to δ 5.81 (as dd, J = 2.1 and 12.1 Hz, 5[/]a) and 5.77 (as dd, J = 2.2 and 12.3 Hz, 5[/]b) from their usual values[33] in the precursor compound (**1**) and the resonances of other protons in their anticipated positions, showed the presence of the octanoyl group at position 5[/]. The formation of 5[/]-*O*-octanoyluridine (**2**) might be due to higher reactivity of the sterically less hindered primary hydroxyl group of the ribose moiety of uridine (**1**). By complete analysis of the FTIR, ^{1}H-NMR and elemental data, the structure of this compound was assigned as 5[/]-*O*- octanoyluridine (**2**).
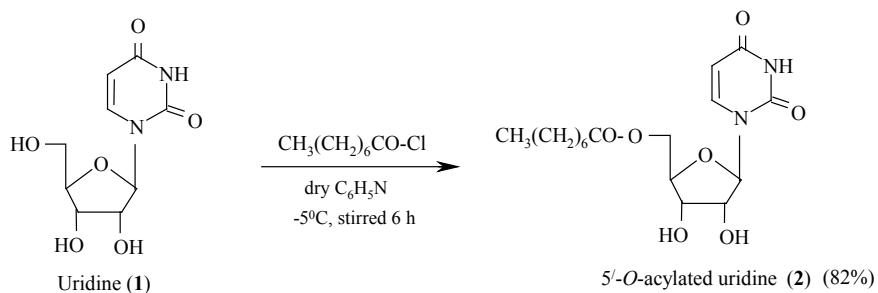
Scheme 1. Synthesis of 5´-O-octanoyluridine (Compound 2).
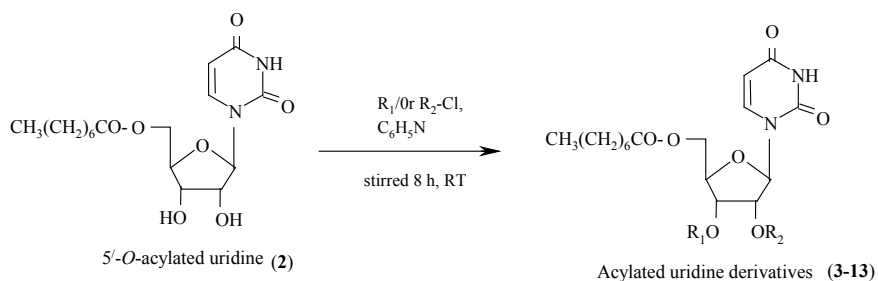
Scheme 2. Synthesis of 2/,3/-di-O-acylated 5´-O-octanoyluridine esters (Compounds 3-13).

Table 3. Synthesized of uridine derivatives (Compounds 2-13)

Compounds	$R_1=R_2$	Compounds	$R_1=R_2$
2	H	8	$CH_3(CH_2)_{14}CO-$
3	$CH_3(CH_2)_3CO-$	9	$(CH_3)_3CCO-$
4	$CH_3(CH_2)_4CO-$	10	CH_3SO_2-
5	$CH_3(CH_2)_8CO-$	11	$C_6H_5SO_2-$
6	$CH_3(CH_2)_{10}CO-$	12	$2-Br.C_6H_4CO-$
7	$CH_3(CH_2)_{12}CO-$	13	$4-Cl.C_6H_4CO-$

The diol **(2)** was then allowed to react with pentanoyl chloride in dry C_6H_5N at freezing temperature. Usual work-up procedure provided the $2'$,$3'$-di-*O*-pentanoyl derivative **(3)**. The FTIR spectrum of compound **3** showed absorption band at 1758 cm^{-1} for carbonyl stretching. In the ^{1}H-NMR spectrum of compound **3**, the resonance peaks three four-proton multiplets at δ 2.35 {2×CH$_3$(CH$_2$)$_2$C*H*$_2$CO-}, δ 1.61 {2×CH$_3$CH$_2$C*H*$_2$CH$_2$CO-} and δ 1.38 {2×CH$_3$C*H*$_2$(CH$_2$)$_2$CO-} and one six-proton multiplet at δ 0.88 {2×C*H*$_3$(CH$_2$)$_3$CO-} correspond to the presence of two pentanoyl groups in the molecule. The deshielding of H-$2'$, and H-$3'$ protons to δ 4.52 (as d, J= 5.2 Hz) and δ 4.33 (as dd, J= 7.7 and 5.6 Hz) from their usual values (~ 4.00 ppm), showed the attachment of the two pentanoyl groups at positions $2'$ and $3'$. The mass spectra of the compound **3** showed a molecular ion peak at *m/z* [M+H]$^+$ 539.60 which is corresponding to a molecular formula $C_{27}H_{42}O_9N_2$. Complete analysis of the FTIR, ^{1}H-NMR, mass spectra and elemental data, the structure of this compound was assigned as $5'$-*O*-octanoyl-$2'$,$3'$-di-*O*-pentanoyluridine **(3)**.

Further support for the structure accorded to the octanoyl derivative **(2)** was obtained by preparation and identification of the dihexanoate **(4)**. The FTIR spectrum of this compound **4** showed absorption band at 1730 cm^{-1} (C=O), thereby suggesting the presence of carbonyl group. In its ^{1}H-NMR spectrum provided two four-proton multiplets at δ 2.35 {2×CH$_3$(CH$_2$)$_3$C*H*$_2$CO-}, and δ 1.62 {2×CH$_3$(CH$_2$)$_2$C*H*$_2$CH$_2$CO-}, an eight-proton multiplet at δ 1.27 {2×CH$_3$(C*H*$_2$)$_2$CH$_2$CH$_2$CO-} and one six-proton multiplet at δ 0.85 {2×C*H*$_3$(CH$_2$)$_4$CO-} indicating the presence of two hexanoyl groups in the compound. The resonance for H-$2'$, and H-$3'$ protons appeared at δ 4.95 (as d, J= 5.2 Hz) and δ 4.39 (as dd, J= 7.8 and 5.6 Hz) which shifted downfield from their precursor compound **(2)** suggesting the attachment of the hexanoyl groups at positions $2'$ and $3'$. Mass spectra of the compound **4** showed a molecular ion peak at *m/z* [M+H]$^+$ 567.50 which is corresponding to a molecular formula $C_{29}H_{46}O_9N_2$. The rest of the FTIR, ^{1}H-NMR, mass spectra and elemental data was in complete agreement with the structure accorded to the hexanoyl derivative as, $2'$,$3'$-di-*O*-hexanoyl-$5'$-*O*-octanoyluridine **(4)**.

Table 4. Physicochemical properties of the synthesized of uridine derivatives (2-13).

Compounds	RT (h)	R$_f$ value	(%) Yield	State
2	6.0	0.50	82	semi solid
3	5.5	0.51	91	pasty mass
4	6.0	0.52	88	thick syrup
5	6.0	0.50	92	pasty mass
6	6.0	0.51	91	needles, m.p. 49-50°C
7	6.5	0.52	86	needles, m.p. 64-66°C
8	6.0	0.55	76	needles, m.p. 65-67°C
9	5.5	0.51	89	semi solid
10	6.0	0.51	72	syrupy
11	6.5	0.50	76	thick syrupy
12	6.0	0.52	93	pasty mass
13	5.5	0.50	89	thick syrupy

In addition, confirmation of the structure accorded to compound **(2)** was achieved by its conversion to and identification by ¹H-NMR of its di-*O*-decanoyl derivative **(5)**. The ¹H-NMR spectrum of compound **5** provided the following characteristic peaks: two four-proton multiplets at δ 2.36 {2×CH$_3$(CH$_2$)$_7$*CH*$_2$CO-} and 1.60 {2×CH$_3$(CH$_2$)$_6$*CH*$_2$CH$_2$CO-}, a twenty four-proton multiplet at δ 1.26 {2×CH$_3$(*CH*$_2$)$_6$(CH$_2$)$_2$CO-} and a six-proton multi-plet at δ 0.85 {2×*CH*$_3$(CH$_2$)$_8$CO-} indicating the introduction of two decanoyl groups to the molecule. In the showed a molecular ion peak at *m/z* [M+H]⁺ 680.29 which is corresponding to a molecular formula C$_{37}$H$_{62}$O$_9$N$_2$. On the basis of complete analysis of the FTIR, ¹H-NMR, mass spectra and elemental data, the structure of this compound was accorded as 2/, 3/-di-*O*-decanoyl-5/-*O*-octanoyluridine **(5)**.

Next effort was to carry out lauroylation of the octanoate **(2)** and provided the lauroyl derivative **(6)**. The FTIR spectrum of the compound **(6)** displayed

absorption band at 1758 cm^{-1} due to carbonyl stretching. It's ^{1}H-NMR spectrum exhibited two four-proton multiplets at 2.37 {2×CH$_3$(CH$_2$)$_9$CH$_2$CO-} and δ 1.59 {2×CH$_3$(CH$_2$)$_8$CH$_2$CH$_2$CO-} a thirty two-proton multiplet at δ 1.21 {2×CH$_3$(CH$_2$)$_8$(CH$_2$)$_2$CO-} and a six-proton multiplet at δ 0.88 {2×CH$_3$(CH$_2$)$_{10}$CO-}, therefore, suggesting the presence of two lauroyl groups in the compound **(6)**. Complete analysis of the FTIR, ^{1}H-NMR and elemental data was in complete agreement with the structure established as 2$^{/}$,3$^{/}$-di-*O*-lauroyl-5$^{/}$-*O*-octanoyluridine **(6)**. Myristoylation of compound **(2)** provided the FTIR spectrum, absorption band at 1736 cm^{-1} corresponded to carbonyl group. The presence of four-proton multiplet at δ 2.35 {2×CH$_3$(CH$_2$)$_{11}$CH$_2$CO-}, a forty-four-proton multiplet at δ 1.26 {2×CH$_3$(CH$_2$)$_{11}$CH$_2$CO-} and a six-proton multiplet at δ 0.88 {2×CH$_3$(CH$_2$)$_{12}$CO-}, in its ^{1}H-NMR spectrum were due to two myristoyl groups in the molecule. Complete analysis of this compound was in complete agreement with the structure accorded to it as the structure of the myristoate was assigned as 2$^{/}$,3$^{/}$-di-*O*-myristoyl-5$^{/}$-*O*-octanoyluridine **(7)**.

The palmitoyl **(8)** was ascertained by observing the following resonance peaks: δ 2.36 {4H, m, 2×CH$_3$(CH$_2$)$_{13}$CH$_2$CO-}, δ 1.24 {52H, m, 2×CH$_3$(CH$_2$)$_{13}$CH$_2$CO-} and δ 0.88 {6H, m, 2×CH$_3$(CH$_2$)$_{14}$CO-}. The introduction of the palmitoyl groups at position 2$^{/}$ and 3$^{/}$ were indicated by appearance of H-2$^{/}$ and H-3$^{/}$ resonance peaks at δ 5.02 and δ 4.87, deshielded considerably from its precursor diol **(2)**. The rest of the FTIR, ^{1}H-NMR and elemental analysis was compatible with structure assigned as 5$^{/}$-*O*-octanoyl-2$^{/}$,3$^{/}$-di-*O*-palmitoyluridine **(8)**. The structure of the octanoyl derivative **(2)** was further supported by its conversion to the pivaloyl derivative **(9)**. The FTIR spectrum showed carbonyl stretching band at 1740 cm^{-1}. In its ^{1}H-NMR spectrum, a characteristic eighteen-proton singlet at δ 1.21 {2×(CH$_3$)$_3$CCO-} was due to the methyl protons of two pivaloyl groups. By analyzing the FTIR, ^{1}H-NMR and elemental data completely, the structure of the dipivaloate was established as 5$^{/}$-*O*-octanoyl-2$^{/}$,3$^{/}$-di-*O*-pivaloyluridine **(9)**. Next, we methanesulfonoate **(10)** was obtained in 83% yield and the FTIR spectrum provided the absorption bands at 1765 cm^{-1} due to C=O stretching and 1365 cm^{-1} for −SO$_2$ stretching. The ^{1}H-NMR spectrum, of this compound showed the following characteristic peaks: two three-proton singlets at δ 3.10 and δ 3.05 (2×CH$_3$SO$_2$-) ascertaining the presence of two methanesulfonyl groups in the molecule. Complete analysis of the FTIR, ^{1}H-NMR and elemental data led us to establish its structure as 2$^{/}$,3$^{/}$-di-*O*-methanesulfonyl-5$^{/}$-*O*-octanoyluridine **(10)**.

The 2$^{/}$,3$^{/}$-di-*O*-benzenesulfonyl derivative **(11)** was also prepared and in its ^{1}H-NMR spectrum, the characteristic peaks at δ 7.90 (4H, m), δ 7.56 (2H, m) and δ 7.41 (4H, m) corresponded the aromatic protons of two phenyl groups in

the compound. The downfield shift of H-2$'$ proton to δ 4.76 and H-3$'$ proton to δ 4.56 from their precursor diol **(2)** values, ascertained the attachment of benzenesulfonyl groups at 2$'$ and 3$'$ positions. The rest of the FTIR, ^{1}H-NMR and elemental analysis was in complete agreement with the structure accorded to the benzenesulfonyl derivative as, 2$'$,3$'$-di-*O*-benzenesulfonyl-5$'$-*O*-octanoyl-luridine **(11)**. Further, the confirmation of the structure of the 5$'$-*O*-octanoyl derivative **(2)** was achieved by its transformation into and identification of the di-*O*-(2-bromobenzoyl) **(12)** and di-*O*-(4-chlorobenzoyl) **(13)** derivatives.

Thus, selective octanoylation of uridine **(1)** was successfully carried out using the direct acylation method. A single, monosubstitution product was isolated pure in each case in reasonably high yields. The octanoyl derivative was further transformed into its different acyl derivatives. These transformations were conducted in order to gather supportive evidences for elucidating structures of the parent acylation products and also to obtain new products of synthetic and biological importance. All these newly synthesized products (Table 3) may be employed as important precursors for the modification of the uridine **(1)** molecule at different positions.

Screening of microbial efficacy

From the experimental results obtained by using a number of selected human pathogenic bacteria (as shown in Figure 2, 3 & 5) were found that selectively acylated uridine derivatives **10, 11** and **13** showed good inhibition against Gram-positive bacteria while compounds **10** and **13** were also very active against Gram-negative bacteria. We also observed that some compounds such as **10** and **13** are highly active against both the Gram-positive and Gram-negative organisms. So, these compounds may be targeted for future studies for their usage as broad spectrum antibiotics. In general, it has been observed that antibacterial results of the selectively acylated uridine derivatives obtained by using various acylating agents follow the order for Gram-positive organisms: **10 > 13> 9 > 11 = 3 > 4 > 5 >12 = 7** and Gram-negative bacteria follow the order: **10 > 13 = 11 > 6= 4 > 5 > 9**.
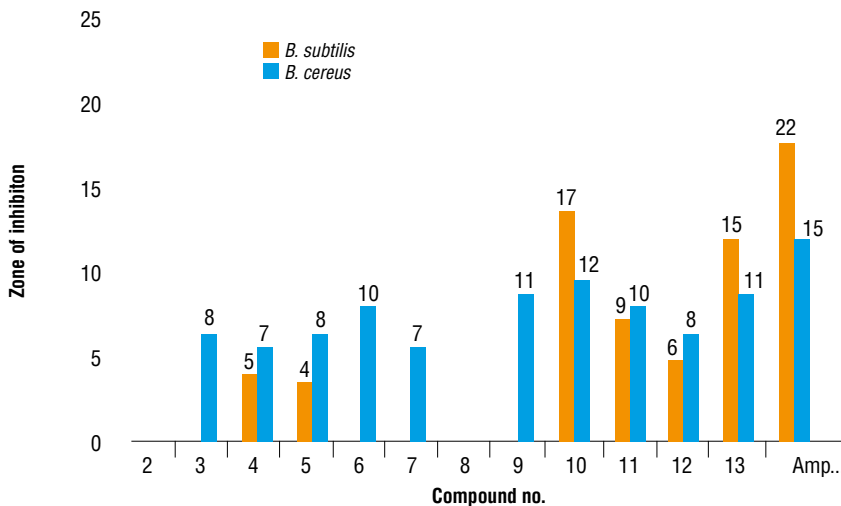
Figure 2. Zone of inhibition observed against Gram-positive bacteria by the test compounds.
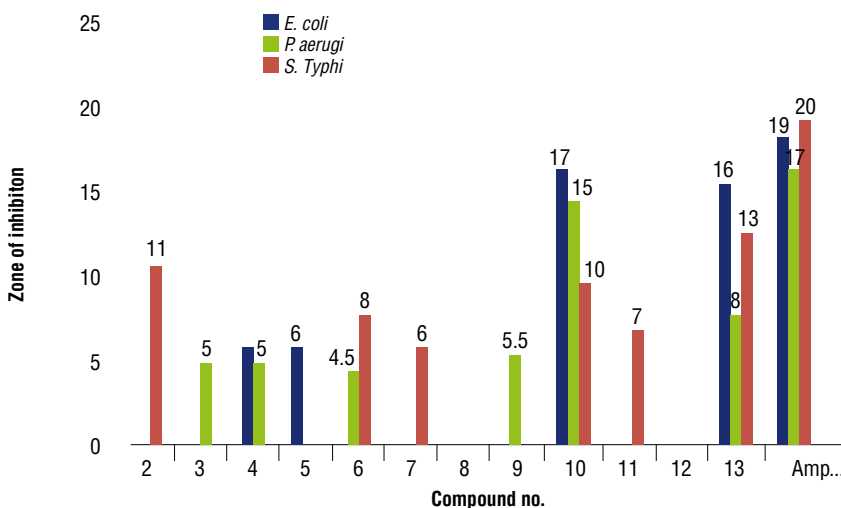
Figure 3. Zone of inhibition observed against Gram-negative bacteria by the test compounds.

From this study we found that among the acylated products, compound **10** showed effective activities (17 mm) against both *B. subtilis* & *E. coli* and compounds **13** (16 mm) and **10** (15 mm) showed high activity against the *E. coli* and *P. aeruginosa* microorganisms, respectively. Some of the tested chemicals showed moderate to marked inhibition against the bacterial pathogens employed. It was also found that some tested chemicals were unable to show any

inhibition at all against the bacterial pathogens employed. It was also observed that the uridine derivatives were found comparatively more effective against Gram-positive bacteria than that of Gram-negative bacteria.

The results obtained from the present investigation of antifungal studies mentioned in Figure 4 and 6 clearly demonstrate that compounds **5** showed the highest inhibition (60.0%) against the *Rhizopers nigricans*. Excellent inhibition was observed in case of compound **10** (55.0%) in which the percent inhibi

tion is very close to the standard antibiotic Nystatin against *Aspergillus niger*. Compounds **4** (50.0%) and **13** (50.0%) showed the good inhibition against the *Aspergillus niger and Rhizopers nigricans*, respectively. However, most of the compounds showed to be less active or toxic to the selected plant pathogens as compared to the standard antibiotic (Nystatin).
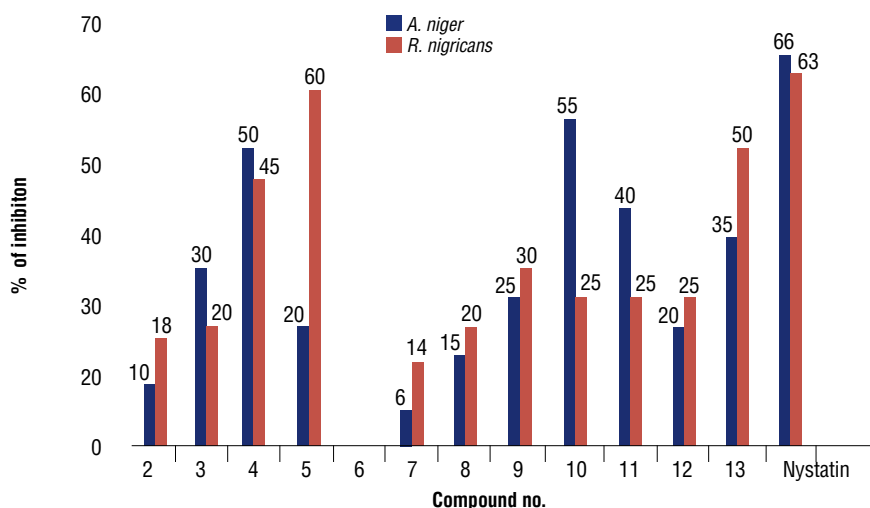
Figure 4. The percentage inhibition of mycelial growth of test fungi by the test compounds.
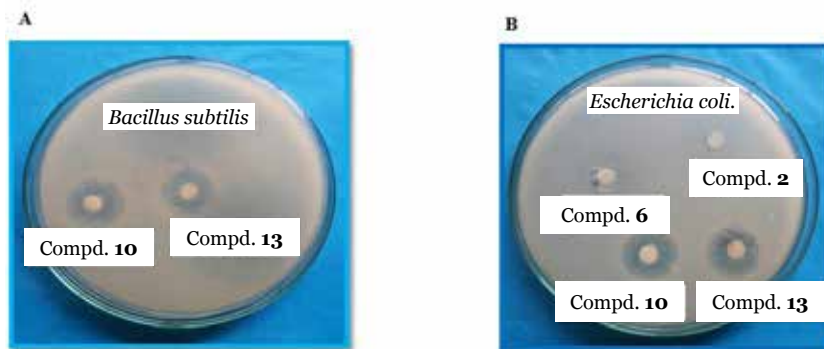
Figure 5. A. Zone of inhibition of the compounds 10 and 13 against *B. subtilis* and B. Zone of inhibition of the compounds 2, 6, 10 and 13 against *E. coli.*
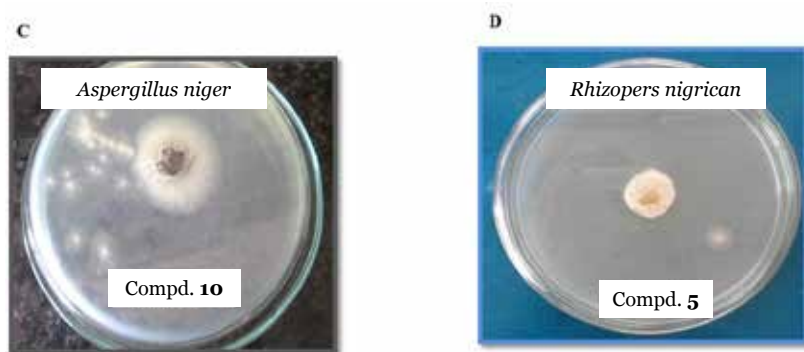
Figure 6. C. The percentage inhibition mycelial growth inhibition of the compound 10 against *A. niger* and D. The percentage inhibition mycelial growth inhibition of the compound 5 against *R. nigricans.*

So, it was found that the newly synthesized and reported compounds **5** and **10** were very much effective against both fungal strains. These antimicrobial efficacies of our tested compounds were in accordance with the results we observed before[34,35]. The brine shrimp lethality assay is considered a useful tool for assessment of toxicity. The cytotoxic activity of the acylated derivatives of uridine (Scheme 1, 2, Table 1) in the brine shrimp lethality bioassay showed different rate mortality with different concentrations. It is expected that this piece of work employing uridine derivatives as test compounds will open the scope for further work on the development of pesticides and medicines sectors.

CONCLUSION

The synthesized uridine derivatives have shown promising antibacterial and antifungal activities. Out of twelve active compounds, three of them (**5**, **10** and **15**) have shown very good antimicrobial inhibiting activity. However, these three compounds have also shown significant cytotoxic activity against brine shrimp lethality assay. Therefore, it is expected that the newly acylated uridine derivatives might show potential antiviral, antidiabetic, anticancer and anti-inflammatory activities.

ACKNOWLEDGEMENT

REFERENCES

1. Carlezon, J. W. A.; Mague, S. D.; Parow, A. M.; Stoll, A. L.; Cohen, B. M.; Renshaw, P. F. Antidepressant-like Effects of Uridine and Omega-3 Fatty Acids are Potentiated by Combined Treatment in Rats. *Biol. Psychiatry.* **2005**, *57*, 343-350

2. Jonas, D. A.; Elmadfa, I.; Engel, K. H.; Heller, K. J.; Kozianowski, G.; Konig, A.; Muller, D.; Narbonne, J. F.; Wackemagel, W.; Kleiner, J. Safety Considerations of DNA in Food. *Annals Nutr. Metabol.* **2001**, *45*, 235-254.

3. Macdonald, G.; Assef, R.; Guiffre, A.; Lo, E. Vasoconstrictor Effects of Uridine and its Nucleotides and their Inhibition by Adenosine. *Clin. Exp. Pharmacol. Physiol.* **1984**, *11*, 381-384.

4. Siggins, G. R.; Gruol, D. L.; Padjen, A. L.; Formans, D. S. In: Iontophoresis and Transmitter Mechanisms in the Mammalian Central Nervous System. Ryall RW, Kelly JS. Editors, *Elsevier*/North-Holland, **1978**, 453-455.

5. Groeningen, C. J.; Leyva, A.; Kraal, I.; Peters, G. J.; Pinedo, H. M. Clinical and Pharmacokinetic Studies of Prolonged Administration of High-dose Uridine Intended for Rescue from 5-FU Toxicity. *Cancer Treat Rep.* **1986**, *70*, 745-750.

6. Morris, D. J. Adverse Effects and Drug Interactions of Clinical Importance with Antiviral Drugs. *Drug Saf.* **1994**, *10*, 281-291.

7. De Clercq, E. A 40-Year Journey in Search of Selective Antiviral Chemotherapy. *Annu. Rev. Pharmacol. Toxicol.* **2011**, *51*, 1-24.

8. De Clercq, E.; Holy, A. Acyclic Nucleoside Phosphonates: a Key Class of Antiviral Drugs. *Nat. Rev. Drug Discovery.* **2005**, *4*, 928-940.

9. Ri, M.; Tashiro, E.; Oikawa, D.; Shinjo, S.; Tokuda, M.; Yokouchi, Y, et al. Identification of Toyocamycin, an Agent Cytotoxic for Multiple Myeloma Cells, as a Potent Inhibitor of ER Stress-Induced XBP1 mRNA Splicing. *Blood Cancer J.* **2012**, *2*, e79.

10. Damaraju, V. L.; Damaraju, S.; Young, J. D.; Baldwin, S. A.; Mackey, J.; Sawyer, M. B.;

Cass, C. E. Nucleoside Anticancer Drugs: the Role of Nucleoside Transporters in Resistance to Cancer Chemotherapy. *Oncogene*. **2003**, *22*, 7524-7536.

11. Najera, I. Resistance to HCV Nucleoside Analogue Inhibitors of Hepatitis C Virus RNA-Dependent RNA Polymerase. *Curr. Opin. Virol.* **2013**, *3*, 508-513.

12. Jordheim, L. P.; Durantel, D.; Zoulim, F.; Dumontet, C. Advances in the Development of Nucleoside and Nucleotide Analogues for Cancer and Viral Diseases. *Nat. Rev. Drug Discovery*. **2013**, *12*, 447-464.

13. Tsuda, Y.; Haque, E. Regioselective Introduction of p-Coumaroyl Group to α-L-Arabinopyranosides. Total Synthesis of Inundoside-G and Inundoside-D1. *Chem. Pharm. Bull.* **1983**, *31*, 1437-1439.

14. Itoh, M.; Hagiwara, D.; Notani, J. A Simple and Mild Esterification Method for Carboxylic Acids Using Sulfonate-type Coupling Reagents. *Synthesis*. **1975**, *7*, 456-458.

15. Kondo, Y. Selective Benzoylation of Methyl α- and β-D-Xylopyranoside. *Carbohydr. Res*. **1982**, *107*, 303-311.

16. Sugihara, J. M. Relative Reactivities of Hydroxyl Groups of Carbohydrates. *Adv. Carbohydr. Chem.* **1953**, *8*, 1-44.

17. Wagner, D.; Verheyden, J. P. H.; Moffatt, J. G. Preparation and Synthetic Utility of some Organotin Derivatives of Nucleosides. *J. Org. Chem.* **1974**, *39,* 24-30.

18. Williams, J. M.; Richardson, A. C. Selective Acylation of Pyranosides-I. Benzoylation of methyl α-D-glycopyranosides of Mannose, Glucose and Galactose. *Tetrahedron*. **1967**, *23*, 1369-1378.

19. Kim, S.; Chang, H.; Kim, W. J. Regioselective Acylation of some Glycopyranoside Derivatives. *J. Org. Chem.* **1985**, *50*, 1751-1752.

20. Kabir, A. K. M. S.; Dutta, P.; Anwar, M. N. Synthesis of some New Derivatives of D-Mannose. *Chittagong Univ. J. Sci.* **2005**, *29*, 01-08.

21. Ichinari, M.; Nakayama, K.; Hayase, Y. Synthesis of 2,4-Dioxoimidazolidines from 2-arylimino-1,3-triazines and their Antifungal Activity. *Heterocycles* (Tokyo). **1988**, *27*, 2635-2641.

22. Gawande, N. G.; Shingare, M. S. Synthesis of Some Thiazolylthiosemicarbazides, Triazoles, Oxazoles, Thiadiazoles & their Microbial Activity. *Ind. J. Chem.* **1987**, *26*, 387-389.

23. Gupta, R.; Paul, S.; Gupta, A. K.; Kachroo, P. L.; Bani, S. Synthesis and Biological Activities of Some 2-Substituted Phenyl-3-(3-alkyl/aryl-5,6-dihydro-s-triazolo[3,4-b][1,3,4]thiazolo-6-yl)-indoles. *Ind. J. Chem.* **1997**, *36*, 707-710.

24. Singh, H.; Shukla, K. N.; Dwivedi, R.; Yadav, L. D. S. Clycloaddition of 4-Amino-3-mercepto-1,2,4-triazole to Heterocumulenes and Antifungal Activity of the Resulting 1,2,4-Triazolo[3,4-c]-1,2-dithia-4,5-diazines. *J. Agric. Food Chem.* **1990**, *38*, 1483-6.

25. Kabir, A. K. M. S.; Matin, M. M.; Kawsar, S. M. A. Synthesis and Antibacterial Activities of Some Uridine Derivatives. *Chittagong Univ. J. Sci.* **1998**, *22*, 13-8.

26. Kawsar, S. M. A.; Kabir, A. K. M. S.; Manik, M. M.; Hossain, M. K.; Anwar, M. N. Antibacterial and Mycelial Growth Inhibition of Some Acylated Derivatives of D-Glucopyranoside. *Int. J. Biosci.* **2012**, *2*, 66-73.

27. Kabir, A. K. M. S.; Kawsar, S. M. A.; Bhuiyan, M. M. R.; Islam, M. R.; Rahman, M. S. Biological Evaluation of Some Mannopyranoside Derivatives. *Bull. Pure Appl. Sci.* **2004**, *23*, 83-91.

28. Kawsar, S. M. A.; Faruk, M. O.; Rahman, M. S.; Fujii, Y.; Ozeki, Y. Regioselective Synthesis, Characterization and Antimicrobial Activities of Some New Monosaccharide Derivatives. *Sci. Pharm.* **2014**, *82*, 1-20.

29. Kawsar, S. M. A.; Sharif, U.; Manchur, M. A.; Fujii, Y.; Ozeki, Y. Acylation of D-Glucose Derivatives Over C_5H_5N: Spectral Characterization and *In Vitro* Antibacterial Activities. *Int. J. Biol. Chem.* **2015**, *9*, 269-282.

30. Bauer, A. W.; Kirby, W. M. M.; Sherris, J. C.; Turck, M. Antibiotic Susceptibility Testing by a Standardized Single Disc Method. *American J. Clin. Pathol.* **1966**, *45*, 439-476.

31. Miah, M. A. T.; Ahmed, H. U.; Sharma, N. R.; Ali, A.; Miah, S. A. Antifungal Activity of Some Plant Extracts. *Bang. J. Bot.* **1990**, *19*, 05-10.

32. Grover, R. K.; Moore, J. D. Toximetric Studies of Fungicides Against the Brown Rot Organisms *Sclerotinia flucticola* and *S. laxa*. *Phytopathology.* **1962**, *52*, 876-880.

33. Kabir, A. K. M. S; Matin, M. M; Kawsar, S. M. A. Selective Acylation of Uridine Using the Dibutyltin Oxide and Direct Methods. *Chittagong Univ. Stud. Part-II: Sci.* **1997**, *21*, 39-45.

34. Kawsar, S. M. A.; Nishat, S. S. B. S.; Manchur, M. A.; Ozeki, Y. Benzenesulfonylation of Methyl α-D-Glucopyranoside: Synthesis, Characterization and Antibacterial Screening. *Int. Lett. Chem. Phys. Astron.* **2016**, *64*, 95-105.

35. Kawsar, S. M. A.; Hamida, A. A.; Sheikh, A. U.; Hossain, M. K.; Shagir, A. C.; Sanaullah, A. F. M.; et al. Chemically Modified Uridine Molecules Incorporating Acyl Residues to Enhance Antibacterial and Cytotoxic Activities. *Int. J. Org. Chem.* **2015**, *5*, 232-245.

Dexketoprofen trometamol-loaded Eudragit® RL 100 nanoparticle formulation, characterization and release kinetics

A. Alper Öztürk[1*], Evrim Yenilmez[1], Yasemin Yazan[1]

1 Anadolu University, Faculty of Pharmacy, Department of Pharmaceutical Technology, Eskişehir, Turkey.

ABSTRACT

Development and *in vitro* evaluation of dexketoprofen trometamol (DT)-loaded nanosized and controlled release drug delivery system was aimed in this study.

DT-loaded Eudragit® RL 100 polymeric nanoparticles were prepared using nano spray-dryer. Structures of DT-loaded polymeric nanoparticles were elucidated by particle size and zeta potential measurements, shape and surface imaging, thermal analysis, X-ray diffraction and FT-IR and ¹H-NMR determinations.

The particle size of the formulations was measured in the range of 475.5-798.7 nm. The droplet size distribution of the formulations was observed in the range of 0.349-0.395. These results showed that nanosized and monodispersed formulations were prepared. The drug content was found to be in the range of 35-38%. DT-loaded particles exhibited nanostructured and spherical shape. In vitro release studies showed extended release of DT. Release was found to fit Korsmeyer-Peppas kinetic model using DDSolver software program.

Depending on the *in vitro* test results obtained, formulations developed in this study seem to extend the release of DT from the nanoparticles prepared which are promising for prolonging analgesic activity.

Keywords: Dexketoprofen trometamol, Eudragit® RL 100, Polymeric nanoparticle, Spray-drying, DDSolver.

INTRODUCTION

DT which is in clinical use since 1996 is the water-soluble salt of dextrorotatory enantiomer of racemic ketoprofen, a non-steroidal anti-inflammatory drug (NSAID). Since dexketoprofen is more lipophilic than ketoprofen, it is rapidly absorbed followed by the activity starting in a short time and reaching

maximum plasma concentration in a short period.[1]

Polymeric nanoparticles are matrix systems that are prepared with natural or synthetic polymers with sizes in the range of 10 to 1000 nm. Nanoparticles are defined as either nanospheres or nanocapsules depending on their structures where the active substance is solubilized, entrapped and/or adsorbed onto the particle surface. Natural (proteins, polysaccharides) and synthetic polymers (synthesized during production, pre-synthesized) are used in the production of polymeric nanoparticles.[2] Both natural and synthetic particulate drug delivery systems are preferred to obtain controlled drug release for increasing the life quality of patients.[3]

A number of approaches can be used to manufacture polymeric nanoparticles such as salting-out, solvent evaporation, supercritical fluid technology, microemulsion, mini-emulsion, surfactant-free emulsion, and interfacial polymerization.[4] Spray-drying subtitues for a single-step, continuous and scalable procedure devoted to transforming liquid systems

Eudragit® RL, also called Eudragit Retard L, is a copolymer of poly(ethyl acrylate, methyl methacrylate and chloro trimethyl ammonium methyl methacrylate) containing 8.8 %-12 % quaternary ammonium groups. It is insoluble at physiologic pH values with limited swelling thus representing a good candidate for drug dispersions.[8]

Drug release is a significant topic in the context of drug development for years. With intensive progress in drug formulation design with increasing revolution and innovation, drug release is introduced giving it a substantial role in drug formulation development and quality control. It is a relatively rapid and inexpensive technique to predict *in vivo* absorption of a drug formulation. Quantitative evaluation of drug dissolution characteristics is of great interest to the pharmaceutical scientists owing to its outstanding advantages.[9]

DDSolver is a menu-driven add-in program which can be used to facilitate the modeling of dissolution data using nonlinear optimization methods based on a built-in model library containing fourty dissolution models. It offers a number of benefits over the other software packages prepared for dissolution kinetic modeling.[10,11,12] Among the dissolution kinetic models for drug release are zero order, first order, Hixson-Crowell, Higuchi, Korsmeyer-Peppas models, etc. [13,14]

In this study, DT-loaded Eudragit® RL 100 polymeric nanoparticles were prepared using Nano Spray Dryer B-90 and characterized. In vitro dissolution data and kinetic modelling were investigated through DDSolver program aiming sustained release of DT.

METHODOLOGY

DT was a kind gift of Abdi İbrahim (İstanbul, Turkey). Eudragit® RL 100 was obtained from Degussa Röhm Pharma Polymers (Germany). Methanol and deutero chloroform were both purchased from Merck (Germany) while acetonitril, potassium phosphate monobasic and sodium hydroxide were purchased from Sigma-Aldrich (Germany). All other chemicals and reagents were used of pharmaceutical and analytical grade.

Preparation of nanoparticles

For the preparation of the polymeric solution with and without DT, Eudragit® RL 100 was dissolved in methanol under a magnetic stirrer at 250 rpm for 2 hrs to obtain a clear solution. DT was added to this clear solution and stirred further for another 5 minutes. Nano spray-dryer (Nano Spray-Dryer B-90, BÜCHI, Switzerland) was conditioned 30 minutes using methanol to obtain the desired levels of spraying, pump level, inlet temperature, outlet temperature, gas flow and ambient temperature prior to delivering the polymeric soluton. Inlet temperature of 120°C, outlet temperature of 54°C and a needle with 4 μm pore size were used during application (Table 1). Dried nanoparticles were collected in the collecting chamber. Contents of formulations prepared were summarized in Table 2.

Table 1. Spray-drying conditions

Inlet temperature	Outlet temperature	Pump level	Spray level
120°C	54°C	3	100 %

Table 2. Content of polymeric nanoparticles

Code	Eudragit® RL 100 (g)	DT (g)	Methanol (mL)
ERL-blank	1	-	100
ERL-1	1	0.05	100
ERL-2	1	0.1	100
ERL-3	1	0.15	100

__Blank:__ Formulation without active ingredient

Characterization

Morphology

Particle shape and surface properties of the freshly prepared polymeric nano-particles (PNP) and pure DT were examined by SEM (Zeiss Ultra Plus Fesem, Germany) after spreading the formulation onto the carbon band and coating with gold.

Particle size, polydispersity index (PDI) and zeta potential

Particle size and distribution of prepared PNPs were measured (Zetasizer Nano ZS, Malvern, UK) by dispersing the formulation in distilled water adjusted to a conductivity of 50 µS with NaCl to avoid measurement deviations. Zeta potential values were determined using the same instrument in a disposable folded capillary zeta cell, at 25°C room temperature and diluted with distilled water.

Thermal analysis (DSC)

Thermal analyses using DSC (Schimadzu DSC-60, Japan) of pure DT, pure polymer and PNPs prepared were performed against an aluminum reference and nitrogen gas at a flow rate of 50 mL. min^{-1} with a temperature increase of 10°C.min^{-1} in the 30-300°C range.

X-ray diffraction (XRD)

XRD analyses of pure DT, pure polymer and PNPs prepared were performed with Rikagu generator (XRD Rikagu Rint 2000, Japan) at a speed of 40 kV, 30 mA current intensity, 2Θ angle and 2°min^{-1} in the range of 2-40°.

Fourier transform infrared spectrophotometry (FT-IR)

FT-IR spectra of pure DT, pure polymer and PNPs prepared were determined at 4000-500 cm^{-1} wavelength using FT-IR (Schimadzu IR Prestige-21, Japan).

Nuclear magnetic resonance (NMR)

NMR analysis (^{1}H-NMR) of pure DT, pure polymer and PNPs prepared were determined (Bruker 500 MHz UltraShield NMR, Germany) by dissolving the samples in deutero chloroform ($CDCl_3$).

HPLC method

HPLC (Shimadzu-20 A, Japan) equipped with reversed- phase NUKLEODUR column (diameter, 4.6 mm; length, 250 mm, C_{18} Gravity, 5 µm pore size) was used. Determination of DT was achieved by a modified HPLC method. 25:75 (v/v) acetonitrile-methanol was selected as the mobile phase following preliminary tests for the best resolution of DT. Flow rate of mobile phase was 1

mL·min⁻¹ and constant amount of 25 μL was injected using an automatic injector (Shimadzu, Japan). Fluorescent detector (Shimadzu, Japan) was used at 258 nm and the column temperature was set to 30°C. HPLC method used was validated in reference to previous studies.[15]

Encapsulation efficiency (EE %)

Distilled water was used as a solvent for determining DT amount. 5 mg accurately weighed ERL-1 was put in a 2.5 mL-Eppendorf tube and 2 mL distilled water was added. After ultrasonication for 5 minutes, the upper transparent portion was removed by centrifugation at 11.000 rpm for 5 minutes and the sample was analyzed following dilution and filtration.

To determine DT incorporated into PNPs, 2 mL of the mobile phase where both DT and Eudragit® RL 100 were previously dissolved was added to the remaining particles. Following ultrasonication for 5 minutes, the clear solution obtained was filtered through the polyamide filter after adequate dilutions. Tests were repeated 3 times for each formulation. Loading capacity was calculated using the equation given below.[16]

EE %= [[(Drug concentration in formulation)-(Drug concentration in supernatant)]/ (Drug concentration in formulation)]x100   Eq. 1

In vitro release study

In vitro release of DT from Eudragit® RL 100 PNPs was investigated over 48 hrs using a dialysis membrane. PNP containing 1 mg DT was placed in a cellulose acetate dialysis bag (MW cut off 12-14 kDa, Sigma). After the addition of 1 mL of dissolution medium, the bag was sealed at both ends. Dialysis bag was then placed into an amber glass beaker containing 100 mL PBS (pH 7.4) at 37°C±0.5°C as the dissolution medium under continuous stirring of 100 rpm. The receptor compartment was closed to prevent evaporation of the dissolution medium. Samples were withdrawn at regular time intervals and the same volume was replaced by fresh dissolution medium. DT concentration in the samples was quantified by HPLC method.

Determination of *In vitro* kinetics with DDSolver program

Data obtained in the *in vitro* drug release studies was further investigated for release kinetics using DDSolver software program.[9]

Statistical Analysis

Each experiment was carried out three independent times and the data are presented as mean ± standard error (SE). Microsoft Excel and DDSolver were employed for statistical analysis.

RESULTS AND DISCUSSION

Morphology

SEM images of pure DT and PNPs were given in Figure 1. Figure 1 clearly shows that crystal structure of DT was diminished in the SEM images of PNPs indicating successful loading of DT into the polymer.
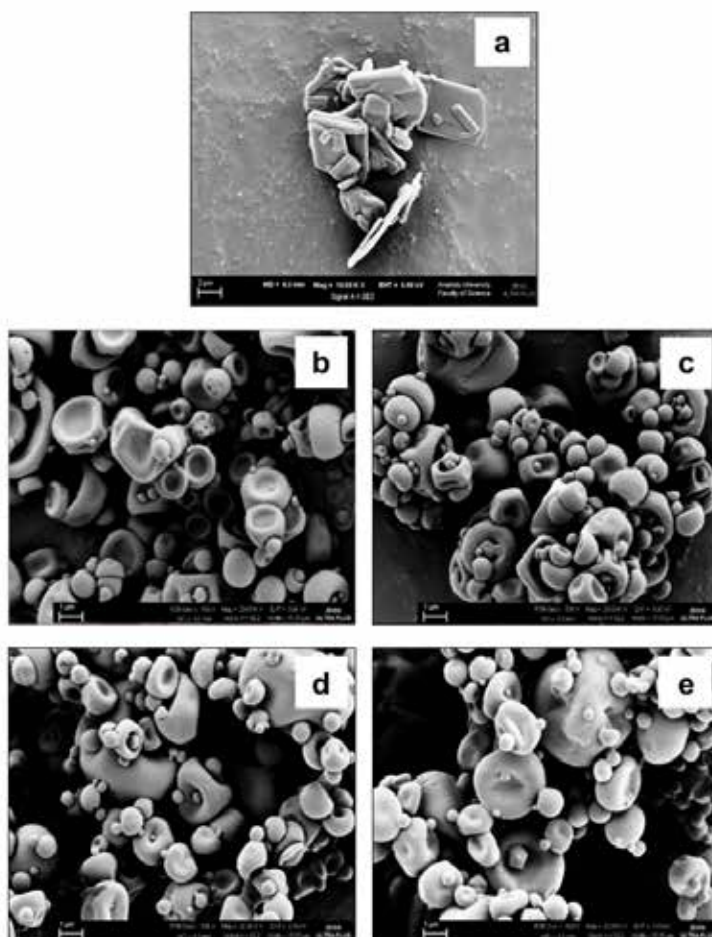

Figure 1. SEM images of pure DT and PNPs, **a:** DT, **b:** ERL-blank, **c:** ERL-1, **d:** ERL-2, **e:** ERL-3

Particle size, PDI and zeta potential

Results of particle size, PDI and zeta potential measurements were given in Table 3. PDI value, used to define particle size distribution, is between 0.01 and 0.5-0.7 for single phase systems. A value higher than 0.7 is indicative of heterogeneous distribution.[17] PDI value of all PNPs prepared in this study was determined to be <0.395±0.015 (mean±SE) meaning uniform particle distributions for all PNPs.

Since Eudragit® RL 100 contains 8.8 %-12 % quaternary ammonium groups, it stands out as a suitable cationic polymer for preparing pharmaceutical dispersions.[18] All PNPs prepared with Eudragit® RL 100 were found to have positive zeta potential value owing to the cationic ammonium groups in its structure. Zeta potential values of all PNPs were in the range of +20.15±0.51 mV and +45.05±0.46 mV. The lowest zeta potential value (+20.15±0.51 mV) was obtained for ERL-3 with the highest DT content when compared to ERL-2, ERL-1 and ERL-blank.

Stability of nanoparticles dispersed in aqueous media is dependent on electrostatic or stearic stability, or both, and high zeta potential value ($\geq$ +/- 30 mV) is correlated with good colloidal dispersion stability.[19] Depending on this knowledge, it can be interpreted that the PNPs prepared were stable.

Table 3. Particle size, PDI and zeta potential values

Code	Particle size (nm) ± SE	Polydispersity index ± SE	Zeta potential ± SE
ERL-blank	475.501±3.852	0.381±0.012	+ 39.11±0.40
ERL-1	540.400±1.715	0.395±0.015	+ 45.05±0.46
ERL-2	571.500±0.615	0.349±0.026	+ 43.81±2.10
ERL-3	798.700±2.312	0.351±0.060	+ 20.15±0.51

*SE: Standard Error

Thermal analysis (DSC)

Thermograms of ERL-blank and all the other freshly prepared formulations were presented in Figure 2 in comparison to DT and Eudragit® RL 100. DSC analyses showed the disappearance of endothermic DT peak observed at 105.1°C in thermograms of all PNPs. Complete disappearance of DT peak is most probably due to homogeneous polymer matrix formation or dilution effect of the polymer.[20] In any case, disappearance of DT peak in all PNPs indicates successful DT loading into nanoparticles, homogenous matrix formation and amorphous DT structure with incorporation significantly reducing its crystal structure.[21]

Figure 2. Thermograms of DT, pure polymer and PNPs, **a:** DT, **b:** Eudragit® RL 100, **c:** ERL-blank, **d:** ERL-1, **e:** ERL-2, **f:** ERL-3

X-ray diffraction (XRD)

XRD profiles of ERL-blank and all the other freshly prepared formulations were shown in Figure 3 in comparison to DT and the polymer. XRD analysis is a well-defined analytical method frequently used in research because it reveals the molecular structure of PNPs, examines the crystal state, performs polymorphism studies and also provides information about stability.[22,23] DT dispersion in the polymer matrix at the molecular level and amorphous form of PNPs were determined in this study.[24] The fact that even low intense DT peaks in XRD profiles of PNPs are not seen suggests quite low DT amount adhering to the PNP surface.[16] Disappearance of DT peak for all PNPs may be due to the dilution effect of the polymer network.[18]

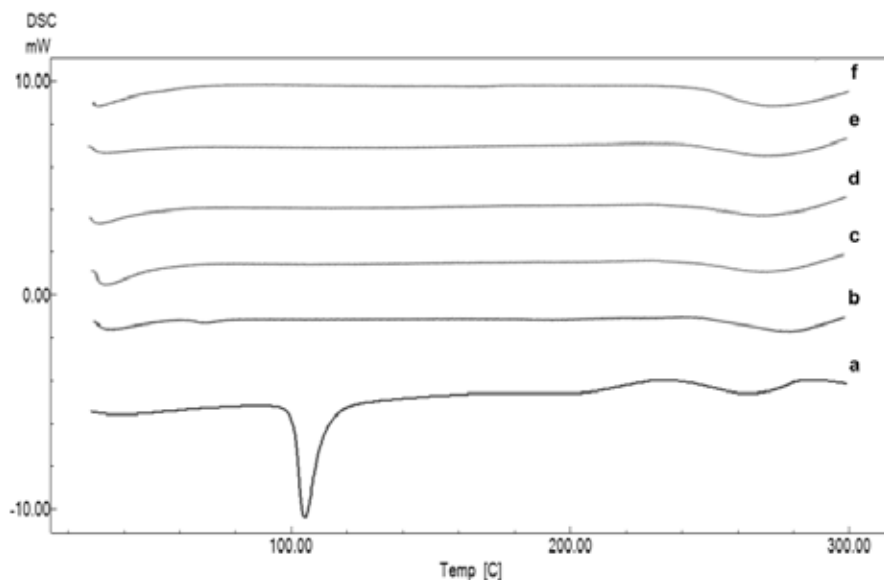**Figure 3.** XRD profiles of DT, pure polymer and PNPs, **a:** DT, **b:** Eudragit® RL 100, **c:** ERL-blank, **d:** ERL-1, **e:** ERL-2, **f:** ERL-3

Fourier transform infrared spectrophotometry (FT-IR)

FT-IR spectra of ERL-blank and all freshly prepared PNPs were given in Figure 4 in comparison to DT, Eudragit® RL 100 and the physical mixture. The same spectra of both ERL-blank and pure polymer indicates that production parameters of PNPs had no affect on preparation.[25] No new peak formation of DT in FT-IR specta of PNPs prepared can be evaluated as no existence of chemical interaction between DT and the polymer.[18] It was thought that DT was molecularly dispersed in the polymeric matrix due to the decrease in DT peaks seen in ERL-1, ERL-2 and ERL-3 spectra. This was also supported by thermal and XRD analyses.[26]
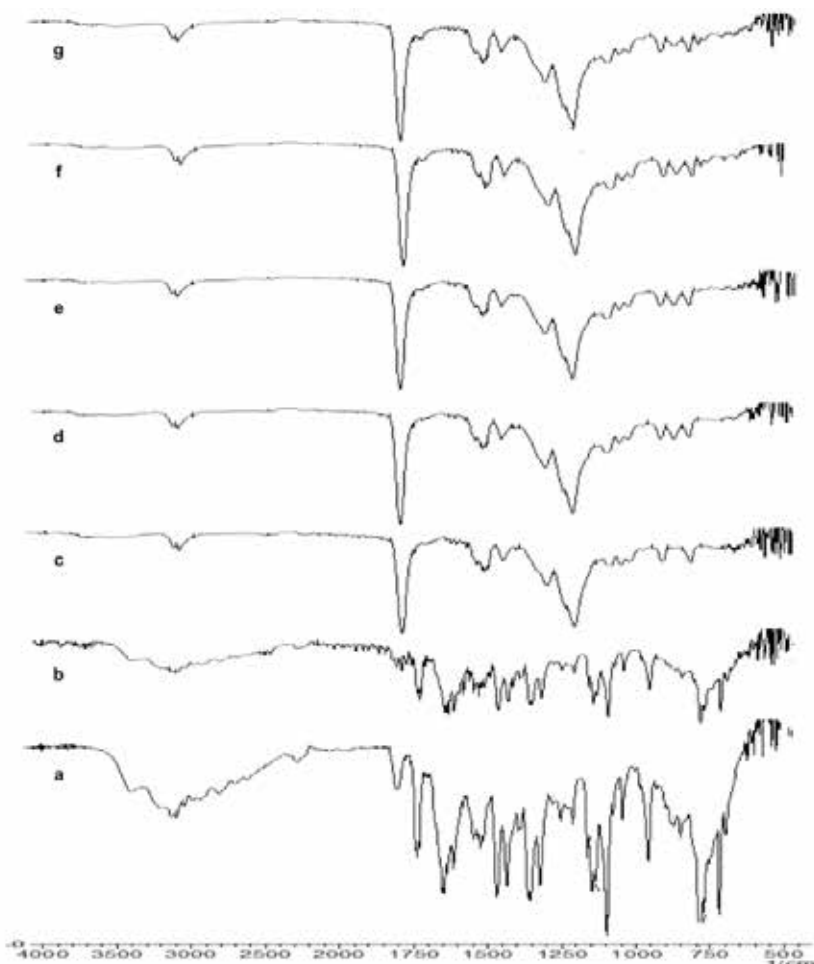
Figure 4. FT-IR spectra of DT, pure polymer, physical mixture and PNPs, **a:** DT **b:** Physical mixture, **c:** Eudragit® RL 100, **d:** ERL-blank, **e:** ERL-1, **f:** ERL-2, **g:** ERL-3

Nuclear magnetic resonance (NMR)

^{1}H-NMR spectra of ERL-blank and all freshly prepared PNPs were presented in Figure 5 in comparison to DT and the pure polymer. ^{1}H-NMR analysis performed in this study is significant for showing the interaction of DT with the polymer and any change in the polymeric structure with addition of DT. Similar spectra of ERL-blank and pure polymer and no peak existence of DT at 7-8 ppm were determined.[16] Presence of characteristic DT peaks was observed in spectra of ERL-1, ERL-2 and ERL-3. Peak intensity which was affected by the

amount of DT added to PNPs was higher in the spectrum of ERL-3 containing the highest DT amount. It was decided that DT was molecularly dispersed in the polymeric structure depending on the correlation between characteristic DT peak and molecular distribution and also DT concentration.[16] This was also interpreted as DT loading into nanoparticles.

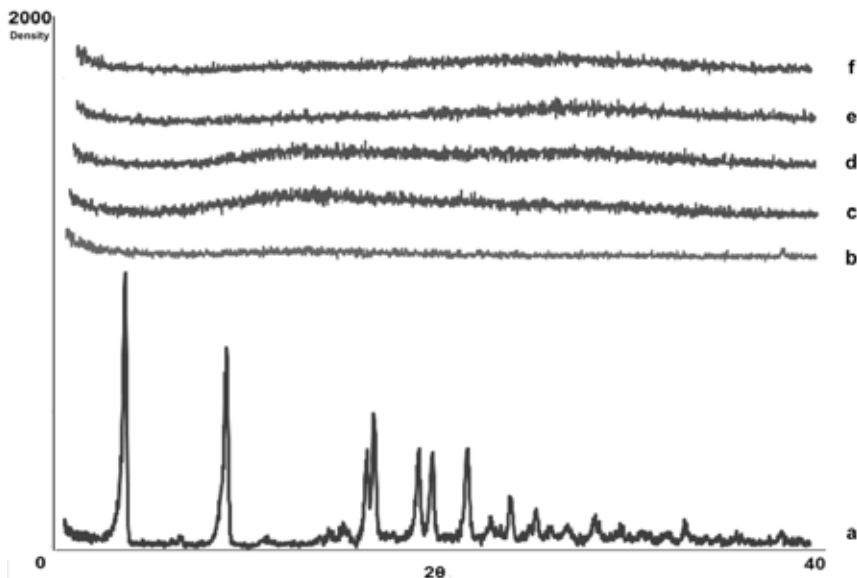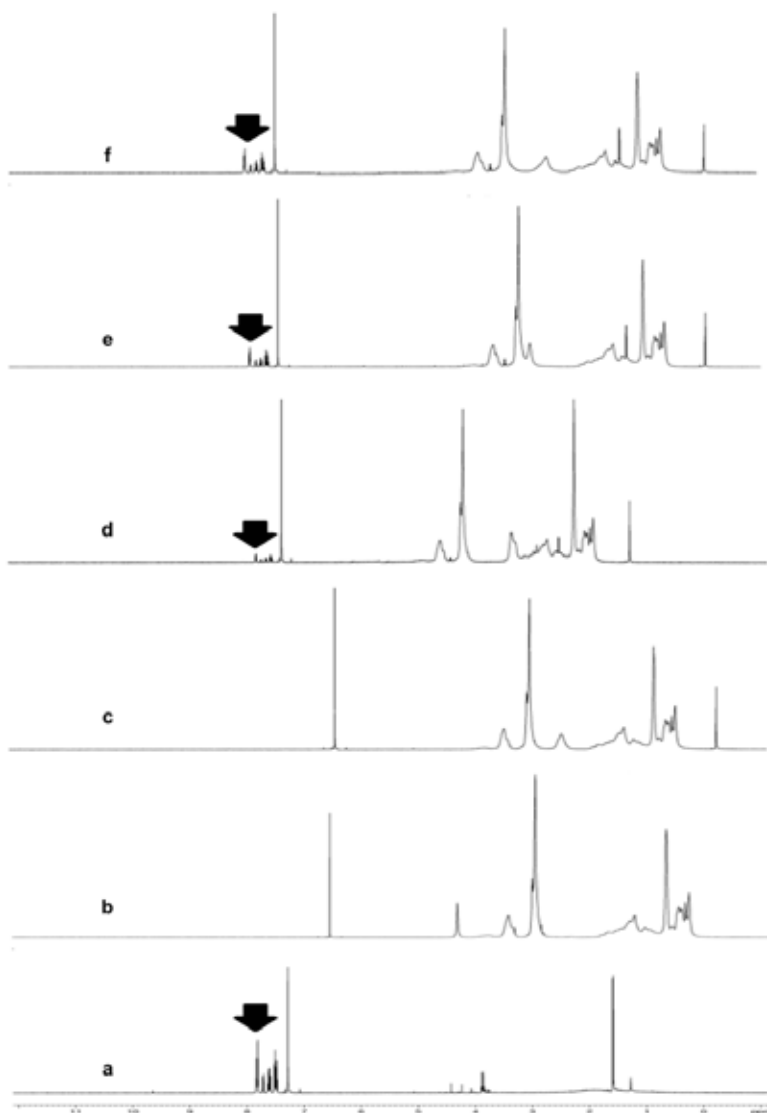**Figure 5.** 1H-NMR spectra of DT, pure polymer and PNPs, **a:** DT, **b:** Eudragit® RL 100, **c:** ERL-blank, **d:** ERL-1, **e:** ERL-2, **f:** ERL-3

HPLC method

Modified HPLC method for DT quantification was validated for linearity, specifity, precision and accuracy.[27] Linearity was determined to be at the concentration range of 10-80 µg·mL^{-1} with the regression equation of y = 67363 x - 243811 (r²=0 9999). The method used was decided to be precise owing to RSD values of < 2 % for repeatability and intermediate precision. Accuracy of the method was determined to be 100.768 % ± 0.3975, 99.964 % ±0.439 and 99.533 % ± 0.312 for the DT concentrations of 20 µg.mL^{-1}, 40 µg.mL^{-1} and 60 µg.mL^{-1}, respectively (n = 6). Recovery of the method was found satisfactory depending on the <2 % RSD value. Limit of detection (LOD) was found to be 0.5613 µg.mL^{-1} while limit of quantitation (LOQ) was 1.7010 µg.mL^{-1}. Conclusively, procedure proposed in this study suggests routine, simultaneous and concurrent use for DT quantification.

Encapsulation efficiency (EE %)

EE % values calculated according to Eq. 1 were given in Table 4. Nanoparticles composed of natural/synthetic polymers or lipids are usually smaller than 1000 µm in size. Active drug ingredient may either be incorporated into the matrix or superficially adsorbed. Therefore, both the amount of encapsulated and the amount of adsorbed to the polymer surface should be determined in analyzing the total amount in the nanoparticulate system.[16] In this study, loading capacity of ERL-2 was found to be the highest among the other formulations. EE% of ERL-3 was lower among the prepared particles. It can be said that the amount of DT loaded on the polymer matrix decreases as the amount of the active ingredient increases.

Table 4. EE % values

Code	ERL-blank	ERL-1	ERL-2	ERL-3
EE % ± SE	-	37.079±1.340	38.873±1.027	35.177±0.458

*SE= standard error

In vitro release

In vitro release and also detailed 2-hr release profiles of pure DT and PNPs prepared were presented in Figure 6. In vitro release test results are frequently used not only for monitoring stability of drugs but also for predicting *in vivo* absorption.[9] Due to the short half-life of DT and rapid release from the conventional tablet formulations marketed, patients need to take the drug at least 3 times a day. Therefore, preparing polymeric nanoparticles to provide initial dose with the superficial DT and maintenance dose with DT entrapped

was aimed in this study. Testing *in vitro* release of pure DT resulted in 92.217 %±0.682 (mean±SE) release within the first 2 hrs while release from all PNPs prepared were sustained. Initial rapid release observed from PNPs was most probably dependent on the rapid dissolution of superficially adsorbed DT and it was found that DT entrapped in PNPs was released in a sustained pattern. ERL-3 demonstrated higher amounts of DT release in 48 hrs with a release of 51.870±1.505 (mean±SE).

In vitro release kinetics

As a result of applying *in vitro* release study data obtained to different kinetic models using DDSolver program, rate constant (k), determination coefficient (r^2) and Akaike information criterion (AIC) found were shown in Table 5. Korsmeyer-Peppas model was determined to be the most appropriate kinetic model for DT release from all PNPs. Release kinetic profiles of all PNPs corresponding to the Korsmeyer-Peppas model were presented in Figure 7.
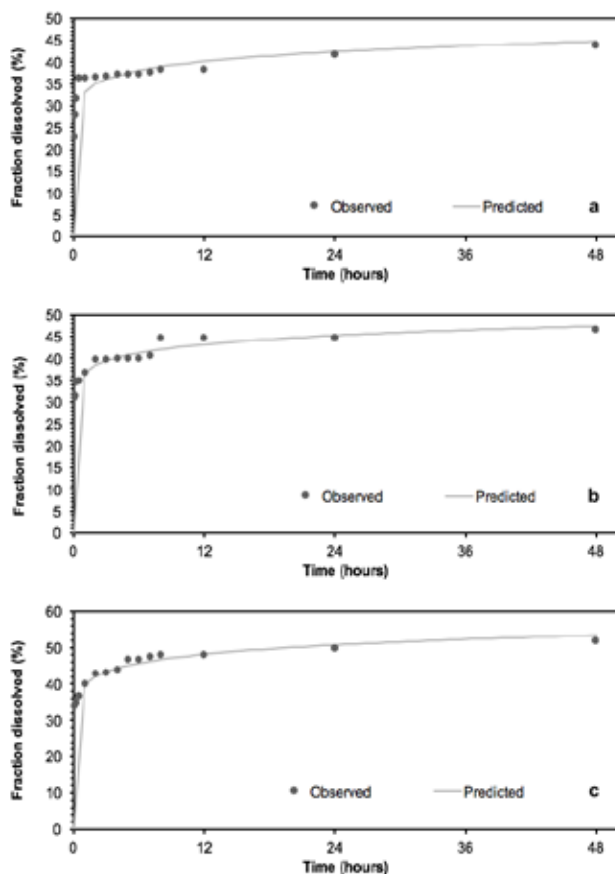
Figure 7. Automated release kinetic profiles of Korsmeyer-Peppas model, **a:** ERL-1, **b:** ERL-2, **c:** ERL-3

Table 5. Release kinetic modeling of PNPs

Kinetic Model	Evaluation Criteria	ERL-1	ERL-2	ERL-3
Korsmeyer- Peppas	k	33.112	36.719	39.984
	r^2	0.815	0.945	0.968
	AIC	67.525	47.284	45.040

Evaluation of drug release data is achieved using many mathematical models and statistical parameters. However, most of those models contain nonlinear equations. In the DDSolver computer program which can evaluate 40 different dissolution parameters, the highest k and r^2 values and the lowest AIC values were used for determining the best fit.[16] Higuchi and Korsmeyer-Peppas models both were determined to give good correspondance. Comparing those two models according to the 3 criteria mentioned above, Korsmeyer-Peppas model was selected to be the best kinetic model which describes controlled release from matrix nano-systems.[16]

CONCLUSIONS

As a result of all particle size, PDI, zeta potential, SEM, DSC, XRD, FT-IR, NMR, EE % and *in vitro* release data obtained, it was decided that sustained release matrix systems could be prepared in this study. Correspondance to Korsmeyer-Peppas model describing controlled release from matrix nano-systems also confirmed the formation of matrix systems in this study. ERL-3 containing the highest amount of active ingredient among the other PNPs prepared was found to be promising for providing sustained analgesic activity. Eudragit® RL polymer containing quaternary ammonium groups represents a good matrix ingredient for further *in vivo* studies due to its cationic character.

CONFLICT OF INTEREST

The authors declare no conflict of interest, financial or otherwise.

ACKNOWLEDGEMENTS

REFERENCES

1. Eroglu, C.; Durmus, E.; Kiresi D. Effect of low-dose dexketoprofen trometamol and paraceta-mol on postoperative complications after impacted third molar surgery on healthy volunteers: A pilot study. *Med Oral Patol Oral Cir Bucal.* **2014**, 19 (*6*), 622-627.

2. Derman, S.; Kızılbey, K.; Akdeste, Z. M. Polymeric nanoparticles. *J Eng Natur Sci.* **2013**, *31*, 107-120.

3. Fu, Y.; Kao, W. J. Drug release kinetics and transport mechanisms of non-degradable and degradable polymeric delivery systems. *Expert Opin Drug Deliv.* **2010**, 7 (*4*), 429-444.

4. Rao, J. P.; Geckeler, K. E. Polymer nanoparticles: Preparation techniques and size-control parameters. *Prog Polym Sci.* **2011**, *36*, 887-913.

5. Re, M. Formulating Drug Delivery Systems by Spray Drying. *Dry Technol.* **2006**, 24, 433-446.

6. Li, X.; Anton, N.; Arpagus, C.; Belleteix, F.; Vandamme, T. F. Nanoparticles by spray dry-ing using innovative new technology: the Büchi nano spray dryer B-90. *J Control Rel.* **2010**, *147*, 304-310.

7. Aundhia, C. J.; Raval, J. A., Patel, M. M.; Shah, N. V.; Chauhan, S. P.; Sailor, G. U.; Javia, A. R.; Mahashwari, R. A. Spray Drying in the Pharmaceutical Industry – A Review. *IAJPS.* **2011**, 2 (*1*), 125-138.

8. Das, S.; Suresh, P. K.; Desmukh, R. Design of Eudragit RL 100 nanoparticles by nanopre-cipitation method for ocular drug delivery. *Nanomedicine: NBM.* **2010**, *6,* 318-323.

9. Zhang, Y.; Huo, M.; Zhou, J.; Zou, A.; Li, W.; Yao, C.; Xie, S. DDSolver: an add-in program for modeling and comparison of drug dissolution profiles. *The AAPS J.* **2010***, 12*, 263-271.

10. Di Colo, G.; Baggiani, A.; Zambito, Y.; Mollica, G.; Geppi, M.; Serafini, M. F. A new hy-drogel for the extended and complete prednisolone release in the GI trac *Int J Pharm.* **2006**, *310*, 154-161.

11. Phaechamud, T. Variables Influencing Drug Release from Layered Matrix System Com-prising Hydroxypropyl Methylcellulose. *AAPS PharmSciTech.* **2008**, *9*, 668-674.

12. Korsmeyer, R. W.; Gurny, R.; Doelker, E.; Buri, P.; Peppas, N. A. Mechanisms of solute release from porous hydrophilic polymers. *Int J Pharm.* **1983**, *15*, 25-35.

13. Singhvi, G.; Singh, M. Revıew: In-Vıtro Drug Release Characterızatıon Models. *IJPSR.* **2011**, 2(*1*), 77-84.

14. Öztürk, A. A.; Yenilmez, E.; Yazan, Y. Development and validation of high performance liquid chromatography (HPLC) modified method for dexketoprofen trometamol. *Eur. Int. J. Sci. Tech.* **2017**, 6(*4*) 33-41

15. Öztürk, A.A.; Yenilmez, E.; Arslan, R.; Şenel, B.; Yazan Y. Dexketoprofen Trometamol-Loaded Kollidon® SR and Eudragit® RS 100 Polymeric Nanoparticles: Formulation and In Vitro-In Vivo Evaluation. *Lat. Am. J. Pharm.* **2017**, 36*(11),* 2153-2165.

16. Lopedota, A.; Trapani, A.; Cutrignelli, A.; Chiarantini, L.; Pantucci, E.; Curci, R.; Manuali, E.; Trapani, G. The use of Eudragit® RS 100/cyclodextrin nanoparticles for the transmucosal administration of glutathione. *Eur J Pharm Biopharm.* **2009**, *72*, 509-520.

17. Pignatello, R.; Ricupero, N.; Bucolo, C.; Maugeri, F.; Maltese, A.; Puglisi, G. Prepara-

tion and characterization of eudragit retard nanosuspensions for the ocular delivery of cloricromene. *AAPS Pharm Sci Tech*. **2006**, 7(*1*), 1-7.

18. Nagarwal, R.C.; Kant, S.; Singh, P. N.; Maiti, P.; Pandit J. K. Polymeric nanoparticulate system: a potential approach for ocular drug delivery. *J Control Release*. **2009**, *136*, 2-13.

19. Pagar, K.; Vavia, P. Rivastigmine-Loaded L-Lactide-Depsipeptide Polymeric Nanoparticles: Decisive Formulation Variable Optimization*Sci Pharm*. **2013**, *81*, 865-885.

20. Mainardes, R. M.; Evangelista, R.C. PLGA nanoparticles containing praziquantel: effect of formulation variables on size distribution. *J Microencapsul*. **2005**, 2(*1*), 13-24.

21. Sapsford, K. E.; Tyner, K. M.; Dair, B. J.; Deschamps, J. R.; Medintz, I. L. Analyzing nanomaterial bioconjugates: a review of current and emerging purification and characterization techniques. *Anal Chem*. **2011**, *83*, 4453-4488.

22. Lin, P. C.; Lin, S.; Wang, P. C.; Sridhar, R. Techniques for physicochemical characterization of nanomaterials. *Biotechnol Adv*. **2014**, *32*, 711-726.

23. Shin, S. B.; Cho, H.Y.; Kim, D. D.; Choi, H. G.; Lee, Y. B. Preparation and evaluation of tacrolimus-loaded nanoparticles for lymphatic delivery. *Eur J Pharm Biopharm*. **2010**, *74*, 164-171.

24. Öztürk, A. A.; Martin Banderas, L.; Cayero Otero, M.D.; Yenilmez, E.; Yazan Y. New Approach to Hypertension Treatment: Carvediol-Loaded PLGA Nanoparticles, Preparation, In Vitro Characterization and Gastrointestinal Stability. *Lat. Am. J. Pharm*. **2018**, 37*(9),* 1730-1741

25. Öztürk A. A., Güven U. M., Yenilmez E, Şenel B. Effects of Different Derivatives of Eudragit Polymer on Entrapment Efficiency, In Vitro Dissolution, Release Kinetics and Cell Viability Results on Extended Release Flurbiprofen Loaded Nanomedicines. *Lat Am J Pharm*. **2018**, 37(*10*), 1981-1992.

26. Öztürk A. A., Güven U. M., Yenilmez E. Flurbiprofen Loaded Gel Based Topical Delivery System: Formulation and In Vitro Characterization with New Developed UPLC Method. Acta Pharm Sci. **2018**, 56(*4*), 81-105.

Determination Amount of Silymarin and Pharmaceutical Products from Milk Thistle Waste Obtained from Cold Press

Derya Duran[1*], Semih Ötleş[1], Ercüment Karasulu[2]

1 Graduate School of Natural and Applied Science, Food Engineering, Izmir, Turkey
2 Institue of Health Science, Drug Research and Pharmacokinetic Development and Applied Center, Izmir, Turkey

ABSTRACT

In this study, the compounds that contain active ingredients beneficial for health and disposed from t he fruits of milk thistle which from oil was extracted after cold press was obtained, and end products were provided.

At this stage, total ash, insoluble ash in HCl, loss on drying, foreign matter, heavy metal and microbiology analyses were carried out on the milk thistle waste supplied as seeds. The seeds were treated to cold press, then oil and waste were obtained. Peroxide value, FFA, refractive index, fatty acid composition, saponification and iodine number were investigated in the oil. The waste had silymarin compounds significantly, therefore verification was performed for the quantitation of silymarin active ingredient in the waste. The waste contained up to 2% silymarin.

As a result, a formulation was created for the standardized active ingredient and milk thistle oil, and end product was provided in the form of soft capsule.

Keywords: cold press, milk thistle (*Silybum marianum*), silymarin, soft capsule

INTRODUCTION

Silybum marianum (L.) Gaertn (synonym *Carduus marianus* L.) is known as milk thistle. It belongs to Asteraceae family. It originates from the Mediterrane-an area. However, it has spread to other countries in Europe, Asia, Australia and both Americas[1]. The primary content of *S. marianum* is the presence of a group of flavonolignans known as silymarin in the pericarp and seed coat [2]. The rate of flavonolignans is usually between 1.5% and 3.5% of the fruit weight[1]. Silymarin consists of silybin, isosilybin, silydianin, silychristin, isosilychrystin and isosi-lybinin[1-3]. Since among flavonolignan compounds silybin has detoxificationing

properties, it stabilizes the functions of the liver. Therefore, *S. marianum* has been grown for pharmaceutical purposes in some European and Asian countries. In recent years, silymarin has been used in various treatments because of its properties in the medical, pharmaceutical and veterinary fields[1,4]. In addition to their hepatoprotective effect, flavonolignans also have antioxidant, anti-inflammatory, antifibrotic, hypolipidemic, neurotrophic and neuroprotective effects[3]. Silymarin is also known with its effects of reducing chemotherapy side effects and protecting against radiotherapy-induced toxicity[3,5].

Milk thistle has a wide area of usage due to the chemical composition of its fruits and biomasses, and oil yield. Byproducts are produced from silymarin extraction, and these biomass is used in various fields including food, fodder, cosmetic and bioenergy.

Cold press is a simple, ecological and energy-efficient method. For these reasons, it is a more economical technique compared to the other methods[6] such as solvent extraction and hot press. It has been reported to be the best way to produce high-quality oil. When compared with hot pressing and solvent extraction, its oil yield is lower[7]. Cold press has hence drawn the interest of consumers because of nutritional contents and naturality of the oils[8]. Since no heat treatment and chemical process is used during the cold press process, all beneficial nutritional properties of the raw material are transmitted to the oil. Therefore, cold pressed seed oils have high dietary and sensory properties and contain useful elements with significant chemical properties for health [9,10,11]. Cold pressed seed oils contain natural phytochemicals such as tocopherols, fatty acids, sterols and antioxidant phenolic compounds[12,13,14,15].

Milk thistle seed contained high silymarin levels as it was seen in the literature data. In this study, the seeds were treated to cold press, then oil and waste were obtained. Silymarin remained in the waste, it didin't pass to oil. The quantitation of silymarin active ingredient in the waste analyzed. After that, active ingredients were quantified in a product that was not evaluated as waste, formulations were created for mixture with oil which is rich in its own fatty acids, and the end product was produced as capsule. Based on the data obtain from the study, all necessary quality control analyses were conducted on the plantal waste that was the source of silymarin, the biomass of milk thistle, and extraction of end product by dosing was aimed.

METHODOLOGY

Materials

Seed and oil samples

Seed samples were supplied from an approved supplier in Konya province. These samples were approved after the relevant quality control analyses. The cold pressing technique was applied with an industrial scale in ZADE VİTAL Pharmaceuticals Inc. (200 kg seed/day capacity, single head, 2,2 kW power) cold press machine. The cold pressing procedure was set by a 10-mm exit die, and 40 rpm of screw rotation speed and 40 ºC of exit temperature was used[16].

Glycerin, gelatine and pure water

Gelatine was supplied from SEL-JEL Inc. vegetative glycerin from the approved supplier, and pure water from ZADE VITAL Pharmaceuticals Inc. in order to produce soft capsule from the material, namely from the biomass generated after cold press.

Chemicals

Potassium hydroxide was supplied from T. Baker, nitric acid, hydrogen peroxide, phosphoric acid, methanol was supplied from Sigma-Aldrich, media for microbiology was supplied from VWR companies. Pure water and ultrapure water were used to meet the pharmacopeia requirements.

Methods

Analysis Performed in the Seed

Total aflatoxin and ochratoxin analysis

Eueropean Pharmacopoeia 8.0, 2.8.18 method[17] and Eueropean Pharmacopoeia 8.0, 2.8.22 method[17] were used for aflatoxin and ochratoxin analyses respectively.

Heavy Metal Analysis

The analysis is made with Shimadzu / ICPE 9000 device. Burner unit temperature is as follows: Process temperature was gradually increased for 15 minutes up to 200ºC. At the end of this period, the temperature was fixed at 200ºC for 15 minutes. Then, it was conditioned to cool after the process of 30 minutes. Argon gas was used in ICPE 9000 device conditions. The cooler temperature was set at -15ºC, and the gas pressure at 450-460 Pa. Nitric acid of 1% was prepared. Reference standard solution was prepared as 1, 5, 10, 20, 50, and 100 ppb. At the application steps, 0.5 g sample was weighed in weighing bottle

on an assay balance. Then the sample was taken to the burner unit container. 7 mL nitric acid and 1 mL hydrogen peroxide were added into the container[17].

The Analysis of Total Ash, Insoluble Ash in HCl, Loss on dryimg, and Foreign Matter

Because all these analyses were performed under the title of the control of vegetable drugs, European Pharmacopoeia methods were used[17]. The total ash was analyzed using EP 2.4.16, insoluble ash in HCl EP 2.8.1, loss on drying EP 2.2.32, and foreign matter EP 2.8.2 methods.

Microbiological Analysis

Since microbiology analyses in the seed were made based on drug control, *the total bacteria, total yeast and mold, bile tolerant gram-negative bacteria, Escherichia Coli* and *Salmonella* strains specified in European Pharmacopoeia were taken into close scrutiny. All these analyses are made according to EP 2.6.12 and 2.6.13 methods[17].

Oil Analyses

Analyses of Peroxide Value, FFA, Saponification Number, Amount of Unsaponifiable Matter and Iodine Number

After oil extraction from the seed the resultant waste and milk thistle oil provide of end product. For this reason, analyses in the pharmacopoeia is also carried out in milk thistle[17]. These analyses include peroxide value using EP 2.5.5, free fatty acids (FFA) value EP 2.5.1, saponification number EP 2.5.6, amount of unsaponifiable matter EP 2.5.7, and iodine number EP 2.5.4 methods.

Fatty Acid Composition

Fatty acid composition was made with a validated method in the company. Oil sample of 60 mg was weighed and put into a screwed covered tube then 2 mL 2N methanolic potassium hydroxide solution (KOH) was added on it. It was then mixed with a vortex for 5 minutes after that, 2 mL of n-Heptane was added on the oil sample and methanolic potassium hydroxide mixture and mixed for 1 minute with the vortex. The oil sample mixed with vortex was centrifuged at 3000 rpm for 5 minutes. Supernatant (organic phase) of the centrifuged sample was taken, filtered and transferred into a GC vial. Schimadzu GC and SUPELCO SP 2560 column were used. Fatty acid was identified using FAME-MIX 37 standard.

Furnace temperature was kept at 140°C for 5 minutes. The temperature was raised to 240°C with 4°C increase per minute and kept for 20 minutes. The

sample of 1 µL was injected. Flow rate was set at 1.1 mL/min and nitrogen gas was used as the carrier gas. The analysis lasts 50 minutes. Percentile fatty acid composition was obtained after 50 minutes.

Capsule Analysis

Disintegration test

One capsule was put into 6 tubes. Each tube was added a disk. Pure water was used for the fluid medium to be immersed. Fluid medium temperature had to be kept at $37 \pm 2°C$. The equipment was run for 30 minutes. After the time determined for the control of disintegration duration was up, the reservoirs in which the tubes were inserted were removed from the immersed fluid.

Uniformity of dosage units

Twenty soft gelatine capsules were obtained. At first, each filled capsule was weighed, then the capsule was cut with a knife and the matter in it was removed, and then the capsule was irrigated with chloroform, dried, and the empty gelatine was weighed. The weight difference between the filled and empty states of the capsule was calculated, and the weight of the vegetative preparation in the capsule was found.

Verification of the waste

Verification of silymarin and its components

In this study, the active ingredient should be quantified for the dose adjustment of the milk thistle waste used in its finished dosage form. Therefore, since milk thistle was found in the United States Pharmacopoeia, the verification of the active ingredient was carried out.

The used reactives were methanol and phosphoric acid, the used standard Milk Thistle Extract (E.P) and the used placebo was milk thistle waste supplied from ZADE VITAL. The acceptability criteria were considered as RSD% value ≤ 2.0.

Mobile phase: According to the USP 54.2 analysis method, the mobile phase was prepared as two separate phases as Mobile phase A and Mobile phase B. For the mobile phase A, 400.0 mL methanol and 1600 mL ultrapure water were put into the mobile phase bottle of 2000 mL with measuring cylinder and 10 mL phosphoric acid was added on it. For mobile phase B, 1600 mL methanol and 400 mL ultra pure water were put into the mobile phase bottle with measuring cylinder and on which 10 mL phosphoric acid was added on it. After the prepared mobile phases were filtered through vacuum, the mobile phase was put into the bottle and degased. 1000 ppm main stock solution, and

10, 20, 50, 100, and 250 ppm silymarin calibration solutions were prepared[30].

Linearity

As the acceptability criteria, R^2 value should be between $1.00 \geq R^2 \geq 0.99$. Three injections were made at each of 6 separate concentrations.

Limit of Detection (LOD)

Signal/noise ratio was calculated. This ratio was expected to be ≥ 3.00.

Limit of Quantification (LOQ)

Signal/noise ratio was calculated. This ratio was expected to be ≥ 10.00

Accuracy

Each recovery was expected to be between 98.0% and 102.0% and RSD value between the injections < 2.00. The samples of 80%, 100%, and 120% were prepared as three in each, and three injections were made from each one.

Reproducibility

RSD% value was expected to be ≤ 2%. Six sample solutions of 100% were prepared. Three injections were made from each sample.

Repeatability of the Method

RSD% value was expected to be ≤ 2%. Six sequential injections were given from 100% sample solution. Repeatability values of the methods were given in the following table. The results were appropriate according to the acceptability criteria.

Capsule production

The vegetable material obtained after cold press of milk thistle oil was ground in the grinder, and then filtered through 250-micron screens and the granule size was standardized. The obtained standardized powder mixture was mixed with lecithin, beeswax and milk thistle oil and the end product was obtained. End product which soft capsule formulation was occured about 1% lecithin, 2% beewax, 25% milk thistle waste powder and 72% of milk thistle oil.

Statistical analysis: Data collected on proximate composition were analyzed by simple descriptive statistics[18].

RESULTS AND DISCUSSION

Results of milk thistle seed

In a study by Mehring[19], total ash amounts were analyzed in various seeds and spices. The total ash values in the anise seed 6%, in the bay leaf 9%, in the caraway 8%, in the cinnamon 5%, in the celery 10%, in the cinnamon 5%, in the carnation 7%, in the coriander 8.5%, in the cumin 9%, in the in the ginger 5%, in the mustard 5% and in the thyme 14% were found.

The insoluble ash in HCl value of Morus nigra seeds were found 5.817% by Shukla et al. [20] the amount of insoluble ash in HCl should not exceed 1% and loss on drying max. 8%, according to the Fructus Silybi Mariae monograph in WHO[21],

Inorganic residues were found by William[22] in some spices and seeds as follows; in the chili powder abaout 43.1 mg/10 g, in the celery seed 85.7 mg/10g, in the cinnamon 63.4 mg/10g.

According to the analyses that should be made under the Herbal Drugs title of European Pharmacopoeia[17], total ash, insoluble ash in HCl, loss on drying, foreign matter, total aflatoxin, ochratoxin, heavy metal and microbiology analyses were made. In the analysis, the total ash were found as 4.38%, insoluble ash in HCl as 0.01%, and loss on drying as 6.38%, while foreign matter, total aflatoxin, and total ochratoxin could not be found. As a result, in this studuy analyses values were found to be in close proximity with other literature values.

Table 1. Physicochemical analyses of milk thistle seeds

Analysis	Specifications	Results
Total ash	Max. 5.00	4.38%
Insoluble ash in HCL	Max. 5.00%	0,01%
Loss on drying	Max. 10.00%	6,83%
Foreign matter	Absent / 100 g	Not detected

Another analysis group which were expected to be performed in the seeds was microbiological controls with the following results in Table 2.

Table 2. Microbiological analysis in milk thistle seeds

Controls	Specifications	Results
Total bacteria	Max. 5 x 10^4 CFU/g	Conforms
Total yeast and mould	Max. 5 x 10^2 CFU/g	Conforms
Bile-tolerant gram-negative bacteria	Max. 5 x 10^2 CFU/g	Conforms
Escherichia coli	Absent/ g (Absent / g)	Conforms
Salmonella	Absent/25 g (Absent / 25g)	Conforms
Aflatoxin	Max. 5.0 µg / kg	Not detected
Ochratoxin	Max.10.0 µg / kg	Not detected

Turkish Food Codex Contaminant Statement and the mean of relevant values were considered when acceptability criteria were sought in the seed in heavy metals, and the limit was found as 0.10 mg/kg, while no limit was detected in mercury and cadmium as specification of it should not contain.

In a study[23], concentration of metals (aluminum, arsenic, lead, and cadmium) was examined using atomic absorption spectrophotometry in medicinal plants including: Thymus vulgaris, Melissa officinalis, Achillea millefolium, Rosmarinus officinalis, and Salvia officinalis around Arak city/Iran. The minimum and maximum levels of toxic metals in these plants was reported to be 3.022µg/g and 0.254µg/g for lead and 0.031 µg/g and 0.144 µg/g for cadmium, respectively.

Table 3. Heavy metal analysis in milk thistle seeds

Controls	Specifications	Results
Lead	Max. 0.10 mg / kg	Not detected
Mercury	Absent/ g	Not detected
Cadmium	Absent/ g	Not detected

Given all these analysis results, milk thistle seed complies with all acceptability criteria as a vegetable drug.

Results of the analysis of milk thistle seed oil

In a study by Iman Nasrollahi[24] peroxide values were respectively found as 0.51, 0.69, 0.68 and 0.57, and refractive index values as 1.4646, 1.46482, 1.4656, and 1.4651 in four separate milk thistle oils. In the present study, peroxide value was found as 1.16 meqO$_2$/kg oil, and refractive index as 1.46. In a study by Faiza et al.[24]; saponification number was found as 126.2 mg KOH/g, number of free fatty acids (FFA) as 2.53 mg/g, iodine number as 2.79 mg/g and specific weight as 0.8129. In a study by Meddeb[21]; refractive index was found as 1.47, specific weight as 0.91 g/mL, acidic value as 5.48 mgKOH/g oil, peroxide values as 2.83 meqO$_2$/kg oil, iodine number as 112.41 mgKOH/g oil, and amount of unsaponifiable matter as 1.57. In our study, peroxide value (moqO$_2$/kg oil) was found as 1.16, FFA (in terms of oleic acid) (%) (m/m) as 1.70, amount of unsaponifiable matter (g/kg) as 14.14, saponification number (mgKOH/ g oil) as 200.13, iodine number (mgKOH/g oil) as 118.03, refractive index (40 °C) as 1.46, and specific weight (g/mL) (20°C) as 0.92. Therefore, our results were close to those of the previous studies.

Table 4. Physicochemical analysis of milk thistle oil

Analysis	Results
Peroxide (meq O$_2$/kg oil)	1.16
FFA (in terms of oleic acid) (%)(m/m)	1.70
Amount of unsaponifiable matter (g/kg)	14.14
Saponification Number (mg KOH/g oil)	200.12
Iodine Number (mg KOH/g oil)	118.03
Refractive Index (40° C)	1.46
Concentration (gr/mL)(20°C)	0.92

Table 5. Fatty acid composition of milk thistle

Carbon Number	Fatty Acid	Percentage (%) value
C 14:0	Myristic Acid	0.06
C 16:0	Palmitic Acid	7.75
C 16:1	Palmitoleic Acid	0.05
C 18:0	Stearic Acid	5.07
C 18:1	Oleic Acid	23.91
C 18:2	Linoleic Acid	55.49
C 20:0	Arachidic Acid	3.18
C 20:1	Gondoic Acid	0.86
C 18:3	Linolenic Acid	0.42
C 22:0	Behenic Acid	2.30
C 22:1	Erucic Acid	0.10

In another study[25], nine fatty acids were detected. Linoleic acid (18:2n-6) was the dominant fatty acid, it was followed by oleic (18:1n-9), palmitic acid (16:0) and stearic (18:0) acid. The amount of polyunsaturated fatty acid was about 50-54%, and amount of saturated fatty acid was about 19-21% in the extracted milk thistle oil.

Herein, the important point was that polyunsaturated fatty acids play an important role in cellular communication, membrane structure, prostaglandin synthesis, nervous, endocrine and immune systems[26].

In study by Iman Nasrollah [27]; fatty acid compositions were studied in 4 different milk thistle oil; and palmitic acid (16:0) was respectively found as 8.55%, 8.36%, 7.99% and 9.26%; stearic acid (18:0) as 5.609%, 7.72%, 5.607% and 5.01%; oleic acid (18:1) as 28.68%, 35.85%, 28.54%, and 30.42%, while linoleic acid (18:2) was found as 54.5%, 43.57%, 54.71%, and 52.78% and finally linolenic acid (18:3) as 2.50%, 4.48%, 3.13% and 2.51%.

In our study, 11 fatty acids were studied, and the results were given in Table 5. Main results included palmitic acid (16:0) as 7.75%, stearic acid (18:0) as 5.07%, oleic acid (18:1) as 23.91%, linoleic acid (18:2) as 55.49%, and arachidic acid (20:0) as 3.18%. In conclusion, milk thistle oil is rich in polyunsaturated fatty acids.

Results of the analysis of end product soft capsule

Disintegration time

In a study by Gurley et al.[28] disintegration time of milk thistle oil soft capsule was found as 12.6 minutes. It has a total daily dose of 440 mg.

In another study[29], disintegration times were studied in different soft capsules. Disintegration time was found as 9.7 minutes in amantadine soft capsule at covered room temperature, considering storage conditions, and the time increased to 10 minutes 2 weeks after room temperature, and 10.3 minutes after 2 further weeks at 40°C. When the same processes were made in flaxseed oil soft capsule; again the disintegration time was found as 8.2 minutes at room temperature, 7.7 minutes 2 weeks after the storage, and 8.3 minutes after 2 weeks at 40°C. The same studies were conducted in soy oil, and ginseng soft capsules. In our soft capsule that we produced with milk thistle waste and milk thistle oil, disintegration time was found as 13 minutes at 37 ± 2 °C.

Uniformity of dosage units

Because milk thistle substance was in the range of 90-110% 'Milk Thistle Capsule Monograph' title of USP 38 NF 33[30], we predicted an amount of vegetative preparation in the range of 810-990 based on the capsules of 900 mg. For this purpose, 20 capsules were selected and analyzed. The mean capsule value was about 900 mg, and this value was within the limits.

Verification of active ingredients in the waste

The analysis was conducted using the Powder Milk Thistle method in USP. Verification procedure was applied since the method was registered in American United States Pharmacopeia (USP)[30]. Within the verification, following parameters was analyzed.

- Linearity

- Limit of Detection (LOD)

- Limit of Quantification (LOQ)

- Accuracy

- Reproducibility

- Repeatability

The results for linearity was summarized in the following Table 6.

Table 6. Accuracy values for total silymarin

Sample No	Theoretical Concentration (%)	Concentration (mg / mL)	Peak Areas (mAU * s)	Mean Peak Areas (mAU * s)	RSD%
1	25	0,025	408713,0	407872,00	1,16
			402782,0		
			412121,0		
2	75	0,075	1112058,0	1125253,33	1,06
			1135179,0		
			1128523,0		
3	100	0,100	1465893,0	1477306,00	1,14
			1496567,0		
			1469458,0		
4	150	0,150	2223280,0	2210673,33	0,84
			2219508,0		
			2189232,0		
5	200	0,200	3166932,0	3188459,00	0,59
			3197370,0		
			3201075,0		
6	250	0,250	4025934,0	4036681,67	0,23
			4043571,0		
			4040540,0		

STATISTICAL EVALUATION	
Correlation Factor (R^2)	0,9961
Slope	16230
Intercept	89617

Silymarin solution was prepared at 6 different concentrations of 25, 75, 100, 150, 200, and 25 ppm for linearity among the verification parameters. A linear chart was obtained according to device result, area values, and equation of y = ax + b (Chart 1). Again, recovery percentage (RSD%) was found as ≤ 2.

Tablo 7. Accuracy values for silymarin.

Sample No	Concentration (mg / mL)	Peak Areas (mAU *s)	Mean Areas (mAU *s)	Recovery (%)	Mean Recovery (%)	% RSD
1	0,080	3014038,0 3055221,0 2955533,0	3008264,00	100,64	99,66	1,39
2	0,080	3005572,0 2937406,0 2846391,0	2929789,67	98,06		
3	0,080	2947268,0 3084160,0 2960685,0	2997371,00	100,28		
4	0,100	3805910,0 3819263,0 3817707,0	3814293,33	101,66	101,65	0,20
5	0,100	3834192,0 3832395,0 3797175,0	3821254,00	101,84		
6	0,100	3788289,0 3809254,0 3821343,0	3806295,33	101,45		
7	0,120	4449077,0 4457120,0 4692136,0	4532777,67	100,43	100,41	0,72
8	0,120	4464181,0 4513701,0 4498404,0	4492095,33	99,54		
9	0,120	4498404,0 4690313,0 4524867,0	4571194,67	101,27		

STATISTICAL EVALUATION	
MEAN RECOVERY %	100,01
STANDARD DEVIATION	0,90
RSD %	0,90

For accuracy parameters, each recovery was between 98.0% and 102.0%, and RSD value was <2.00%. The samples of 80%, 100%, and 120% were prepared as three in each, and three injections were made from each one.

Table 8. Total silymarin recovery values

Sample No	Concentration (mg / ml)	Peak Areas (mAU * s)	RSD (%)	Mean Area (mAU * s)	Recovery (%)
1	0,100	1487466,5	0,39	1487223,83	99,60
		1481366,5			
		1492838,5			
2	0,100	1474817,5	1,77	1471510,83	98,51
		1495767,5			
		1443947,5			
3	0,100	1488724,5	0,60	1488637,50	99,69
		1497576,5			
		1479611,5			
4	0,100	1489920,5	0,68	1494016,83	100,07
		1486511,5			
		1505618,5			
5	0,100	1471985,5	1,48	1497598,83	100,31
		1509519,5			
		1511291,5			
6	0,100	1471832,5	0,54	1472499,17	98,58
		1480743,5			
		1464921,5			

STATISTICAL EVALUATION	
MEAN RECOVERY %	99,46
STANDARD DEVIATION	0,75
RSD %	0,76

Recovery values from 100% concentration were found between 98% and 102%, indicating the method worked correctly.

Table 9. Total silymarin repeatability values

SAMPLE	AREA (mAU*s)
1	1502274,5
2	1492981,5
3	1488446,5
4	1489787,5
5	1492166,5
6	1491073,5
Mean	1492788,33
RSD %	0,33

Six sequential injections were given from 100% solution. Area values were highly close to each other, indicating repeatability of the method.
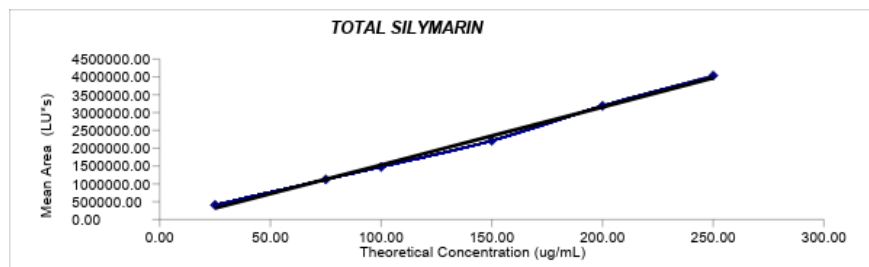

Figure 1. Total silymarin accuracy chart

CONCLUSION AND RECOMMENDATIONS

Milk thistle is a plant which can easily grow almost all countries worldwide including our country. With flavonolignan compounds named fatty acids and silymarin that it contains in seed and the oil, milk thistle found a wide area of use in many field such as medicine, cosmetic, and food. The oil, rich in poly-unsaturated fatty acids were obtained after cold press, but compounds that are named as hepatic protectors especially silymarin are not transported to the oil. They remain in vegetative pomace called waste. In this study, active ingredients were quantified in a product that is not evaluated as waste, for-mulations were created for mixture with oil which is rich in its own fatty acids, and the end product was produced as capsule. By this way, we aimed to pro-duce a standardized product, and obtained a value-added product from waste material. Thus, we demonstrated that this product which we made pilot test at laboratory scale can be produced at industry scale.

ACKNOWLEDGEMENT

REFERENCES

1. Morazzoni P., Bombardelli E. *Silybum marianum* (*Carduus marianus*). *Fitoterapia*, **1995**, *66*, 3–42.

2. Cappelletti E.M., Canaito R. Silymarin localization in the fruit and seed of *Silybum marianum* (L.) Gaertn. *Herba Hungarica*, **1984**, *23*, 53–62.

3. Abenavoli L., Capasso R., Milic N., Capasso F. Milk thistle in liver diseases: past, present, future. *Phytotherapy Research*, **2010**, *24*, 1423–1432.

4. Thanonkaew, A., Wongyai, S., McClements, D. J., & Decker, E. A. Effect of stabilization of rice bran by domestic heating on mechanical extraction yield, quality, and antioxidant properties of cold-pressed rice bran oil (Oryza saltiva L.). *LWT-Food science and technology*, **2012**, 48(*2*), 231-236.

5. Meddeb W., Rezing L., Abderrabba M., Lizard G., Mejri M., Tunisian Milk Thistle: An Investigation of the Chemical Composition and the Characterization of Its Cold-Pressed Seed Oils. *Int. J. Mol. Sci.*, **2017**, *18*, 2582.

6. Radko L., Cybulski W. Application of silymarin in human and animal medicine. *Journal of Pre-Clinical and Clinical Research*, **2007**, *1*, 22–26.

7. Yilmaz, E., Aydeniz, B., Guneser, O., & Arsunar, E. S. Sensory and Physico-Chemical Properties of Cold Press-Produced Tomato (Lycopersicon esculentum L.) Seed Oils. *Journal of the American Oil Chemists' Society*, **2015**, 92(*6*), 833-842.

8. Thanonkaew, A., Wongyai, S., McClements, D. J., & Decker, E. A., Effect of stabilization of rice bran by domestic heating on mechanical extraction yield, quality, and antioxidant properties of cold-pressed rice bran oil (Oryza saltiva L.). *LWT-Food science and technology*, **2012**, 48(*2*), 231-236.

9. Argon Z., & Gokyer A. Determination of Physicochemical Properties of Nigella sativa Seed Oil from Balıkesir Region, Turkey, *Chemical and Process Engineering Research*, **2016**, *41*, 43-46.

10. Gharibzahedi, S. M. T., Mousavi, S. M., Hamedi, M., Rezaei, K., & Khodaiyan, F. Evaluation of physicochemical properties and antioxidant activities of Persian walnut oil obtained by several extraction methods. *Industrial crops and products*, **2013,** *45*, 133-140.

11. Topkafa, M. Evaluation of chemical properties of cold pressed onion, okra, rosehip, safflower and carrot seed oils: triglyceride, fatty acid and tocol compositions. *Analytical Methods*, **2016**, 8(*21*), 4220-4225.

12. Bozan, B., & Temelli, F. Chemical composition and oxidative stability of flax, safflower and poppy seed and seed oils. *Bioresource Technology*, **2008**, 99(*14*), 6354-6359.

13. Lutterodt, H., Slavin, M., Whent, M., Turner, E., & Yu, L. L. Fatty acid composition, oxidative stability, antioxidant and antiproliferative properties of selected cold-pressed grape seed oils and flours. *Food Chemistry*, **2011**, 128(*2*), 391-399.

14. Gumus, Z. P., Guler, E., Demir, B., Barlas, F. B., Yavuz, M., Colpankan, D., & Timur, S. Herbal infusions of black seed and wheat germ oil: Their chemical profiles, in vitro bio-investigations and effective formulations as phyto-nanoemulsions. *Colloids and Surfaces B: Biointerfaces*, **2015**, *133*, 73-80.

15. Kozłowska, M., Gruczyńska, E., Ścibisz, I., & Rudzińska, M. Fatty acids and sterols composition, and antioxidant activity of oils extracted from plant seeds. *Food chemistry*, **2016**, *213*, 450-456.

16. Yilmaz E, Aydeniz B, Güneser O., Arsunar E.S., Sensory and PhysicoChemical Properties of Cold PressProduced Tomato (Lycopersicon esculentum L.) Seed Oils *J Am Oil Chem Soc.* **2015**, *92*, 833–842.

17. European pharmacopoeia, 8th ed. Council of Europe, **2014**.

18. Annongu, A. Azor, Joseph J. K., Proximate Analysis of Castor Seeds And Cake, *J. Appl. Sci. Environ. Manage.* **2008**, 12(*1*) 39 − 41.

19. A. L. Mehrıng, Total Ash Determınatıon In Spices, *Journal of Agricultural Research*, **1924**, *11* 81-87.

20. Shukla R.K., Painuly D., Shukla A., Kumar V., Singh J., Porval A., Vats S**.**, Physical Evaluation, Proximate Analysis and Antimicrobial Activity of Morus Nigra Seeds *Int J Pharm Pharm Sci*, **2015**, 7(*1*), 191-197.

21. WHO Monographs on Selected Medicinal Plants - Volume 1, **1999.**

22. William V. Eisenberg, Inorganic Particle Content of Foods and Drugs *Environmental Health Perspectives* **1974**, Vol. 9, pp. 183-191

23. Fytianos K, Katsianis G, Triantafyllou P, Zachariadis G., Accumulation of heavy metals in vegetables grown in an industrial area in relation to soil. *Bulletin of Environmental Contamination And Toxicology.* **2001**, 67(*3*), 0423-30.

24. Faiza A, Naveed I R, Noor-Ul-Ain, Uneeza J, Farhat Y. Some Physio-Chemical Properties of Silybum marianum Seed Oil Extract. *Curr Trends Biomedical Eng & Biosci.* **2018**, 13(*5*), 555875.

25. Fathi-Achachlouei B., Azadmard-Damirchi S., Milk Thistle Seed Oil Constituents from Different Varieties Grown in Iran *J Am Oil Chem Soc.* **2009,** *86*, 643–649.

26. Yehuda S PUFA: mediators for the nervous, endocrine, immune systems. In: Mostofsky DI, Yehuda S, Salem N (eds) Fatty acids: physiological and behavioral functions. Humana, Totowa, **2001,** pp 403–420.

27. Nasrollahi I, Talebi1 E, Nemati Z. Study on *Silybum marianum* Seed through Fatty Acids Comparison, Peroxide Tests, Refractive Index and Oil Percentage. *Pharmacognosy Journal.* **2016**, 8(*6*), 595–597.

28. Gurley B. J., Barone G. W., Williams D. K., Carrier J., Breen P., Yates R. C., Song P, Hubbard A. M., Tong Y., Cheboyina S. Effect of Milk Thistle (*Silybum Marianum*) And Black Cohosh (*Cimicifuga Racemosa*) Supplementation On Digoxin Pharmacokinetics In Humans. *American Society for Pharmacology and Experimental Therapeutics*, **2005**, 34, 69–74.

29. Almukainzi M., Salehi M., Chacra N. A. B., Löbenberg R., Comparison of the Rupture and Disintegration Tests for Soft-Shell Capsules. *Dissolution Technologies*, **2011**, 21-25.

30. United States Pharmacopeia 38 National Formulary 33, **2014.**

Antimicrobial Evaluation of Trisubstituted 2-piperazinyl Thiazoles

Betül Giray[1*], Leyla Yurttaş[2], Zafer Şahin[3], Barkın Berk[3], Şeref Demirayak[3]

1 Istanbul Medipol University, School of Medicine, Department of Pharmaceutical Microbiology, 34083 İstanbul, Turkey.
2 Anadolu Üniversitesi, Faculty of Pharmacy, Department of Pharmaceutical Chemistry, 26470 Eskişehir, Turkey.
3 Istanbul Medipol University, School of Pharmacy, Department of Pharmaceutical Chemistry, 34083 İstanbul, Turkey.

ABSTRACT

Thiazole and basic nitrogen containing rings are important chemical moieties of antimicrobial drugs. In recent, third generation cephalosporins include thiazole ring system. In this study, we synthesized 33 piperazine thiazole derivatives which were thought to show antimicrobial activity. Synthesize were realized with good yield using the method which reports the anticholinesterase properties of these compounds. Similar compounds with the same scaffold (2, 4, 5 trisubstituted thiazoles) are investigated for antimicrobial activity. Compounds **23-27** exhibited MIC: 256 μM against *S. aureus* ATCC 25923. Besides, 27-33 group showed MIC: 256 μM against *K. pneumoniae* UC57 and *B. cereus*. It is remarkable that the compound **27** showed antimicrobial activity against 4 different microorganisms and **26** showed antimicrobial activity against *L. monocytogenes by* MIC: 32 μM which is same as the standart chloramphenicol.

Keywords: thiazole, piperazine, antimicrobial, trisubstituted thiazole, N-benzoylthioamide.
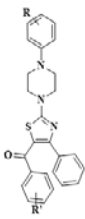
INTRODUCTION

Bacterial resistance to the treatment of infectious diseases is the main problem. Many classes of antibiotics are facing resistance and have initiated new efforts to develop new derivatives and discover new chemical classes.[1] Gram positive and gram-negative bacteria such as *Escherichia coli, Staphylococcus aureus, Micrococcus luteus, Bacillus subtilis, Bacillus cereus, Pseudomonas aeruginosa* etc. are responsible for many diverse infections which even can cause of death.[2]

Thiazole and basic nitrogen containing rings are important chemical moieties of antimicrobial drugs. Recently, third generation cefepime, ceftriaxone, cefix-

ime, ceftazimide drugs are wide spectrum cephalosporins containing thiazole ring system. Also, new studies on compounds with thiazole moiety are investigated.[3-5] List of the synthesized compounds, which were first evaluated for their acetylcholinesterase inhibitor activity by our group[6] is given in Table 1.

Table 1. Synthesized compounds

|	C. no	R	R'	C. no	R	R'	C. no	R	R'
	1	2-Cl	H	12	3-Cl	H	23	4-Cl	H
	2	2-Cl	3-CH$_3$	13	3-Cl	3-CH$_3$	24	4-Cl	3-CH$_3$
	3	2-Cl	4-CH$_3$	14	3-Cl	4-CH$_3$	25	4-Cl	4-CH$_3$
	4	2-Cl	3-OCH$_3$	15	3-Cl	3-OCH$_3$	26	4-Cl	3-OCH$_3$
	5	2-Cl	4-OCH$_3$	16	3-Cl	4-OCH$_3$	27	4-Cl	4-OCH$_3$
	6	2-Cl	3-F	17	3-Cl	3-F	28	4-Cl	3-F
	7	2-Cl	4-F	18	3-Cl	4-F	29	4-Cl	4-F
	8	2-Cl	3-Cl	19	3-Cl	3-Cl	30	4-Cl	3-Cl
	9	2-Cl	4-Cl	20	3-Cl	4-Cl	31	4-Cl	4-Cl
	10	2-Cl	3-NO$_2$	21	3-Cl	3-NO$_2$	32	4-Cl	3-NO$_2$
	11	2-Cl	3-NO$_2$	22	3-Cl	3-NO$_2$	33	4-Cl	3-NO$_2$

Similar compounds with the same scaffold (2, 4, 5 trisubstituted thiazoles) are investigated for antimicrobial activity. These compounds also have the same substituents on the thiazole ring such as piperazine (morpholine) at 2nd position, phenyl at 4th position and benzoyl at 5 th position.

As a pioneer of this study, 2, 4, 5-trisubstituted thiazole derivatives (I) were screened for antimicrobial activity against *E. coli, S. aureus, M. luteus, B. subtilis, B. cereus, P. aeruginosa* bacterial strains by paper disc diffusion method. In this study, all 7 compounds showed moderate to good activity. According to zone diameters, activity was found approximately %40-45 of ciprofloxacin.[7]
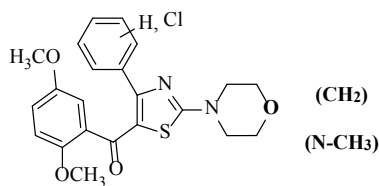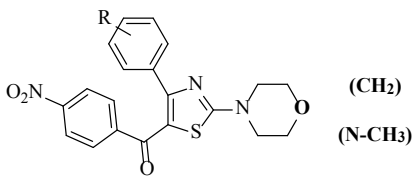
**Figure 1.** Trisubstituted thiazole compounds with antimicrobial activity

In another study of the same group, similar compounds (II) were evaluated for antimicrobial activity against same strains. 7 of 8 compounds exhibited good activity, which was very close to standard ciprofloxacin. [8]

In this study, we synthesized 33 compounds, which are thought to show antimicrobial activity. Synthesize were realized with good yield using the method which reports the anticholinesterase activity of these compounds.[6]

METHODOLOGY

Chemistry

Synthesis of 33 compounds were carried out by the method used in a recent study.[6] Following the method, N'-benzoyl piperazine thioureas (10 mmol) and bromoacetophenones (10 mmol) reacted to give the compounds. The equivalent mole of materials was boiled in ethyl alcohol until the reaction was being completed. After cooling, it was poured into the water and neutralized with NaHCO$_3$ solution. The products were crystallized from ethanol. [6,9]
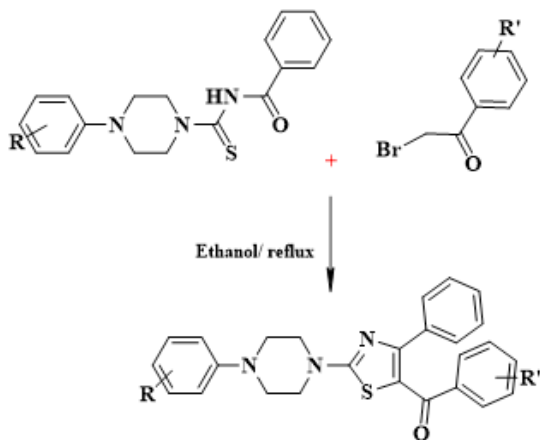
Scheme 1. Synthesis of compounds

Antimicrobial Activity Test

Antimicrobial activity test was determined on both gram positive and gram-negative bacteria strains including, *Escherichia coli* ATCC 25922, *Klebsiella pneumonia* UC57, *Enterococcus faecalis* ATCC 29212, *Listeria monocytogenes* ATCC 7644, *Salmonella typhi* ATCC 19430, Pseudomonas aeriginosa ATCC 27853, *Staphylococcus aureus* ATCC 25923, *Bacillus cereus* ATCC 7064, *Listeria monocytogenes* ATCC 7644. Clinically isolated *Acinetobacter baumannii* and *Shigella dysenteria* were provided by Hospital of İstanbul Medipol University. All these compounds were dissolved in DMSO to prepare stock solution at 10 mg/mL. Broth microdilution method was carried out in accordance with the relevant 2012 CLSI standard. [10,11] The bacterial strains were inoculated and grown to mid-log phase in Muller Hinton Broth (MHB) at 37 degrees. Bacterial inoculum suspensions were prepared at a final concentration of approximately 1×10^5 cfu/ml. Materials were 2-fold serially diluted to make different concentration, from 0.5 to 256 micromolar. Equal volumes of inoculum suspensions were than added to each well of sterile 96 well-plate with different concentration of materials, and the plate was incubated 18 h at 37 °C. Positive or negative control were set to wells with and without bacteria, respectively. Besides, chloramphenicol is used as positive control. MIC was defined as the lowest concentration of materials that prevented visible turbitidy by visual inspection. Experiments were performed duplicate.

RESULTS

Chemistry

Synthesis of compounds were carried out up to %80 yield. Characterizations were corresponded our previous study IR, ^{1}H-NMR and ^{13}C-NMR results were previously reported in the related paper.[6]

Antimicrobial activity

No antimicrobial activity was detected against *E. coli, S. Typhii, P. aeriginosa*, *S. dysanteria* ve *A. Baumanni* bacteria. Activity on the other bacteria is summarized in Table 2.

27-33 compound series against *K. pneumoniae* and *B. Cereus* microorganisms are effective. It is important that these compounds are effective against two different microorganisms in serials. When the whole table was examined, the compounds in the range 23-33 were found to be effective against to the microorganisms. This indicates that the 4-chlorophenyl structure attached to the piperazine ring is beneficial for antimicrobial activity. The structures in

the 23-27 group against *S. aureus* have been found effective. In this group, electron donating substituents (R') were prominent. 13, 17, 27, 31 (MIC: 256 μM), 32 (MIC: 128 μM), 33 (MIC: 64 μM) effects have been found against *E. facealis*. Chloramphenicol has no effect on this microorganism.

Table 2. MIC of te materials against bacteria.

Compounds	MIC (μM)				
	K. pneumoniae UC57	S. aureus ATCC 25923	E. faecalis ATCC 29212	B. cereus	L. monocyto-genes ATCC 7644
1	-	-	-	-	-
2	-	-	-	-	-
3	-	-	-	≥ 256	-
4	-	-	-	-	-
5	-	-	-	-	-
6	-	-	-	-	-
7	-	-	-	-	-
8	-	-	-	-	-
9	-	-	-	-	-
10	-	-	-	-	-
11	-	-	-	-	-
12	-	-	-	-	-
13	-	-	≥ 256	-	-
14	-	-	-	-	-
15	-	-	-	-	-
16	-	-	-	-	-
17	-	-	≥ 256	-	-
18	-	-	-	-	-
19	-	-	-	-	-
20	-	-	-	-	-
21	-	-	-	≥ 256	-
22	-	-	-	-	≥ 256
23	-	≥ 256	-	-	-
24	-	≥ 256	-	≥ 256	-
25	-	≥ 256	-	-	-
26	-	≥ 256	-	-	≥ 32
27	≥ 256	≥ 256	≥ 256	≥ 256	-
28	≥ 256	-	-	≥ 256	-
29	≥ 256	-	-	≥ 256	-
30	≥ 256	-	-	≥ 256	-
31	≥ 256	-	≥ 256	≥ 256	-
32	≥ 256	-	≥ 128	≥ 256	-
33	≥ 256	-	≥ 64	≥ 256	-
Chloramphenicol	≥ 256	≥ 256	-	≥ 32	≥ 32

Against *L. monocytogenes*, compounds 22 (MIC: 256 μM) and 26 (MIC: 32 μM) were found active. Although it is not appropriate to make a chemical interpretation here, the activity of compound 26 is the same as the standard compound chloramphenicol.

CONCLUSION

Compound 27 has effect on 4 of 5 microorganisms with 256 MIC values. Besides, 27-33 has 256 μM MIC value against *K. pneumoniae* and *B. cereus* as series. This empowers the idea that activity is related to chemical structure. Furthermore 23-27 on *S. aureus* has antimicrobial effect as a chemical series. These results can be associated with the chemical structure and efforts can be continued in these chemical groups for investigating new antimicrobial drugs.

REFERENCES

1. Levy, S.B.; Marshall, B.; Antibacterial resistance worldwide: causes, challenges and responses. *Nat Med.* **2004**, *10*, 122–129.

2. Seifert, S.; Dirita V. Evolution of microbial pathogens, ASM Press, Washington, (**2006**).

3. Holla, B.S.; Karthikeyan, M.S.; Prasad, D.J.; Mahalinga, M.; Kumari, N.S.; Synthesis of some novel 2, 4-disubstituted thiazoles as possible antimicrobial agents, *Eur. J. Med. Chem.* **2008**, *43*, 261–267.

4. Holla, B.S.; Malini, K.V.; Rao, B.S.; Sarojini, B.K.; Kumari, N.S.; Synthesis of some new 2, 4-disubstituted thiazoles as possible antibacterial and anti-inflammatory agents, *Eur. J. Med. Chem.* **2003**, 38 (*3*), 313-318.

5. Sarojini, B.K.; Darshanraj, C.G.; Bharath, B.R.; Manjunatha, H. Synthesis, characterization, in vitro and molecular docking studies of new 2, 5-dichloro thienyl substituted thiazole derivatives for antimicrobial properties, *Eur. J. Med. Chem.* **2010**, 45 (*8*), 3490–3496.

6. Sahin, Z.; Ertas, M.; Bender, C., Bulbul, E. F., Berk, B., Biltekin, S. N., Yurttas, L., Demirayak, S. Thiazole-substituted benzoylpiperazine derivatives as acetylcholinesterase inhibitors. *Drug Dev Res.* **2018**, *79*, 406-425.

7. Darji D.N.; Pasha T.Y.; Bhandari, A.; Molvi, K.I.; Desai, S.A.; Makwana, M.V. Synthesis and Spectral characterization of some novel (2, 5-dimethoxyphenyl)-(2,4-disubstituted-thiazol-5-yl) methanone as possible antibacterial agents, *Der Pharma Chemica.* **2012**, 4(*2*), 808-812.

8. Darji D.N.; Pasha T.Y.; Bhandari, A.; Molvi, K.I.; Desai, S.A.; Makwana, M.V. Synthesis of some novel 2, 4, 5 –trisubstituted thiazoles as possible antibacterial agents. *J. Chem. Pharm. Res.* **2012**, 4(*4*), 2148-2152.

9. Ried, W.K.; L. Neuartige Synthese substituierter 2-Morpholino- und 2-Athox ythiazole. Liebigs. Ann. Chem. **1976**, 395-399.

10. Balouriri, M.; Sadiki, M.; Ibnsouda S. K. Methods for in vitro evaluating antimicrobial activity: A review. J. Pharm. Anal. **2016**, 6(*2*) 71-79.

11. Cockerill et al., CLSI, Methods for Dilution Antimicrobial Susceptibility Tests for Bacteria That Grow Aerobically, Approved Standard, 7th ed., CLSI document M7- A7 Clinical and Laboratory Standart Institute, 950 West Valley Road, Suite 2500, Wayne, Pennsylvania 19087, USA **2012**.